MODELING AND INTERPRETATION OF FIBER ORIENTATION-BASED FAILURE MECHANISMS IN MACHINING OF CARBON FIBER-REINFORCED COMPOSITES

BY

KEVIN A. CALZADA

THESIS

Submitted in partial fulfillment of the requirements
for the degree of Master of Science in Mechanical Engineering
in the Graduate College of the
University of Illinois at Urbana-Champaign, 2010

Urbana, Illinois

Advisers:

Professor Shiv G. Kapoor
Professor Richard E. DeVor

Abstract

Fiber-reinforced polymer composites have recently emerged as novel materials capable of playing a unique role in industrial applications. The advantage of these materials over traditional metals or polymers comes from the material property enhancements that can be achieved by combining appropriate fiber and matrix materials into the microstructure. While these materials have recently become popularized, many complications arise in the manufacturing process of the two-phase microstructures, specifically in the machining of FRP composites. Due to the complex nature of FRP two-phase microstructures, the fiber failure mechanisms occurring in the machining process are not fully understood. Many experimental and modeling techniques have been implemented to more fully explain the nature of the fiber failure mechanisms in the machining process, but these have fallen short of a complete understanding of the machining complexities. This research seeks to gain a fundamental understanding of the fiber orientation-based fiber failure mechanisms occurring in the micro-machining of FRP composites by employing two unique modeling techniques.

In this research, both experimental and finite element-based modeling approaches are undertaken. Fibers oriented in 0, 45, 90, and 135 degrees with respect to the direction of tool motion are investigated and unique failure theories are developed for each of these orientations. The model based on experimental observations is focused on explaining the micro-scale failure mechanisms occurring in the machining process. The finite element machining model developed in this work uses a unique modeling approach, which is capable of explaining the fiber failure mechanisms occurring throughout the chip formation process. After development of the two machining models, the machining responses are compared to a set of machining experiments for validation purposes.

Fibers orientated in the 45 and 90 degree orientations were found to fail in compressive crushing-dominated failure while fibers oriented in the 135 degree orientation were found to fail in bending below the surface of the cut. In the 0 degree orientation, the fibers were proposed to fail in buckling or bending-dominated failure, depending on the depth of cut, and tool geometry of the process. The micro-scale fiber failure mechanisms were observed to differ significantly from their macro-scale counterparts. The machining responses of the two models were found to agree well with the experimental validation analyses indicating that these models are an accurate representation of the chip formation process.

Acknowledgements

I would first like to thank my advisors, Professor Shiv Kapoor and Professor Richard DeVor for giving me this opportunity and their continual guidance throughout these last two years. Their high standards throughout this work have assisted greatly in developing many of my academic and professional skills. I would also like to specifically thank Professor Kapoor for his mentoring in my undergraduate studies and for sparking my interest in micro-scale manufacturing process technologies.

I would also like to thank Techsolve Inc., Cincinnati, OH and the Grayce Wicall Gauthier Chair in Mechanical Engineering for the funding of this research along with the Frederick Seitz Materials Research Laboratory Central Facilities, University of Illinois, which is partially supported by the U.S. Department of Energy under grants DE-FG02-07ER46453 and DE-FG02-07ER46471 for use of their facilities.

I would like to thank my colleagues here in the research group throughout my time here including Johnny, Ken, Keith, Isha, Kurt, Jimmy, Bingyi, and Alex. Their input, ideas, and recommendations assisted my work in a large part and for that I am grateful. I would like to specifically thank Johnny and Ken for their great friendship and for their leadership in the research group.

Lastly, I want to thank my parents, Manuel and Linda, and brothers, David and Daniel for their unending support over the last 22 years and even specifically over the last two. I am grateful to my mom for teaching me everything I needed to know up until my time here at the University of Illinois and my dad for giving me the inspiration to pursue a career in engineering. I would also like to thank Amy for her love and support and for being with me every step of the way during my graduate studies and for the rest of my life to come. Finally I want to thank God for the endless encouragement and lessons he’s taught me over my time here. These far outweigh the worldly knowledge and academic achievements I have gained and for that I am eternally grateful.

Table of Contents

List of Figures

List of Tables

1. Introduction

1.1.Background and Motivation

Composite materials have the potential to play an important role in the drive for product miniaturization. Their appeal comes from the unique material property enhancements that can be achieved by using appropriate combinations of the reinforcing phase (carbon fiber, alumina, etc.) and matrix phase (polymer, ceramic, metals, etc.). Carbon fiber-reinforced polymer composites (CFRPs) are often used in structural components for micro-scale devices such as microrobots including micromechanical flying insects, crawling robots and biomimetic fishbots [1] because of their ability to provide the combination of high stiffness with high aspect ratio geometries. These devices are currently manufactured using expensive laser-based cutting operations. Micro/meso-scale mechanical manufacturing technologies like micro-milling/drilling/turning have recently emerged as economically-feasible manufacturing processes for making micro-scale parts. However, though the micro-scale applications of CFRPs are many, their machining performance, in particular, the fiber failure mechanisms during machining at the micro-scale, is not clearly understood.

At the macro-scale, a wide range of experimental and theoretical failure theories have been proposed to explain the fundamental failure mechanisms occurring during the machining of aligned CFRPs. According to Koplev et al. [2], the tool does not shear the material as observed in conventional metal machining, but rather induces a compressive stress at the contact point with the fiber, which results in crushing of the fiber. Bhatnagar et al. [3] claims that the fibers experience tensile failure from the side of the fiber opposite the tool. According to Pwu et al. [5], the tool itself does not fracture the fiber but rather it induces a bending stress at a point below the surface resulting in fracture at that location as well as sub-surface damage.

In an aim to better understand the complex nature of the fiber failure mechanisms, several researchers have employed finite element machining models to aid in the interpretation of the experimental machining responses. Finite element machining models have been developed for a variety of CFRP microstructures, some having the ability to predict cutting forces, chip formation mechanisms, and material damage in the machining of a complex multi-phase, anisotropic material. Two methods of microstructure development in finite element machining studies have been implemented: a micro-mechanical approach and a macro-mechanical approach. The micro-mechanical approach describes the local material microstructure as two individual phases (carbon fiber and epoxy) each being assigned unique material properties. Using the micro-mechanical approach, the modeling of the fiber-matrix interface is accomplished with cohesive zone elements in order to accurately model material damage in the form of phase separation. The macro-mechanical approach replaces the two-phase carbon fiber/epoxy microstructure with a homogenous microstructure with equivalent anisotropic properties referred to as an equivalent homogenous material (EHM).

The EHM approach has serious limitations as it is not capable of describing factors such as chip formation mechanisms, material damage, and fiber-matrix interactions. The microstructure-based CFRP finite element machining models (FEMMs) that have been developed are all quasi-static machining models and thus, are only capable of predicting the failure mechanisms at the end of the displacement-based cutting operation. Thus, in predicting the fiber failure mechanisms, quasi-static models are only capable of predicting the location of failure in the first fiber encountered by the tool rather than describing the failure mechanisms in the formation of a full chip. Quasi-static models are further limited by the fact that, it is difficult to identify the locations of failure in an entire chip by simply examining the fiber stress-distribution in a single fiber.

All of the proposed failure theories and finite element machining models are geared towards explaining the fiber failure mechanisms in a macro-scale machining process and none of the models adequately explain the micro-scale failure mechanisms. Micro-scale failure mechanisms are likely to differ from their macro-scale counterparts for several reasons. The chip loads encountered in micro-machining are at times equal to or even lower than the critical diameter of the fibers (5-8 μm). This, coupled with the relatively high tool edge radius-to-chipload ratios encountered at the micro-scale, implies that the failure modes of individual fibers at various fiber-orientations with respect to the cutting direction become more critical in dictating the machining responses of aligned CFRPs at the micro-scale.

In summary, while studies have been done to understand the fiber failure mechanisms encountered in the machining of CFRP composites, there are several shortcomings. Of the experimental and modeling studies in literature, none are capable of explaining the exact nature of the orientation-based fiber failure mechanisms encountered in the full chip formation process. Furthermore, none of these studies shed light on the unique failure mechanisms that occur when machining CFRPs at the micro-scale. In this thesis, a study will be performed to gain a fundamental understanding of the specific nature of the micro-scale failure mechanisms using various modeling techniques.

1.2. Research Objectives Scopes and Tasks

1.2.1. Objectives and Scope

The overall objective of this research is to gain a better understanding of the orientation-based fiber failure mechanisms occurring in the micro-scale CFRP machining processes. Both a model based on experimental observations and a unique approach to a finite element machining model will be implemented to aid in the interpretation of the micro-scale fiber failure mechanisms.

The scope of this research will be focused on the effects of fiber orientation on the micro-scale failure mechanisms in both milling and orthogonal machining processes. Throughout this thesis, four fiber orientations will be considered: 0, 45, 90, and 135 degrees with respect to the direction of motion of the tool tip. These fiber orientations will be studied to cover the full range of fiber orientations encountered in a milling process as each has shown to yield different and distinct fiber failure mechanisms [1]. While many of the fiber failure mechanisms are comparable between different unidirectional fiber-reinforced polymers (FRPs), the focus of this study will be on carbon fiber-reinforced polymer (CFRP) composites with 5-8 μm diameter fibers and 60 percent fiber volume fraction.

1.2.2. Tasks

To accomplish the objectives of this thesis, the following tasks will be undertaken:

1. Micro-endmilling slotting experiments will be conducted on aligned CFRPs at fiber orientations of 0, 45, 90, and 135 degrees with respect to the direction of tool motion. Chip morphology, delamination along the edge of the slot, and machining forces are the specific machining responses investigated in the experimental study.

2. The results from the experimental study are used as the basis for the development of the experimentally-based model to explain the micro-scale fiber failure mechanisms.
3. The model is validated by comparing the proposed failure mechanisms with those inferred from the results of the experimental study. Chip morphology, delamination, and machining forces are the machining responses used for model validation purposes.
4. A unique finite element machining model capable of describing the specific nature of the fiber failure mechanisms throughout the orthogonal machining process will be developed. In order to facilitate the unique modeling approach, a new fiber-matrix interfacial model will be developed and implemented into the finite element machining model allowing the interfacial elements to fail in tension or compression. Similar to the experimental-based model, fiber orientations of 0, 45, 90, and 135 degrees will be investigated in this study.
5. For model validation purposes, the model-based machining performance predictions are compared to the machining responses from a set of orthogonal machining experiments.
6. The developed finite element machining model is employed to investigate the effects of tool geometry and fiber size on the fiber failure mechanisms and general machining performance of CFRP composites.

1.3. Outline of this Thesis

The remainder of this thesis is outlined as follows. Chapter 2 provides a comprehensive literature review on previous work done by other researchers relating to the machining of FRP composites. The first section discusses experimental studies which have been employed to determine the failure mechanisms encountered in the machining of FRP composites. The second section covers various modeling techniques which have been used to predict machining responses including fiber failure mechanisms, machining forces, and material damage. The third section outlines the gaps in the current state of knowledge.

Chapter 3 presents an experimental study used to predict the failure mechanisms encountered in the micro-scale machining of CFRP composites. The first section discusses the key differences between micro and macro-scale machining and how these are taken into consideration in the development of the experimental-based micro-milling model. The third section outlines the experimental design with the fourth section covering details as to the validation of the model based on experimental observations using the experimental results.

Chapter 4 explains the development of the finite element machining model. The first section introduces the need for the new modeling approach while the second section discusses the development of the finite element machining model. The third section is dedicated to presenting the modeling results specifically relating to the fiber failure mode, characteristic fiber length in the chips, and machining forces.

The first part of Chapter 5 is dedicated to the validation of the finite element machining model developed in Chapter 4 by comparing the model simulation results with the results from a set of orthogonal machining experiments. In the second part, the finite element machining model is employed in a parametric study used to determine the effects of tool geometry and fiber size on the fiber failure mechanisms in the machining of CFRPs, and to find a tool which improves machining performance.

Chapter 6 outlines the specific conclusions, which can be taken from this work and presents areas of possible future work.

2. Literature Review

The literature reported in this chapter contains investigations of the cutting process for fiber-reinforced polymers and highlights specific factors which affect their machining performance. The focus of this review will remain on studying the fiber failure mechanisms occurring in the machining process and how these are affected by process parameters such as tool geometry and fiber orientation. Section 2.1 outlines some mechanical properties of FRP composites and presents some issues occurring in the machining of these materials. Section 2.2 discusses various experimental studies in literature and covers topics including cutting mechanisms, cutting forces, and material damage and focuses on the unique orientation-based failure mechanisms encountered in the machining of FRPs. Section 2.3 covers experimental and theoretical modeling approaches used to predict machining forces while Section 2.4 outlines several finite element-based machining models. Section 2.5 discusses gaps in the current state of the literature.

2.1. Fiber Reinforced Composites

2.1.1. Fiber Reinforced Composite Constituents

Fiber-reinforced polymers consist of a combination of two separate phases within a single material microstructure, typically a fiber and matrix phase. The fibers in the microstructure typically carry the primary load and have a high strength and stiffness. The ductile matrix material provides several key functions including stabilizing the fibers in compression, distributing and transmitting loads between fibers, and providing off-axis properties [2]. Common fiber-reinforcement materials include carbon, glass, aramid, and boron fibers while the matrix typically consists of a thermoset or thermoplastic such as epoxy, polycarbonate, or polyester.

Table 2.1 shows typical mechanical properties of carbon and glass fibers. Fibers are typically produced by a pultrusion process, which results in the alignment of molecules in the fiber longitudinal direction. This molecular alignment leads to high strength and stiffness in the fiber longitudinal direction [1].

Table 2.1 . Properties of Typical Fiber-Reinforcement Materials [3]

Fiber Property	Carbon Fibers	Glass Fibers
Diameter (µm)	5-9	8-14
Density (kg/m3)	1950	2560
Longitudinal Modulus of Elasticity (GPa)	390	76
Transverse Modulus of Elasticity (GPa)	12	76
Tensile Strength (GPa)	2.2	1.4-2.5
Elongation at Fracture (%)	0.5	1.8-3.3

Table 2.2 shows typical mechanical properties of epoxy and polyester matrix materials [3]. The polymeric matrix phase typically used in FRPs consists of long polymer chains of high molecular weight organic compounds [1]. The high toughness of polymer matrix materials comes from the restructuring of these polymer chains occurring during material deformation allowing for high deformation before failure occurs.

Table 2.2 . Mechnical Properties of Typical Matrix Materials [3]

Matrix Property	Epoxy	Polyester
Density (kg/m3)	1100-1400	1200-1500
Modulus of Elasticity (GPa)	3-6	2-4.5
Tensile Strength (GPa)	0.035-0.10	0.04-0.09
Compressive Strength (GPa)	0.1-0.2	0.09-0.25
Elongation at Fracture (%)	1-6	2

In examining the mechanical properties it can be noted that the combination of the two properties are what give FRP composites their unique mechanical properties, namely, high specific strength and stiffness. Furthermore, the fact that the fibers in a typical FRP composite are long and unidirectional, the stiffness and strength of the composite in the fiber direction can be an order of magnitude higher than in the transverse direction. This anisotropic nature of FRP composites is one of the unique features, which must be accounted for in the design and manufacturing of FRP composites.

2.1.2. Issues Encountered in the Machining of Fiber Reinforced Composites

While FRP composite materials are generally fabricated net-shape, post-processing operations are often unavoidable [4]. Net-shape composite manufacturing technologies generally have very loose tolerances and as such, post-curing machining operations are often required to improve dimensional accuracy [1]. Post-processing is also required in joining technologies as attaching the composite component into a structure generally requires milling, drilling, and grinding operations for the implementation of mechanical fasteners. While the machining studies of traditional metal materials are many, studies on the machining behavior of fiber-reinforced composite (FRP) materials are comparatively few and more recent. Due to the anisotropic and highly abrasive nature of typical fiber reinforcements, several machining complications arise which must be accounted for when designing the machining process for a FRP composite, as these have been observed to affect the fiber failure mechanisms occurring in the machining process.

First, unlike most traditional metals, unidirectional FRP composites are highly anisotropic with non-homogenous microstructures. Just as the fiber direction dictates the strength and stiffness properties of the composite; it also affects the machining behavior of the composite. Specifically, chip formation mechanisms and cutting forces are dictated primarily by fiber orientation with respect to the direction of motion of the tool [5,6].

Second, due to the two-phase nature of most FRP composites, several new failure mechanisms and damage modes exist, which do not exist in the machining of homogenous metals. These include matrix cracking, transverse cracking, delamination, fiber pull-out, and fiber-matrix interfacial failure [1,7,8]. These failure modes caused by fiber-matrix interactions dictate the chip formation mechanisms occurring in the different fiber orientations. Furthermore, these failure modes lead to machining-induced damage as material cracks tend to propagate along the fiber axial direction rather than along a shear plane as observed in the machining of ductile homogenous materials [9]. The extent of damage typically observed in the machining of FRP composites is a major material manufacturing limitation.

Third, the highly abrasive nature of the fiber reinforcement phase leads to stringent cutting tool requirements to account for high levels of tool wear typically encountered in the machining process [6,10,11]. In many cases tools with high positive rake angles and a small edge radius are required to minimize the abrasive damage on the cutting tool [1]. Furthermore, a tool material with high stiffness and hardness and low coefficient of friction is often implemented to combat the rapid tool wear as high speed steel and cemented carbide have been observed to be unsuitable tool materials for the machining of FRPs [1,10,12]. For these reasons, new tool geometries and tool materials have been studied, which are better suited to the machining of FRP composites.

2.2.Experimental Machining Studies

2.2.1. Orientation-Based Cutting Mechanisms

Because of the anisotropic nature of fiber-reinforced composites, distinctly different cutting mechanisms have been observed depending on the fiber orientation with respect to the direction of tool motion [13,14]. Figure 2.1 shows the definition of fiber orientation with respect to the direction of tool motion used throughout this review. Generally, the four fiber orientations investigated by researchers are 0, 45, 90, and 135 degrees as each of these fiber orientations has been shown to yield differing fiber failure mechanisms.

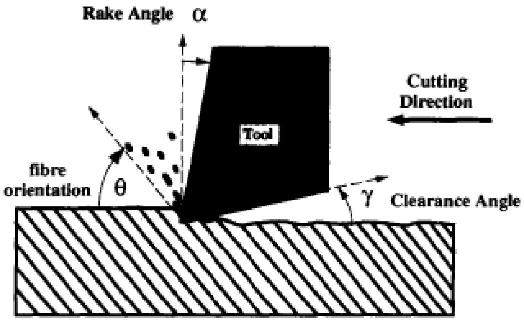

Figure 2.1. Fiber Orientation Definition [15]

0 Degree Fiber Orientation. Figure 2.2 shows the fiber failure mechanisms, which have been observed to occur in the 0 degree orientation when machining with a positive tool rake angle. As the tool enters the workpiece, it applies pressure in the axial direction of the fibers causing the fibers to split or peel along the fiber-matrix interface [16,17,15,18]. This causes a crack to appear ahead of the cutting tool, which propagates along the fiber axial direction. As the tool progresses into the workpiece, the peeled layers move up the rake face of the tool as stresses in the fibers due to bending develop [5]. After sufficient bending stresses develop in the fibers, they fail ahead of the tool under cantilever loading [15,19].

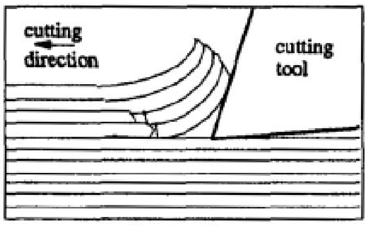

Figure 2.2. 0 Degree Failure Mechanisms with Positive Rake Angle [20]

Figure 2.3 shows the failure mechanisms that occur when machining in the 0 degree fiber orientation with a negative tool rake angle [20]. As the tool progresses into the workpiece, the fibers are subjected to compressive loading along the axial direction. This compressive loading then leads to fiber-matrix interfacial failure in the form of interfacial cracks ahead of the cutting tool similar to the positive rake angle case [5]. Because the chip fragments are not allowed to leave the cutting area due to the negative rake angle, the compressive stresses continue to develop until failure due to buckling occurs ahead of the cutting tool [15,18,1,13]. While buckling failure mode is observed in this configuration, bending stresses develop in the fibers similar to the positive rake angle case [1].

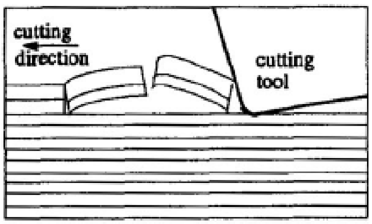

Figure 2.3. 0 Degree Failure Mechanisms with Negative Rake Angle [20]

45 Degree Fiber Orientation. When machining in the 45 degree fiber orientation, the tool edge radius plays a more important role in the failure mechanisms than the tool rake angle. A combination of two distinct cutting mechanisms are observed when machining in the 45 degree orientation depending on the tool edge radius. For a tool with an edge radius comparable to or smaller than the fiber diameter, as the tool progresses into the workpiece, each fiber is observed to fail at the point of contact of the tool due to compressive crushing-dominated failure as seen in Fig. 2.4 for tools with positive and negative rake angles [16,15]. Some researchers claim that a shear-dominated fiber failure occurs, but in both cases, failure occurs at the point of contact of the cutting tool as the small tool edge radius can provide a concentrated stress on each individual fiber causing failure [17,1]. After an individual fiber is crushed by the cutting tool, the fiber-matrix interface undergoes shear failure allowing the chip flow to occur along the fiber axis as the crushed fibers are removed from the cutting zone [21,1].

The second cutting mechanism occurs when machining with a tool with an edge radius significantly larger than the fiber diameter. In this configuration, a crushing failure is not expected as the large tool edge radius does not provide as concentrated a stress on the individual fibers. Compressive stresses build up at the point of contact of the tool, but do not exceed the fiber strength required to cause fiber crushing. Instead, sub-surface interfacial failure occurs below the trim plane allowing a bundle of fibers to separate from the workpiece and eventually fail due to bending-dominated failure at a location below the machined surface [22].

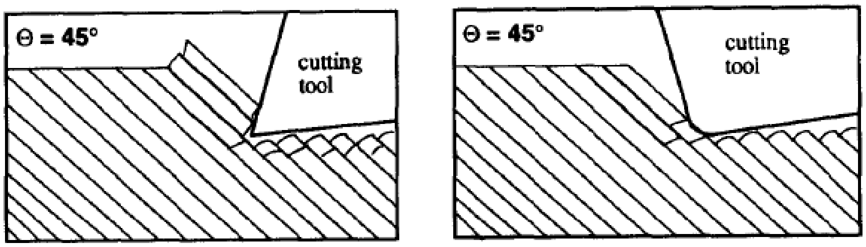

Figure 2.4. Cutting Mechanisms for 45 Degree Fiber Orientation [15]

90 Degree Fiber Orientation. Cutting mechanisms similar to the 45 degree orientation are observed for the 90 degree orientation. When machining with a tool with a small edge radius, crushing-dominated failure takes place at the point of contact of the tool as seen in Fig. 2.5 [16]. The fractured chips then flow from the cutting area vertically along the direction of the fiber axis [15]. This observed failure mode is independent of the tool rake angle [1]. When machining with a large edge radius tool, bending stresses develop below the cutting plane similar to the 45 degree orientation, resulting in sub-surface bending-dominated failure as seen in Fig. 2.6 [22].

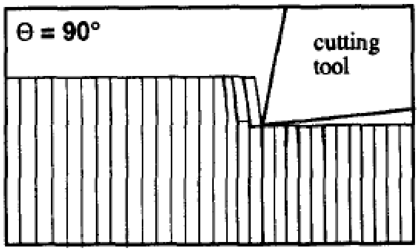

Figure 2.5. Cutting Mechanism for 90 Degree Fiber Orientation with Small Edge Radius [15]

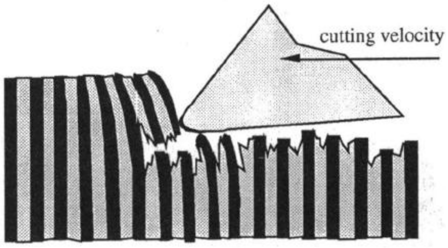

Figure 2.6. Cutting Mechanism for 90 Degree Fiber Orientation with Large Edge Radius [22]

135 Degree Fiber Orientation. Failure in the 135 degree orientation is dominated by bending as seen in Fig. 2.7. As the tool progresses into the workpiece, the tool first contacts the fiber from the rake face rather than the cutting tip due to the fiber angle-rake angle relationship. The tool then continues to move and bend a bundle of fibers. As the fibers bend, interfacial failure is observed below the cutting plane as sections of fibers are peeled from the remaining workpiece and sub-surface bending stresses develop in the fibers [21,23]. When the bending stress reaches the failure stress of the fibers, failure occurs below the trim plane [24,25]. This chip formation event is oftentimes referred to as macro-fracture as the chip produced is large with fibers longer than the DOC of the process as failure takes place away from the cutting tool [15,18,1].

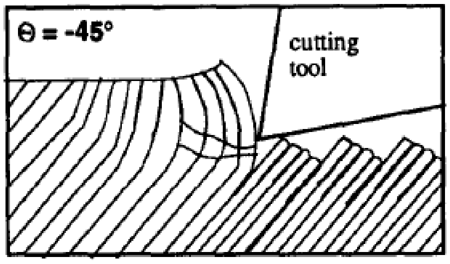

Figure 2.7. Cutting Mechanism for 135 Degree Fiber Orientation

2.2.2. Machining Forces

Machining forces for FRPs are most significantly dictated by fiber orientation rather than process conditions [17,26]. The cutting forces observed in the machining of FRPs are directly related to chip formation mechanisms. Figure 2.8 shows a series of principle (cutting) and thrust force profiles for each fiber orientation under consideration in an orthogonal machining process conducted by wang et al. [15]. This experiment was conducted with a PCD tool with 10 degree rake angle and 17 degree clearance angle. The force signatures were obtained using a 250 µm depth of cut (DOC) and 4 m/min cutting speed. The cutting and thrust force signals are seen to have high variability with the force magnitudes depending primarily on fiber orientation agreeing well with studies by other researchers [27,28]. The force variability arises due to the anisotropic nature of the material, and repeating chip formation events yielding sporadic machining force signals. The force variability is most prevalent when machining in the 135 degree orientation as the sub-surface bending-dominated failure causes the formation of macro-chips at repeating intervals [16,15,21].

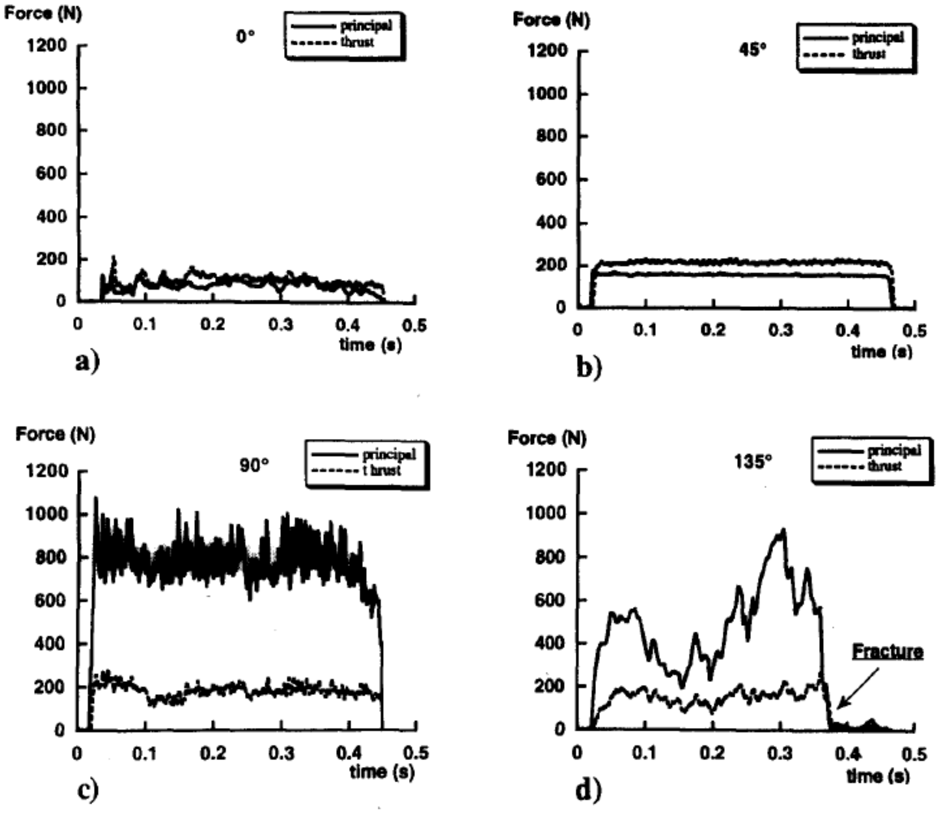

Figure 2.8. Representative Cutting and Thrust Force Profiles for a Series of Fiber Orientations [28]

Figure 2.9 shows the cutting and thrust force trends as a function of fiber orientation for various tungsten carbide tools with clearance angle of 7 degrees and rake angle varying from -20 to 40 degrees [24]. Generally the lowest cutting and thrust forces exist in the 0 degree orientation while the maximum force magnitude occurs between the 45 and 90 degree orientations, agreeing well with the experimental results from other researchers [29,15,9]. A lower force is observed when machining in fiber orientations greater than 90 degrees [1]. The lowest cutting force exists in the 0 and 135 degree orientations, indicating that bending-dominated failure requires a lower machining force as compared to crushing-dominated failure. The 45 and 90 degree fiber orientations show similar cutting force magnitudes as the cutting mechanism in these fiber orientations is crushing-dominated [15]. While the rake angle is seen to play a role in the overall force magnitude, it does little to affect the overall cutting and thrust force trends with respect to fiber orientation.

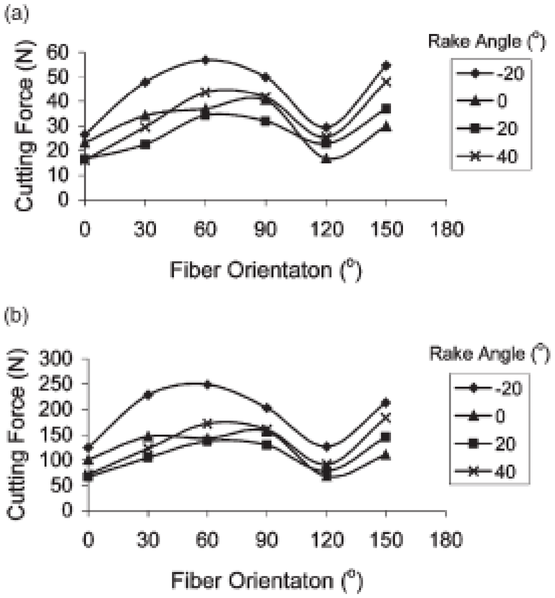

Figure 2.9. Cutting Force Trends as a Function of Fiber Orientation (a. Cutting Force, b. Thrust Force) [24]

2.2.3. Machining Induced Damage and Surface Integrity

One of the major limitations in the machining of FRPs is the sub-surface damage and poor surface quality which is inherent to the machining of fiber-reinforced materials [9,30]. The anisotropic nature of the material allows for failure to take place at locations other than at the tool tip, which causes workpiece damage in the form of fiber-matrix interfacial failure, and sub-surface machining induced fiber failure [31,5,22,27]. These damage modes inherent to the machining process impose a limit on the maximum allowable machining tolerance and the structural integrity of the machined workpiece [9].

The degree of sub-surface damage in the workpiece is primarily affected by fiber orientation over process parameters [24,18,32]. Specifically, the fiber failure mode and location of fiber failure dictates the extent of sub-surface damage. In the 0 degree orientation, the fibers fail in bending- or buckling-dominated failure and occurring ahead of the cutting tool but still along the trim plane as shown in Figs. 2.2-2.3 [26]. Some damage typically exists along the surface of the cut but this damage only extends one or two fiber diameters into the surface of the workpiece [16]. For this reason, negligible sub-surface damage is observed when machining in the 0 degree orientation [29,17].

In the 45 and 90 degree fiber orientations, failure occurs due to crushing at the point of contact of the tool for sharp tools, or bending below the machined surface for tools with a large edge radius. This sub-surface bending failure resulting from machining with large edge radius tools results in an increase in the depth of damage as fibers are removed below the surface of the cut leaving cavities in the material surface [5,22,8,33]. In addition to sub-surface fiber fracture in the 45 and 90 degree orientations, sub-surface interfacial failure and micro-cracks are also typically observed in the orthogonal machining FRPs in 45 and 90 degree fiber orientations [16]. Figure 2.10 shows two types of sub-surface damage occurring below the surface of the cut in an orthogonal machining experiment in the 90 degree orientation conducted by Dandekar et al. [34].

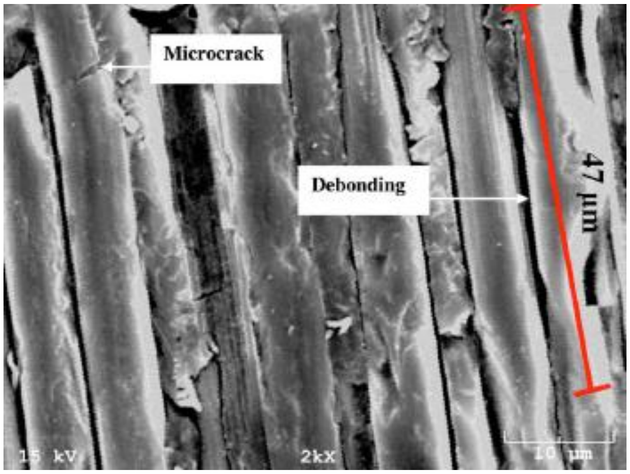

Figure 2.10. Sub-Surface Damage Modes Observed when Machining in the 45 and 90 Degree Fiber Orientaentations [34]

The 135 degree orientation results in the highest depth of damage as the failure is bending-dominated and occurs below the machined surface regardless of other processing conditions as seen in Fig. 2.11 [24]. The cavities and bent fibers caused by residual bending stresses are two forms of damage shown in Fig. 2.11 occurring when machining FRPs with fiber orientations greater than 90 degrees.

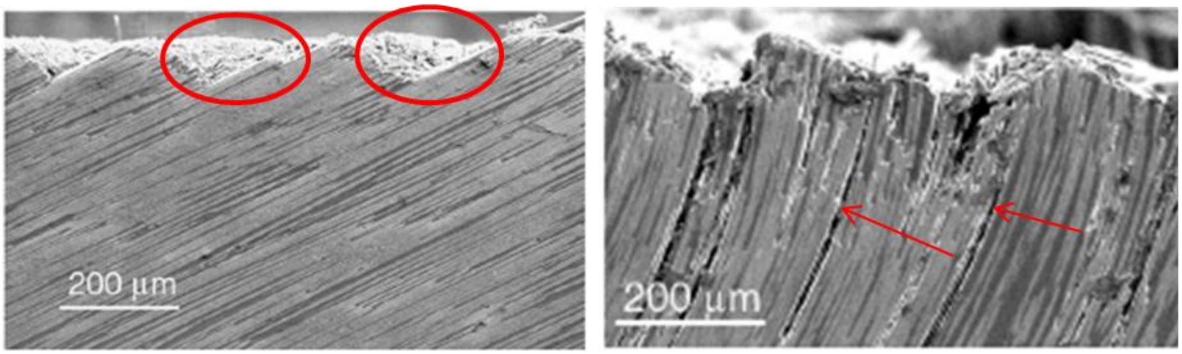

Figure 2.11. Examples of Sub-Surface Damage in the 135 Degree Orientation [24]

2.3. Theoretical and Experimental Modeling

In developing a theoretical or experimental model to capture the cutting process occurring in the machining of FRPs, several considerations must be taken into account. First, it is not accurate to directly apply the merchant shear plane theory from metal cutting as FRPs do not plastically deform along a shear plane as is typical in the machining of metals [35,36]. Instead, the material has been observed to separate along the fiber-matrix interface and cracks tend to grow along the fiber axial direction [15,21]. Thus, in the modeling of the FRP cutting process, the shear angle must always be related to the fiber angle. Second, the shearing behavior along the fiber axis only occurs in fiber orientations between 15 and 90 degrees and thus, new models must be developed outside of this fiber orientation range [35]. Taking these new considerations into account, several researchers have developed theoretical and experimental-based models capable of predicting the machining behavior of FRPs as outlined below.

2.3.1. Continuum Mechanics Approach

<u>Everstine Model.</u> The first modeling work on the machining of FRPs was reported by Everstine et al. [37]. This model is capable of predicting the machining forces when machining in the 0 degree orientation using a continuum mechanics approach [37]. The workpiece in the model is composed of parallel strong fibers embedded in a weaker matrix. The fibers are initially aligned parallel to the direction of motion of the cutting tool. After deformation takes place, it is hypothesized that a 'wrinkle' is formed where the fibers deform in bending while the spacing between the individual fibers remains unchanged. This 'wrinkle' is similar to the cantilever bending observed ahead of the tool tip when machining in the 0 degree orientation [5].

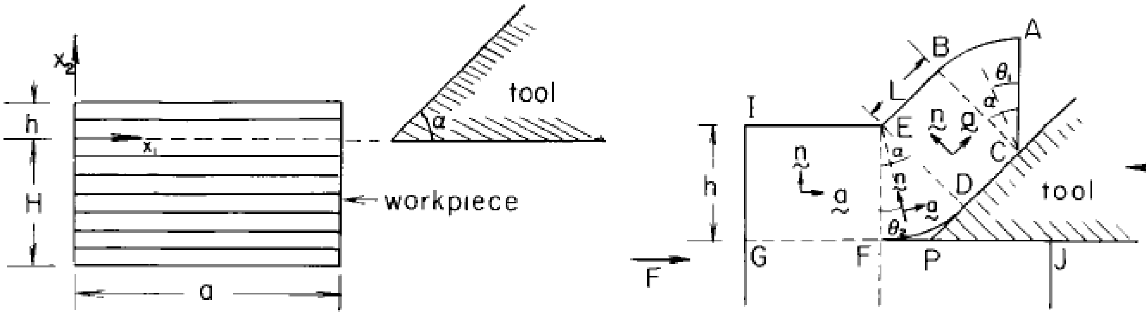

Figure 2.12. Initial configuration and deformation of the chip proposed in Everstine Model [37]

Using a continuum mechanics approach, an expression for the cutting force is derived based on the process parameters and material properties according to:

$$F_C = \varepsilon \pi h T_U (\tan(\pi/2-\alpha)+\tan\delta) \tag{2.1}$$

where h is the depth of cut, T_u is the ultimate tensile strength transverse to the fiber, α is the tool rake angle, δ is a parameter referred to as the angle of downward deflection, and ε is a dimensionless material property parameter given by:

$$\varepsilon^2 = \frac{2(1-\nu)G}{E} \tag{2.2}$$

where ν is the Poisson Ratio, G is the shear modulus, and E is the elastic modulus of the material in the transverse direction.

This model is limited as it lacks experimental validation and only predicts principle cutting forces in the 0 degree fiber orientation. Furthermore, the authors acknowledged that other deformation modes not accounted for by this model are likely to occur.

2.3.2. Cutting Energy Approach

Takeyama Model. The model proposed by Takeyama et al. was the first model to propose machining responses as a function of fiber angle (θ). The model is proposed where cutting force is predicted using a modified version of the minimum cutting energy theory used for the machining of isotropic metals [36]. The shear angle is proposed to vary as a function of fiber orientation and thus, a second parameter is defined referred to as the fiber shear angle (Φ), which is obtained experimentally from a machining chip morphology analysis. Using this new parameter, the model can be implemented for any fiber orientation between 0 and 90 degrees.

Based on the shear angle assumption and the minimum cutting energy principle, the cutting force (F_c) and thrust force (F_t) are defined, respectively, viz.,

$$F_C = \frac{bt\tau(\theta')\cos(\beta-\gamma)}{\cos(\phi+\beta-\gamma)\sin(\phi)} \tag{2.3}$$

$$F_t = \frac{bt\tau(\theta')\sin(\beta-\gamma)}{\cos(\phi+\beta-\gamma)\sin(\phi)}\,, \tag{2.4}$$

where b is the width of cut, t is the depth of cut, θ` is the fiber shear angle, τ(θ’) is the shear strength of the material as a function of fiber shear angle, β is the friction angle, and γ is the tool rake angle as illustrated in Fig 2.13.

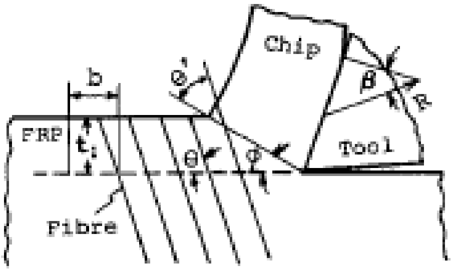

Figure 2.13. Orthogonal machining model proposed by Takeyama et al. [25]

To validate the model, the force predictions calculated according to Eqs 2.3-2.4 were compared with the forces obtained experimentally from an orthogonal machining experiment. Figure 2.14 shows a comparison of the experimental and predicted cutting and thrust forces. The cutting and thrust force values from the model were found to correspond accurately to those obtained from the experimental study.

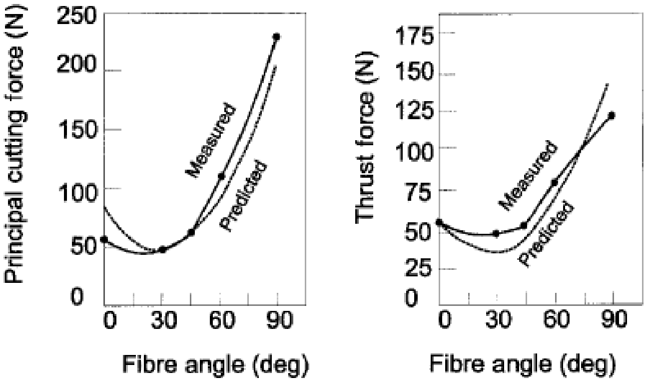

Figure 2.14. Experimental and Predicted Machining Forces in Takeyama Model [25]

While this model does consider the effect of fiber orientation on the machining process and provide experimental validation, it does not discuss the specific failure mechanisms taking place at these orientations. Furthermore, this model has been criticized for several reasons including the method used by the authors to determine the shear plane angle as this is nearly impossible to measure from a chip morphology analysis [27]. In addition to this, no details were given as to the determination of the shear strength of the material under consideration or for the experimental validation study [21].

Bhatnagar Model. The Bhatnagar model aims to overcome some of the shortcomings of the Takeyama model by accurately documenting the experiment used to obtain the material shear strength values along with the model validation experiment. In the Bhatnagar model, the Iosipescu shear test is well-documented and used to characterize the shear strength of the FRP material for each fiber orientation under consideration [38]. The Bhatnagar Model provides a further improvement on the Takeyama Model in that it is developed based on the chip formation mechanisms observed from an orthogonal machining experiment.

The first portion of this study is dedicated to an experimental investigation of the fiber failure mechanisms for fiber orientations between 0 and 135 degrees, which serves as a basis for force prediction modeling. For fiber orientations of 45 and 90 degrees, two events are proposed to take place in the chip formation process. The fibers are first proposed to break in tension followed by shearing of the matrix along the fiber angle. For 135 degree fiber orientations, deep cracks are observed to propagate into the workpiece as the fibers delaminate from the surrounding matrix and fail below the material trim plane.

While chip formation mechanisms are proposed for fiber orientations between 0 and 135 degrees, the cutting forces are only predicted for fiber orientations between 0 and 90 degrees. Similar to the Takeyama Model, fiber cutting forces are predicted by resolving the forces parallel and perpendicular to the fiber orientation as shown in Figure 2.15 for the 45 degree fiber orientation. In the experimental study, the chip was observed to shear along the fiber angle, and thus, it was assumed that the shear angle used in the Takeyama model could be more accurately described directly by the fiber angle. Thus, the cutting and thrust forces are described according to:

$$F_C = \frac{\tau a \cos(\beta - \alpha)}{\cos(\theta + \beta - \alpha)\sin(\theta)} \tag{2.5}$$

$$F_t = \frac{\tau a \sin(\beta - \alpha)}{\cos(\theta + \beta - \alpha)\sin(\theta)} \tag{2.6}$$

where a is the area of the shear plane, θ is the fiber angle, α is the rake angle, β is the friction angle, and τ is the shear strength of the material for a given fiber orientation determined using the Iosipescu Shear Test.

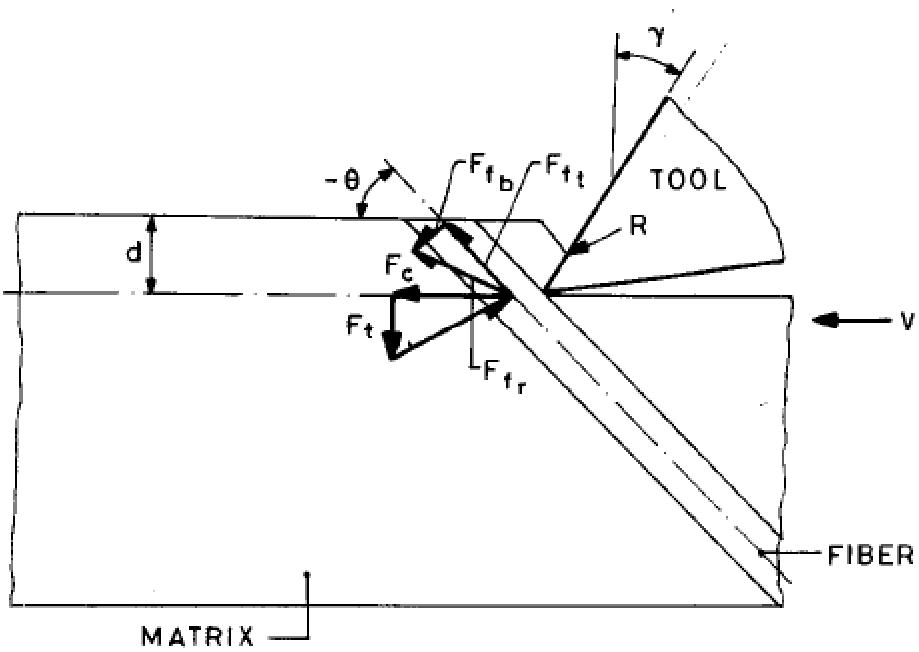

Figure 2.15. Cutting Force Model for 45 Degree Fiber Orientations [21]

While the failure mechanisms proposed in the Bhatnagar Model are based on experimental findings, the force prediction capabilities of the model are not validated experimentally. Furthermore, the model developed by Bhatnagar et al. can predict machining forces for fiber orientations between 0 and 90 degrees; however, the model is incapable of predicting forces for the 135 degree orientation. The authors claim that a force prediction model for the 135 degree fiber orientation would require considerable theoretical modeling work to develop a feasible model to describe the shear plane angle in fiber orientations greater than 90 degrees as the chip formation mechanisms become more complex, and thus, is beyond the scope of this study.

Zhang Model. In the model proposed by Zhang et al., two separate machining models are proposed, the first for fiber orientations between 15 and 90 degrees and the second for fiber orientations greater than 90 degrees. A theory describing the chip formation mechanisms is presented for each of the two cases under consideration.

The cutting zone while machining FRPs in fiber orientations between 15 and 90 degrees is divided into three regions to capture the various deformation mechanisms that occur in the machining process [39]. Figure 2.16a illustrates these three regions. Region 1 in front of the rake face is called the chipping region. In this region fracture occurs at the fiber cross sections and along the fiber-matrix interfaces. This results in the formation of an overall failure plane similar to the shear plane seen in metal machining. The second distinct deformation region takes place under the nose of the cutting tool, where the nose pushes down the workpiece material and is referred to as the pressing region (Region 2). The deformation in Region 2 can be viewed as deformation under a cylindrical indenter. Region 3 is called the bouncing region, where the contact force between the clearance face and the workpiece is caused by the elastic recovery of the workpiece material.

The second distinct failure model is presented for fiber orientation angles greater than 90 degrees with respect to the direction of motion of the tool tip. In this case, the deformation mechanisms become more complex. As seen in Fig 2.16b, the tool first causes fiber-matrix debonding and fiber buckling close to the tool-tip. Only after sufficient deformation has taken place, will the fibers fail in bending along a plane similar to the shear plane as observed in machining of metals.

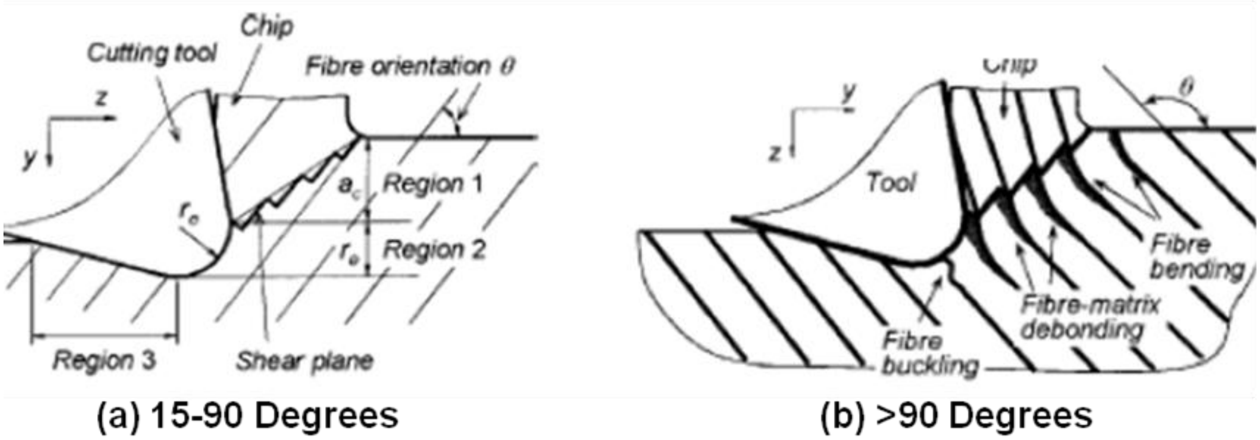

Figure 2.16. Zhang Model for 45 and 135 Degree Fiber Orientations [39]

In addition to predicting the chip formation mechanisms for various fiber orientations, this model is also capable of predicting the machining forces for fiber orientations between 15 and 90 degrees. The cutting and thrust forces are determined for each of the three regions in Fig. 2.16a and the sum of the forces in the three regions is used as the predicted cutting and thrust force response.

Figure 2.17 shows a comparison of the experimental and predicted cutting (F_y) and thrust (F_z) forces for fiber orientations between 0 and 90 degrees and depths of cut (a_c) between 0.05 and 0.15 mm. A comparison of the predicted and experimental force responses show that the model can accurately predict the machining forces. The author then concludes that the accurate force prediction indicates that the model is an accurate representation of the chip formation mechanisms occurring when machining in fiber orientations between 15 and 90 degrees.

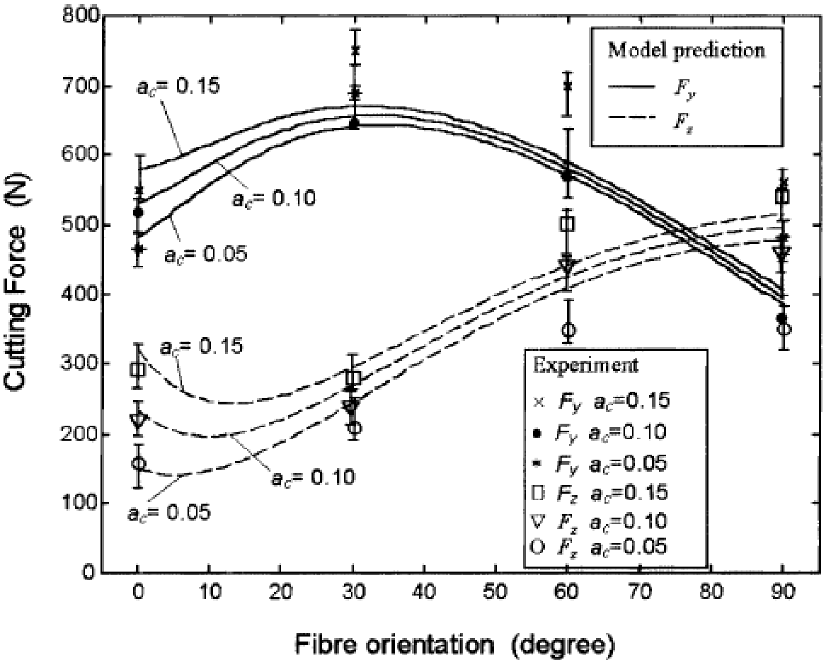

Figure 2.17. Comparison Between Predicted and Experimental Machining Forces [39]

While the force prediction model presented by Zhang et al. is shown to accurately predict machining forces for fiber orientations between 15 and 90 degrees, it does little to model the force response when cutting with fiber orientations greater than 90 degrees and thus, still has many of the same limitations as the other theoretical or experimental force prediction models.

2.4. Finite Element Modeling

While some of the theoretical and experimental models developed in Section 2.3.1 are helpful in predicting chip formation mechanisms and machining forces, they have several limitations. The most significant limitation of these models is the fact that they are not capable of directly illustrating fiber failure mechanisms or machining forces for fiber orientations greater than 90 degrees. Furthermore, the models are not capable of explaining the precise nature of the fiber failure mechanisms encountered in the machining process, as these cannot be observed directly.

More recently, finite element machining simulations have emerged as a standard in FRP machining studies with the aim to improve on many of the experimental and theoretical deficiencies. Finite element models are capable of predicting cutting forces, chip formation mechanisms, and material damage in the machining of a complex multi-phase, anisotropic material for any programmed input parameter [34]. A finite element machining model can be used to understand the physics of the material removal process and identify the microstructural parameters that give a desired combination of properties and machining performance without the need for exhaustive experimentation [40]. Furthermore, a single finite element machining model is capable of predicting machining responses for the full range of fiber orientations.

Orthogonal finite element machining models have been developed for a variety of FRP microstructures using two approaches: a microstructure-based approach (micro-mechanical) and an equivalent homogenous material (EHM) approach (macro-mechanical). The microstructure-based approach describes the local material microstructure as two individual phases (fiber and epoxy) each with unique material properties. In the microstructure-based modeling approach, interfacial elements are typically implemented at the fiber-matrix interface in order to accurately model damage in the form of phase separation. This approach is capable of accurately predicting cutting forces along with damage in the form of fiber-matrix interfacial failure [41,42,43,34]. The EHM approach replaces the two-phase carbon fiber/epoxy microstructure with a homogenous microstructure with equivalent anisotropic properties. The EHM approach is typically used to predict cutting forces rather than sub-surface material damage or chip formation mechanisms [44,45,46,47].

2.4.1. Macro-Mechanical Finite Element Machining Models

The macro-mechanical models developed by researchers are primarily focused on predicting the machining force response in the material. While several of these models have been able to predict machining forces accurately, they are incapable of directly describing the fiber failure mechanisms occurring in the machining process as the fiber-matrix interactions cannot be modeled using the EHM approach.

Arola Model. The first FRP finite element machining model was developed by Arola et al. [47]. The goal of this study was to accurately predict the machining forces for fiber orientations between 0 and 180 degrees and compare the predicted force response to that from a previous experimental study for model validation purposes [18].

The EHM microstructure in this simulation is modeled as elastic and anisotropic. The elastic constants of this material are calculated according to a micromechanics approach with the combined properties of the two constituent materials [48]. The stiffness in the fiber direction (E_1) and the stiffness transverse to the fiber direction (E_2) are calculated according to:

$$E_1 = V_f E_f + V_m E_m \tag{2.7}$$

$$\frac{1}{E_2} = \frac{V_f}{E_f} + \frac{V_m}{E_m} \quad , \tag{2.8}$$

where V_f and V_m are the fiber and matrix volume fractions, respectively, and E_f and E_m are the respective stiffness of each phase. The anisotropic material direction specified for the EHM is the same as the fiber orientation that the model is simulating.

To model the material failure, two separate damage models are studied individually. The first is the maximum stress theory where failure occurs when

$$\left|\sigma_{ij}\right| \geq \left|\sigma_{ij(crit)}\right|, \tag{2.9}$$

where σ_{ij} is the current state of stress at any time in the simulation and $\sigma_{ij(crit)}$ is the strength of the composite in either material direction [48]. The second failure theory used in this simulation was the Tsai-Hill failure criterion where failure is said to occur when

$$\left(\frac{\sigma_{11}}{X}\right)^2 - \frac{\sigma_1\sigma_2}{X^2} + \left(\frac{\sigma_{22}}{Y}\right)^2 + \left(\frac{\sigma_{12}}{S}\right)^2 \geq 1 \text{ ,} \tag{2.10}$$

where σ_1, σ_2, σ_{11}, σ_{22}, and σ_{12} are the various stress components in the anisotropic stress tensor and X, Y, and S are the longitudinal, transverse, and shear strengths of the material, respectively [48]. Separate simulations were run with each of these two failure theories in order to examine the effects of the failure model on the predicted machining forces.

Figure 2.18 shows a comparison of the experimental machining forces and the simulated machining forces for each of the two failure theories under investigation. The simulated cutting forces are seen to agree well with their experimental counterparts for both failure theories. The Tsai-Hill theory is seen to be slightly more accurate. The thrust forces, however, are seen to be significantly underpredicted.

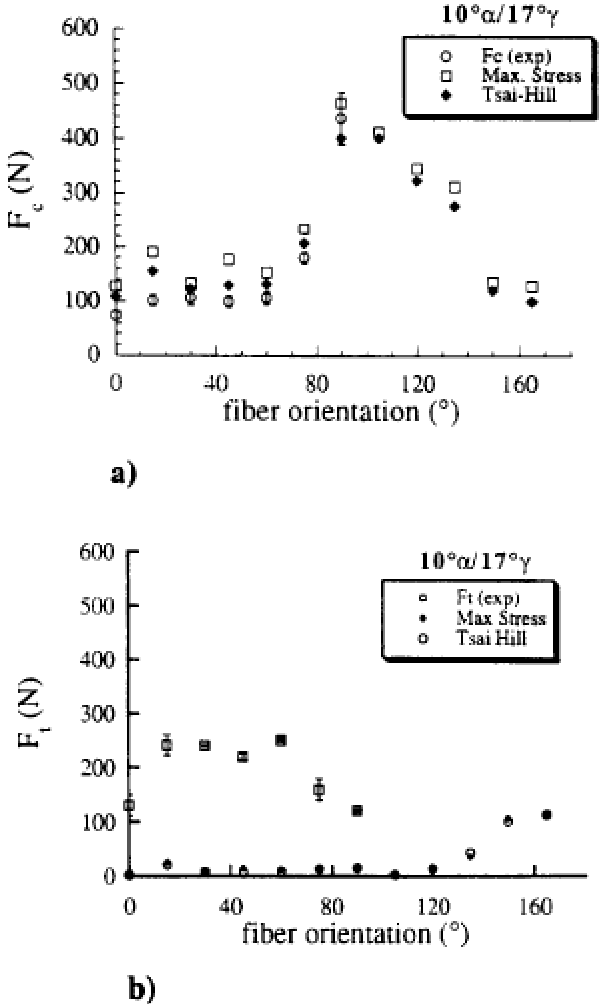

Figure 2.18. Comparison of Predicted and Experimental Force Responses from Arola Model [47]

Mahdi Model. The finite element modeling study by Mahdi et al. is focused on improving the model developed by Arola et al. by examining the effects of mesh density, and element type on the model cutting force prediction.

The material model implemented by Mahdi et al. for the machining simulation is identical to that modeled by Arola et al. according to Eqs. 2.7-2.8. The Tsai-Hill failure criterion was implemented according to Eq. 2.10 because the Arola Model showed a slight improvement in prediction accuracy with the Tsai-Hill failure criterion over the maximum stress failure criterion. Using these material and failure models, separate simulations were run using plane stress and plane strain elements with varying mesh densities.

Figure 2.19 shows the effects of mesh density and element type on the predicted cutting force. It is observed that for the plane stress case, the finer mesh reduces the variation of cutting force with respect to fiber orientation, while in the plane strain case the mesh dependence is negligible.

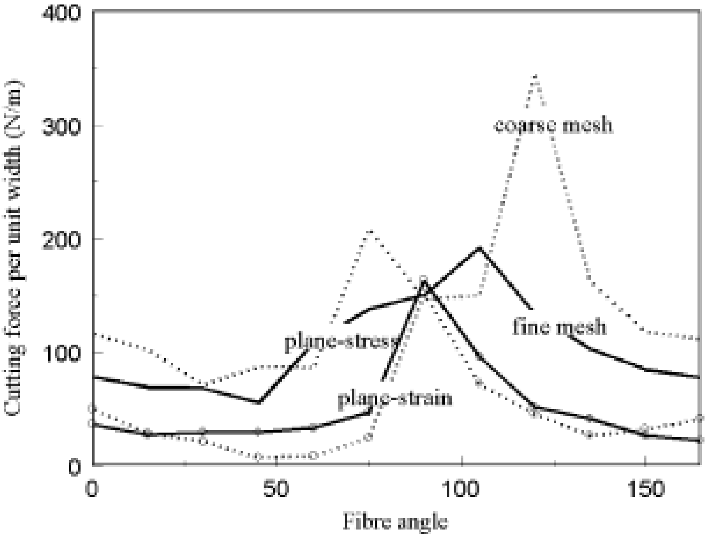

Figure 2.19. Effect of Element Type and Mesh Density on Orientation-Based Machining Forces [44]

While the finite element machining study by Mahdi et al. shows a way to improve the stability of the machining forces, it does little to improve on the major shortcomings of the Arola Model. Namely, the underprediction of thrust force is not addressed.

Ramesh Model. The model developed by Ramesh et al. uses a new material and failure model [45]. Using this failure model, machining forces can be predicted for any fiber reinforced composite material where as the Arola Model is limited to predicting machining forces for graphite-epoxy composites.

Instead of modeling the EHM workpiece material as linear elastic, it is modeled as elasto-plastic. The elastic region is modeled using the anisotropic elasticity matrix identical to that implemented by Arola et al. [47]. The plastic region is modeled using Hill's anisotropic plasticity model where the effective stress ($\bar{\sigma}$) is described as a function of the six three-dimensional stress components (σ_1-σ_6) and anisotropic yield strength parameters [49]. Similarly, the material is said to fail when:

$$\bar{\sigma}_u = \left[\frac{1}{2} \left[\alpha_{12}(\sigma_x - \sigma_y)^2 + \alpha_{23}(\sigma_y - \sigma_z)^2 + \alpha_{31}(\sigma_z - \sigma_x)^2 \right] + 3\alpha_{44}\tau_{xy}^2 \right]^{\frac{1}{2}} \tag{2.11}$$

where $\bar{\sigma}_u$ is the ultimate effective stress in any given element, σ_x, σ_y, and σ_z are the directional normal stresses, τ_{xy} is the shear stress, and α_{12}, α_{23}, α_{31}, and α_{44} are the normalized anisotropic failure strengths. Thus, failure occurs as a combination of individual stress components similar to the Tsai-Hill model presented by Arola et al. while still allowing for plastic deformation before failure.

The key advantage of the Ramesh Model over the Arola Model is that it is capable of predicting the machining force response in any brittle or ductile fiber reinforced composite. In this study, four different materials were investigated, including a boron fiber composite, carbon fiber composite and two different glass fiber composites. It was determined that for all the materials, the cutting forces follow similar trends, namely, the highest cutting forces exist in the 45 and 90 degree fiber orientations with the cutting forces being significantly lower in the 0 and 135 degree orientations [24]. While the machining force trends with respect to fiber orientation predicted by this model agree well with other researchers, it lacks experimental validation.

Rao Model. The macro-mechanical finite element machining study presented by Rao et al. is focused on developing 3-dimensional cutting force prediction model also capable of yielding information regarding the chip formation mechanisms occurring in the machining process.

The Tsai-Hill failure criterion is used to model the material failure; however, it is suitably modified to accommodate a three-dimensional simulation [50]. Failure is said to occur when the following condition is met:

$$\left(\frac{\sigma_1}{X}\right)^2+\left(\frac{\sigma_2}{Y}\right)^2+\left(\frac{\sigma_3}{Z}\right)^2-\sigma_1\sigma_2\left[\frac{1}{X^2}+\frac{1}{Y^2}-\frac{1}{Z^2}\right]-\sigma_2\sigma_3\left[\frac{-1}{X^2}+\frac{1}{Y^2}+\frac{1}{Z^2}\right]-\sigma_1\sigma_3\left[\frac{1}{X^2}-\frac{1}{Y^2}+\frac{1}{Z^2}\right]+\left(\frac{\tau_{12}}{S_{xy}}\right)^2+\left(\frac{\tau_{23}}{S_{yz}}\right)^2+\left(\frac{\tau_{13}}{S_{xz}}\right)^2=1 \tag{2.12}$$

where σ_1, σ_2, and σ_3 are the induced normal stresses, τ_{12}, τ_{23}, and τ_{13} are the induced shear stresses, X, Y, and Z are the directional ultimate strengths, and S_{xy}, S_{yz}, and S_{xz} are the ultimate shear strengths. Instead of directly determining the machining forces from the forces acting on the tool as is typical in other finite element machining models, the cutting forces are obtained by resolving the contact pressure and frictional shear at the workpiece-tool interface.

To validate the developed finite element machining model, the simulated machining process results are compared to the results obtained from an experimental orthogonal machining study. Unlike the other macro-mechanical finite element machining models, this model is found to accurately predict both cutting and thrust forces for depths of cut (t) between 0.10 and 0.20 mm as shown in Fig. 2.20. The improvement in thrust force prediction likely arises from the method used to obtain the machining forces. This model is also capable of accurately predicting the overall chip size and appearance.

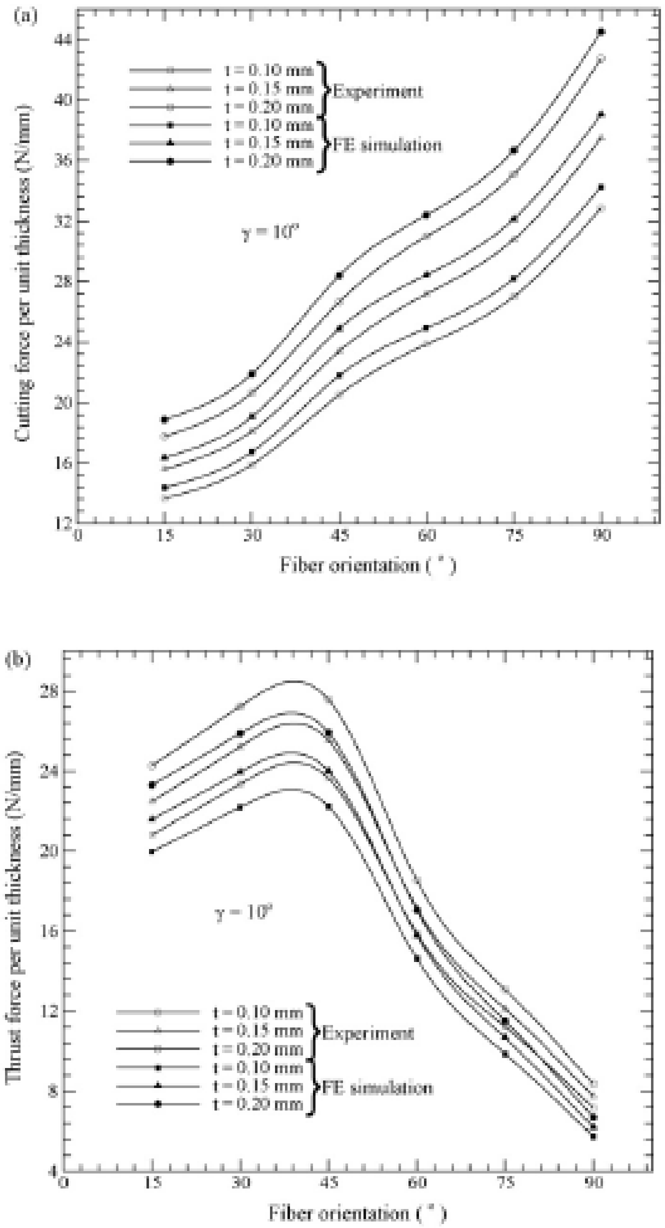

Figure 2.20. Cutting and Thrust Force Prediction for Rao Model [46]

2.4.2. Micro-Mechanical Finite Element Machining Models

While in a macro-mechanical finite element model a single material and failure model is required for the homogenous microstructure, in a micro-mechanical finite element model, separate material and failure models are required for the fiber, matrix, and interface phases.

Having the material constituents modeled as separate phases allows for the prediction of fiber failure mechanisms, and material damage in the form of phase separation, thus providing a significant advantage over the macro-mechanical finite element models.

Nayak Model. The model developed by Nayak et al. was the first micro-mechanical FRP machining model to emerge [42]. To model the fiber-matrix interfacial failure, cohesive zone elements were placed along the material interface to model material separation. Cohesive zone modeling (CZM) is a fracture mechanics approach to model dissimilar material separation [51,52]. Using the cohesive zone elements at the material interfaces, the model can determine the extent of damage below the machining surface in the form of phase separation.

The material interface is modeled using a stress-opening displacement potential function. This potential function allows for both the normal and tangential separation of the cohesive zones using a traction-separation law. The traction vector ($\bar{T}$) across the surface is given by:

$$\bar{T} = \frac{\delta\phi(\bar{\Delta})}{\delta\bar{\Delta}}, \qquad (2.13)$$

where Δ is the work of separation and $\phi(\Delta)$ is the potential function used for two-dimensional cohesive elements allowing for both normal and tangential material separation. The two dimensional potential function is defined according to:

$$\phi(\Delta) = \phi_n + \phi_n \exp\left(-\frac{\Delta_n}{\delta_n}\right)\left\{\left[1 - r + \frac{\Delta_n}{\delta_n}\right]\frac{1-q}{r-1} - \left[q + \left(\frac{r-q}{r-1}\right)\frac{\Delta_n}{\delta_n}\right]\exp\left(\frac{\Delta_t^2}{\delta_t^2}\right)\right\}, \qquad (2.14)$$

where δ is the critical separation, $q = {}^{\phi_t}\!/\!{}_{\phi_n}$, and $r = {}^{\Delta_n}\!/\!{}_{\delta_n}$. In Eq 2.14, the subscripts n and t indicate the normal and tangential components, respectively. When the normal or tangential critical separation is achieved in the cohesive elements, the interface is said to fail, and thus, tensile stresses can no longer be held between fiber and matrix phases.

The overall micro-mechanical microstructure is modeled as a single fiber embedded in the matrix material with the interface only modeled below the cutting plane to ensure that the cutting tool does not cause compressive stresses to develop in the cohesive zone elements. Figure 2.21 shows the overall microstructure used and indicates the location of the cohesive elements below the trim plane.

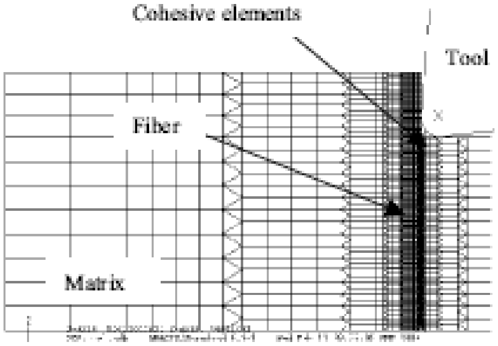

Figure 2.21. Finite Element Mesh and Microstructure used in Nayak Model [42]

It was determined that the CZM model can effectively simulate the interfacial behavior of the material. It was also determined that failure occurs in the fibers due to a combination of compression induced crushing and tensile bending at the point of contact of the tool. Sub-surface damage was found to be lowest with fiber orientations less than 45 degrees with the highest extent of surface damage existing in the 90 degree fiber orientation, agreeing well with the results of experimental studies by other researchers [53,22,8].

In a second study by Nayak et al., the results from an experimental study are compared to both a macro-mechanical model using the Tsai-Hill failure criterion (Eq. 2.10) and the micro-mechanical model developed using cohesive zone interfacial modeling [29,42]. It was determined that the cutting forces obtained from both the micro and macro-mechanical models agreed well with the experimental results while the thrust forces only agreed well with the experimental study for the micro-mechanical model. Furthermore, only the micro-mechanical model was capable of describing the extend of sub-surface damage in the workpiece using the separation of cohesive elements below the machining surface.

While the finite element micro-mechanical model developed by Nayak et al. is helpful in outlining a fiber-matrix interfacial model capable of predicting sub-surface damage in the form of interfacial failure, it does not discuss the material and failure models used for the fiber and matrix phases. Furthermore, the cohesive elements used in the simulations are not allowed to fail in compression, and as such, the model requires that the cohesive elements are strategically placed below the trim plane instead of throughout the entire microstructure. Thus, interfacial failure can only be studied in a single region. This study also does not address the more complex failure mechanisms that have been observed to occur in fiber orientations greater than 90 degrees.

Rao Model. The most comprehensive micro-mechanical finite element machining model in literature was developed by Rao et al. in a two part study for fiber orientations between 0 and 90 degrees [41,40]. The first study is aimed at machining force and damage prediction while the second study examines the chip formation mechanisms in detail. In the Rao model, the material interface is modeled using the cohesive zone model developed by Nayak et al. in Eqs. 2.13-2.14 [42]. Unlike the Nayak Model, however, the fiber and matrix material and failure models are outlined in detail.

The carbon fiber is assumed to be an elastic and anisotropic material and can be fully characterized by the anisotropic elasticity matrix of the material (E). The carbon fibers are assumed to fail when the stress in the fiber exceeds the anisotropic ultimate strengths of the material. The fiber reinforcement phase has been determined to have a very low fracture toughness and does not undergo significant plasticity before failure [54,55].

The epoxy matrix was modeled as an isotropic, elasto-plastic material. The elastic region is characterized by the Elastic Modulus (E) and the poisson ratio (ν). The proportional limit stress (σ_y) is used to define the onset of non-linear plasticity. A progressive damage model was used to capture the failure of the epoxy material caused by brittle cracking and micro-voids [56]. Damage is said to initiate at the point of maximum work hardening. Using the progressive damage approach, the degree of damage can be fully characterized by a scalar damage variable (d). Upon unloading, the current state of damage exhibits itself in the form of a degraded modulus of elasticity (E_d) according to:

$$E_d = (1-d)E \ . \tag{2.15}$$

The damage variable then evolves linearly according to:

$$d = \frac{L_e \varepsilon^{pl}}{u_f^{pl}} , \tag{2.16}$$

where L_e is the characteristic element length, ε^{pl} is the plastic strain and u_f^{pl} is the equivalent plastic displacement at failure calculated according to:

$$u_f^{pl} = \frac{2G_f}{\sigma_y} , \tag{2.17}$$

where G_f is the fracture energy of the material, and σ_y is the static yield stress before the initiation of damage. The material is then said to fail when the damage variable is equal to unity at which point the modulus of elasticity is equal to zero. The degree at which damage progresses can be fully characterized using the yield stress (σ_y), and the fracture energy (G_f). The above damage model is available in the ABAQUS/Explicit finite element code [57].

In this analysis, the workpiece microstructure is modeled as separate phases (micro-mechanical) near the tool contact zone and as an EHM (macro-mechanical) away from the contact zone as seen in Figure 2.22. Using this approach, the number of elements, and thus simulation time can be dramatically reduced without a loss of force prediction accuracy [58].

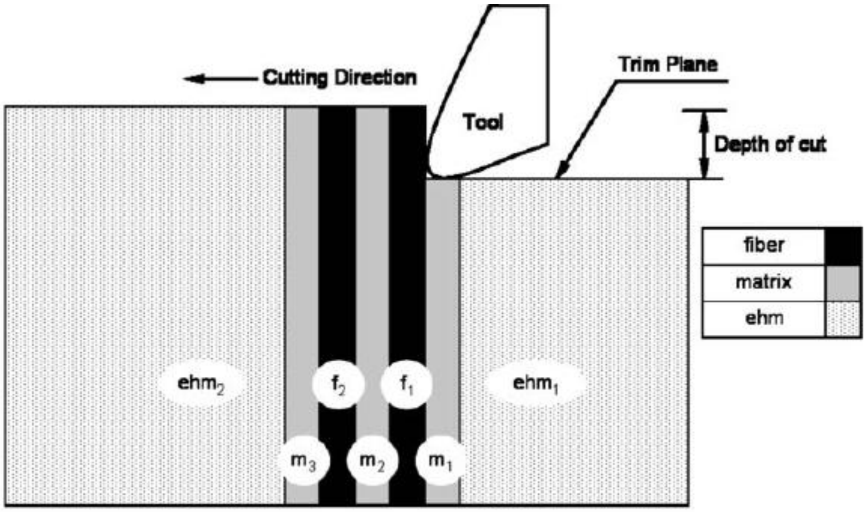

Figure 2.22. Micro-Macro Mechanical Modeling Combination Implemented by Rao et al. [41]

In the first study by Rao et al., the focus remained on the prediction of cutting forces and depth of damage [41]. It was observed that the machining model was capable of accurately predicting both cutting and thrust forces. The machining force results were also compared to the machining forces simulated with the macro-mechanical finite element model developed by Nayak et al. [59] showing that the thrust force trends are more accurately predicted in a micro-mechanical analysis as seen in Fig. 2.23. Furthermore, this model was found to predict sub-surface damage showing that the depth of damage increases with increasing fiber orientation (see Fig. Figure 2.24). The general trends in damage with respect to fiber orientation agree well with the experimental work by other researchers [5,22,8,33]; however, no experimental verification is provided in this study.

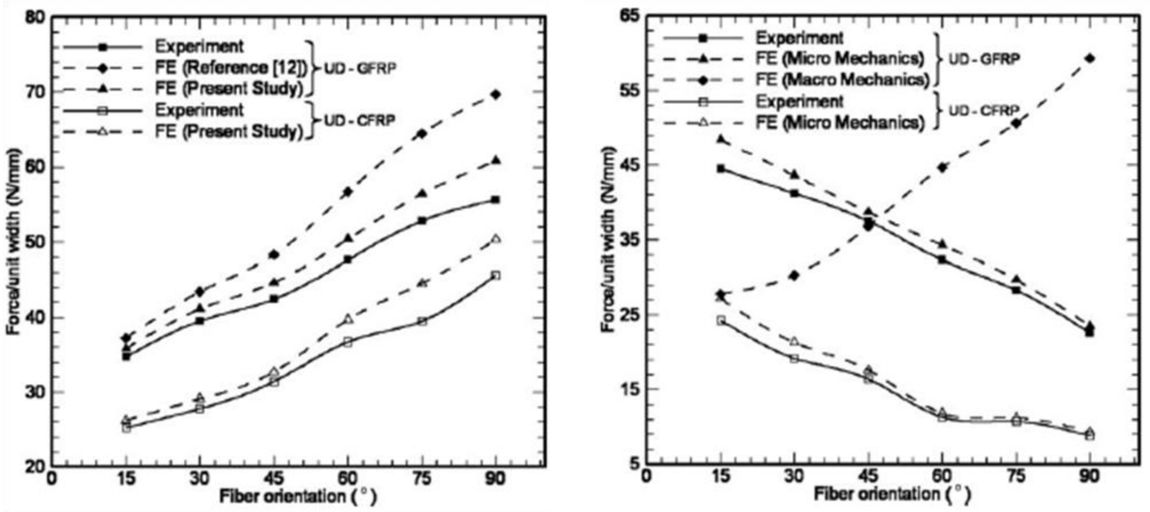

(a) Cutting Forces (b) Thrust Forces

Figure 2.23. Predicted and Experimental Machining Forces for Rao Model [41]

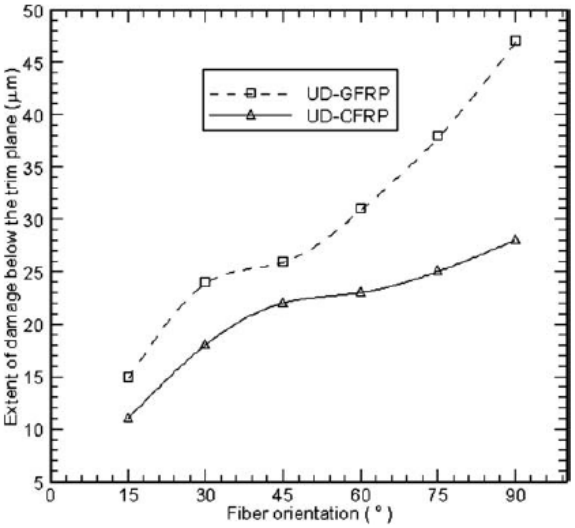

Figure 2.24. Extent of Damage below the Trim Plane for Two FRP Composites [43]

The second study by Rao et al. focused on the chip formation mechanisms occurring in the model simulation [43]. The goal of this study was to determine the failure mode of the fibers for a series of fiber orientations between 15 and 90 degrees. It was determined that for all fiber orientations considered, the fiber failure is likely to take place at the point of contact of the tool by fiber crushing and at the same time, tensile rupture on the side of the fiber opposite the tool due to bending stresses. This contradicts the experimental study of Pwu et al. [22].

While this model is helpful in providing an accurate prediction of machining forces, it has several limitations, most significant of which is the quasi-static nature of the machining simulation. The author admits that it is difficult to identify the location of fracture by examining the stress distribution from a quasi-static machining simulation [43]. Also, because of the cohesive zone elements used in the machining simulation, the interface cannot undergo any compressive stresses and thus, the interface can only be modeled below the trim plane. Furthermore, this study does nothing to explain the complex nature of the fiber failure mechanisms in fiber orientations greater than 90 degrees.

2.5. Gaps in Knowledge

Many experimental studies have been performed with the aim of gaining a better understanding of the fiber failure mechanisms occurring in the machining of FRP composites; however, these fall short of fully describing the specific nature of the fiber failure mechanisms. The material removal mechanisms in the machining process of non-homogenous, anisotropic FRPs are complex and it is difficult to hypothesize on the material failure mechanisms by simply examining the experimental responses, which have a high variability and are sporadic in nature [28].

The modeling studies outlined in Section 2.3 seek to overcome some of the experimental deficiencies; however, these still have several limitations. While the theoretical and experimental-based models are helpful in predicting machining forces for a range of fiber orientations, they do little to describe the specific nature of the fiber failure mechanisms. The macro-mechanical finite element modeling approach has serious limitations as it is not capable of describing factors such as chip formation mechanisms and material damage, relating the fiber-matrix interactions. The micro-mechanical FRP finite element machining models that have been developed are quasi-static in nature and thus, are only capable of predicting the location of failure in the first fiber encountered by the tool rather than describing the failure mechanisms occurring throughout the formation of a full chip. This poses serious limitations as it is difficult to identify the locations of failure in an entire chip by examining the stress-distribution in a single fiber [43]. Furthermore, the cohesive zone model used in micro-mechanical finite element modeling is insufficient as the elements are only allowed to fail in tension and thus, the interface can only be modeled below the trim plane.

The vast majority of the research in the field of machining of FRP composites is focused on fiber orientations between 0 and 90 degrees and does little to explain the complex nature of fiber failure mechanisms when machining in orientations greater than 90 degrees. In the machining of more complex geometries such as rounded edges and curvilinear features, the tool will encounter a full range of fiber orientations, and as such, the process conditions must be selected with this in mind. Thus, the lack of understanding of the machining behavior of FRP composites at fiber orientations greater than 90 degrees poses a serious limitation on the overall machining process.

All of the research on the machining of FRP composites is focused on the macro-scale fiber failure mechanisms and overall macro-scale machining behavior. It is expected that the fiber failure mechanisms at the micro-scale will differ greatly from their macro-scale counterparts for several reasons including the high edge radius to chipload ratios encountered at the micro-scale, and the chiploads being equal or even lower than the critical diameter of the fibers.

3. An Experimental Study on the Failure Mechanisms Encountered in Micro-Milling of Aligned CFRPs

In this chapter, a model capable of describing the fiber failure mechanisms occurring in the micro-scale machining of carbon fiber-reinforced composites (CFRPs) will be proposed. The basis of this experimentally-based model will be developed by examining the general differences between macro and micro-scale machining processes and how these differences will affect the specific nature of the fiber failure mechanisms at the micro-scale. This will then be applied to develop a fiber failure model capable of describing the fiber failure mechanisms at the micro-scale for the full range of fiber orientations under consideration.

The remainder of this paper is organized as follows. Section 3.1 outlines the formulation of the fiber failure model for micro-scale machining of CFRPs followed by Section 3.2 that explains the design of the validation experiments. Section 3.3 discusses the machining responses used to validate the proposed model, and finally, Section 3.4 presents the specific conclusions that can be drawn from this work.

3.1. A Fiber Failure Model for Micro-Scale Machining of CFRPs

This section first reviews the failure mechanisms observed during the machining of CFRPs at the macro-scale, followed by a discussion on the differences between machining at the micro and macro-scale. This section concludes with the proposal of a fiber failure model that describes the failure of CFRPs during machining at the micro-scale.

3.1.1. Summary of Macro-Scale Fiber Failure Mechanisms

Because the compressive and tensile strengths of carbon fibers are comparable, (≈ 3 GPa and 3.5 GPa, respectively [60]) their failure has been observed to be highly dependent on the stress state (i.e. bending/buckling/crushing). The microstructure-based simulation study of Venugoapalrao et al. reveals that for fiber orientations between 15 and 90 degrees relative to the direction of tool motion, failure initiates from the side of the fiber opposite the tool as the tensile stress due to bending in this region reaches the failure value (3.5 GPa). At angles less than 15 degrees the fibers are observed to fail in buckling [17]. Thus, at the macro-scale, the fiber failure for orientations ≤ 90 degrees is bending or buckling-dominated.

For macro-scale machining, the second distinct failure mode occurs for fiber orientation angles greater than 90 degrees with respect to the direction of motion of the tool-tip. The tool first causes fiber-matrix debonding and only after sufficient deformation has taken place, will the fibers fail in bending along a plane similar to the shear plane as observed in machining of metals [21,39]. The bending of the fibers results in a shift in the breakage point of the fibers with the movement of the cutting tool into the workpiece. Thus, the fiber failure for orientations > 90 degrees is bending dominated.

3.1.2. Fiber Failure Mechanism Differences at the Micro-Scale

While the overall fiber failure modes of crushing, bending, and buckling are expected to remain the same at the macro and the micro-scale, the fundamental differences in machining between the two scales is expected to influence the failure mechanisms that come into play at various fiber orientations. In micro-machining, there are at least two things that are fundamentally different from macro-scale machining and each is expected to have a unique and important influence on the machining of CFRPs. First, the relationship between the process geometry and the workpiece microstructure changes as compared to conventional machining operations. Because the feed-per-tooth (FPT) values used are comparable to the nominal carbon fiber diameter (5-8 μm), the tool will encounter individual fibers instead of fiber bundles, as observed at the macro-scale. Therefore, the failure mode of individual fibers in the composite will become significant at the micro-scale.

Second, the relationship between the process geometry and the tool geometry changes as compared to conventional machining operations. In micro-milling, the feedrate is typically on the order of a few microns per tooth, and the endmills have edge radii that are equal to a few microns, limited by the current tool fabrication capability and tool material microstructure. Unlike most conventional endmilling operations in which the chip thickness is at least an order of magnitude larger than the edge radius, in micro-scale machining the edge radius is roughly equal in magnitude or at times even larger than the chip thickness. Therefore, the compressive load exerted by the cutting edge of the tool will also become more prominent in dictating the fiber failure at the micro-scale [42].

3.1.3. Proposed Fiber Failure Model

There are three distinct failure mechanisms observed in the failure of CFRPs at the macro-scale: crushing, bending, and buckling; exhibiting themselves differently depending on fiber orientation. Figure 3.1 shows how these mechanisms are likely to be exhibited at the micro-scale. Figure 3.1a illustrates the failure mechanism for the 90 degree tool-fiber orientation shown, where the tool contacts the fiber at point A. Because in micro-milling, the tool edge radius is small in comparison to that which is typical at the macro-scale, the tool will provide a much more concentrated stress at the point of contact of the tool and the fiber. Furthermore, since the depth of cut (i.e., (FPT) in micro-milling) is comparable to the fiber size, the fiber will likely be crushed due to the compressive stress exerted on it by the tool and a crack will propagate through point A. A similar phenomenon is theorized for the 45 degree tool-fiber orientation shown in Fig. 3.1b.

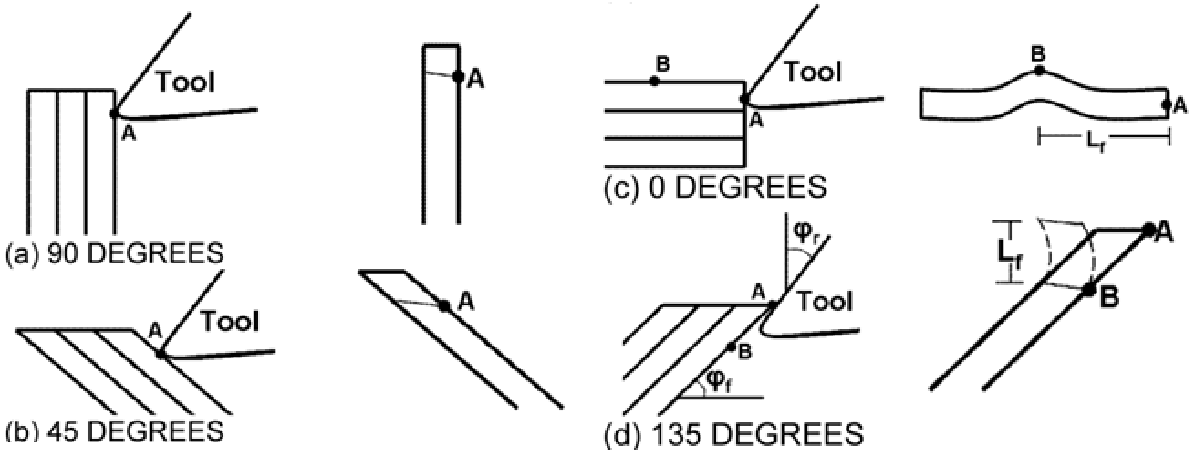

Figure 3.1. Basic CFRP Micro-Scale Failure Mechanisms

For the 0 degree tool-fiber orientation shown in Fig. 3.1c, an entirely different failure mechanism is expected to occur. Given the relatively low FPT values and tool edge radius, the compressive load exerted by the tool is predominantly carried by a single fiber or perhaps two fibers. Because the compressive load exerted on the fiber from the tool is parallel to the fiber axis in this case, the fiber(s) will peel from the matrix as shown in Fig. 3.1c and fracture in tension at point B. Given that the point of load application at the end of the fiber does not significantly vary with change in the FPT value, the buckled fiber length (L_f) of the fibers is expected to be independent of the FPT value (Fig. 3.1c) and significantly larger than the fiber diameter of 5-8 µm. It is also possible that the fibers can fail in bending if the tool contacts the composite material in one of the matrix sections, thus allowing the tool to lift the fiber and bend along the tool rake face.

The fiber failure seen for the 135 degree tool-fiber orientation shown in Fig. 3.1d will likely be dominated by bending. For cases where the fiber angle (φ_f) is greater than the rake angle (φ_r), the tool will first contact the fiber at point A, which will result in fiber bending rather than compressive crushing-dominated failure at point A (Fig 3.1d). The fiber will bend and eventually fail in tension at some location below the tool-path, labeled as point B in Fig. 3.1d. The length L_f of the failed fiber is also expected to be larger than the fiber diameter of 5-8 µm. If the fiber angle is less than or equal to the rake angle, then the tool tip will contact the fiber at point A and a crushing failure is expected, similar to that seen in for the 90 and 45 degree orientations in Figs. 3.1a-b. The failure mechanisms proposed in the model are summarized below:

- Crushing failure at 90º and 45º orientations i.e., $\sigma_{failure} \geq 3$ GPa ($\sigma_{(Max\ compression)}$)
- Tensile buckling failure at 0º and tensile bending failure at 135º orientation, i.e., $\sigma_{failure} \geq 3.5$ GPa ($\sigma_{(Max\ tension)}$).

3.2. Design of Validation Experiments

A micro-milling experiment was employed to validate the proposed fiber failure mechanisms for CFRPs. Three machining responses, viz., chip morphology, delamination, and cutting forces, are used to interpret failure mechanisms and validate the model.

3.2.1. Microstructure Characterization

The specimens used in this experiment were obtained from ACP Composites (www.acp-composites.com [61]). They were in the form of plates of layered, resin-infused carbon fibers with a fiber volume percentage of 60 percent. Each lamina was approximately 180 µm thick. The machining samples were cut from a large 3 mm thick composite panel into 10 x 10 mm samples to fit on the machining testbed. Figure 3.2 shows a scanning electron microscope (SEM) image of the top view of a material sample indicating several fibers along with zones of epoxy. The carbon fibers in the samples were observed to be continuous over the entire length of the workpiece and found to have a diameter between 5 and 8 µm. Note that many fibers in Fig. 3.2 have a generous coating of epoxy making them appear to have a larger diameter.

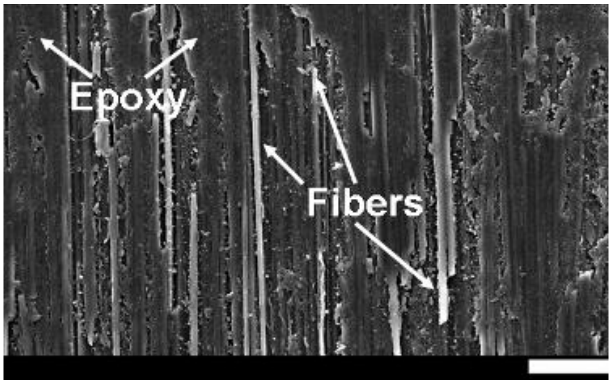

Figure 3.2. SEM Image of CFRP Microstructure (Scale:Bar = 100µm)

3.2.2. Machining Testbed

The micro-milling tests were performed on a three-axis computer numerical control (CNC) micro-scale machine tool (mMT) developed at the University of Illinois. This micro-machine tool is equipped with linear voice coil motors on each axis with encoders having a resolution of 100 nm. Two NSK air-bearing spindles with rated speeds of 50,000 and 150,000 RPM were used on this testbed. This testbed is also equipped with an acoustic emissions-based sensor capable of detecting the surface of the workpiece accurately to within 1 µm, thus allowing for highly accurate workpiece touch-off operations [62]. This guaranteed a consistent axial depth of cut used throughout the experimentation. Figure Figure 3.3a shows the overall experimental setup while Fig. Figure 3.3b shows a close up image of the tool and workpiece.

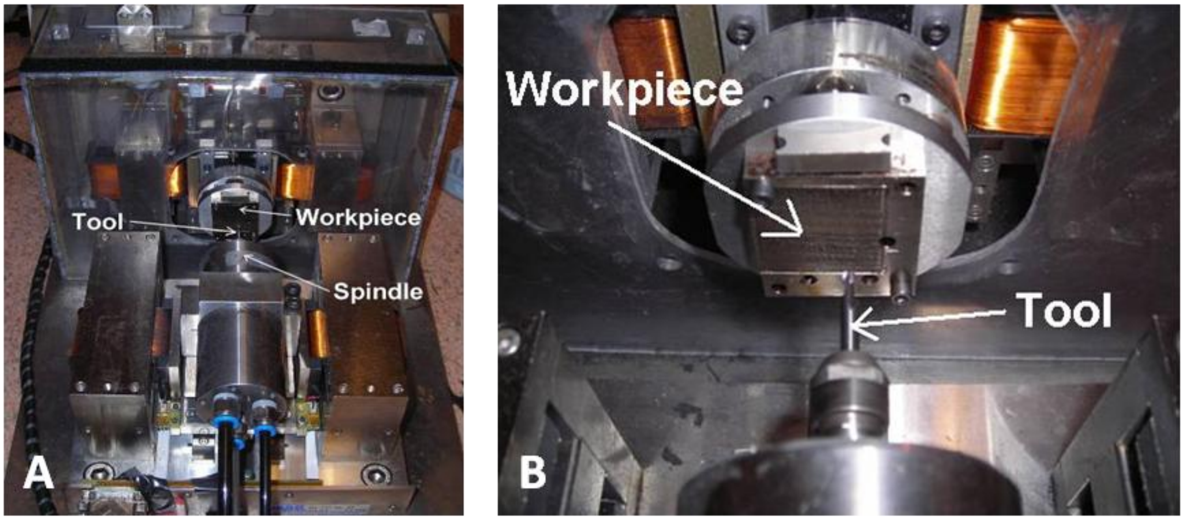

Figure 3.3. Experimental Testbed

A 396 µm diameter, single-fluted, tungsten carbide endmill with an edge radius of 1 µm was used for this study. A single-fluted endmill was chosen because it allows for a precise control of chipload and eliminates effects due to tool run-out. Figure 3.4 shows an image of the one of the tools used in this experimental study.

Figure 3.4. Image of single-fluted tool tip

3.2.3. Experimental Design

Slotting experiments were conducted with an axial depth of cut of 80 µm and FPT values of 2, 4, 5, 6, 7, 8, 10, and 18 µm. Cutting speeds of 62.5 and 187.5 m/min were studied. Four different fiber orientations relative to the feed direction (Fig. 3.5) were examined. For every cutting condition, a 10 mm long slot was machined. A new tool was used for every cutting condition to ensure that the machining responses under consideration were not confounded with tool wear effects.

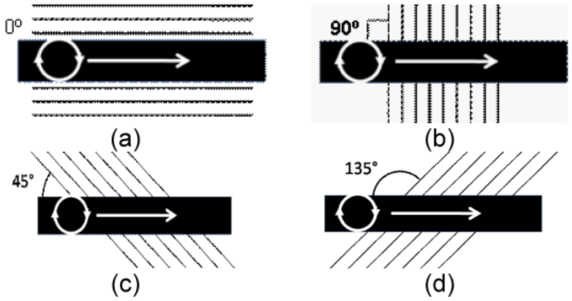

Figure 3.5. Fiber Orientations Relative to Tool Path

3.2.4. Machining Responses for Model Validation

The three machining responses used to validate the proposed fiber failure model were chip morphology, delamination, and cutting forces. This section discusses how each of these were defined and observed.

To analyze the chip morphology, chips were collected around the cutting area. Because many small chips in the form of fractured sections of individual fibers are present, only the larger chips were collected, imaged, and examined using the SEM.

Delamination is a common phenomenon occurring in the milling of CFRPs where sections or layers break out usually along the edges of the machined slot. While machining at the micro-scale, two unique types of delamination were observed depending on the fiber orientation. The first was failure due to entire sections of the fibers being pulled from the matrix, along the top edge of the slot, leaving a series of cavities or irregular ledges as circled in Fig. 3.6a. This type of delamination will be referred to as positive delamination. The second type of delamination failure occurs when the matrix is removed from the fibers leaving stray fibers laying across the slot. This type of failure is pictured in Fig. 3.6b and will be referred to as negative delamination. The positive and negative delamination can be quantified using the positive and negative delamination factors (F_{DP} and F_{DN}, respectively) according to:

$$F_{DP} = \frac{W_{DP}}{W} \tag{1}$$

$$F_{DN} = \frac{W_{DN}}{W} \tag{2}$$

where W_{DP} is the maximum width of positive damage in µm, W_{DN} is the maximum width of the slot without fiber interference, and W the nominal width of cut in µm as indicated in Figs. 4a-b. SEM imaging was used to make the measurements required to determine the two delamination factors. Because of the variability observed along the length of the slot, eight measurements were taken along the entire length of the slot and averaged.

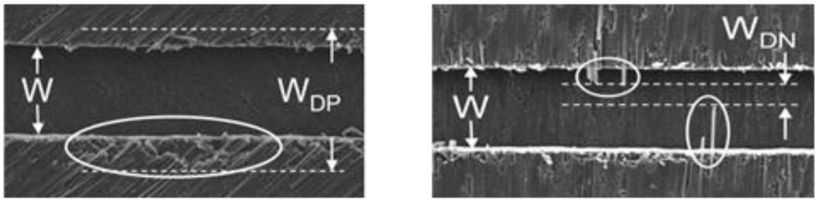

(a) Positive Delamination (b) Negative Delamination

Figure 3.6. Delamination Types

The cutting force signals were obtained using a Kistler 9018 tri-axial load cell embedded in the mMT by sampling at a rate of 50 kHz. Once the forces were obtained, the average peak-to-peak (P-to-P) force orthogonal to the feed direction was calculated over the length of the slot and used as the cutting force response.

Table 3.1 outlines the parameters used in the experimental machining study.

Table 3.1. Experimental Parameters Used in Machining Study

Workpiece Material	Carbon fiber reinforced polymer Layered with unidirectional fibers 5-6 µm fiber diameter
Machine Tool	Linier voice coil motors 100 nm encoder resolution NSK air bearing spindles Acoustic emission touch-off sensor
Tool	Ø 396 µm Single-fluted, tungsten carbide end mill 1 µm edge radius
Axial Depth of Cut	80 µm
Feed per Tooth	2, 4, 5, 6, 7, 8, 10, and 18 µm
Cutting Speed	62.5 and 187.5 m/min
Fiber Orientation	0º, 90º, 45º, and 135º
Machinability Measures	Chip Morphology Cutting forces Positive and Negative Delamination Surface Roughness

3.3.Model Validation

3.3.1. Chip Morphology

Figure 3.7 shows the tool path and three different tool positions along one half tool revolution for all four fiber orientations shown in Fig. 3.5. In Fig. 3.7, the parallel lines denote the orientation of the fibers. Tool positions 1, 2 and 3 in Fig. 3.7 correspond to the entry, center and the exit of the cut, respectively. Because at tool positions (1) and (3) the chipload is low in comparison to the FPT value, the process will likely produce only very small chips formed by crushing a portion of the fiber either longitudinally or transversely. Position (2) is the only point along the cutting path that will experience a chipload equal to the programmed FPT value. Since only the larger chips were collected, it can be inferred that these chips were cut when the tool was in the vicinity of tool position (2). Therefore, in order to properly interpret the chip images, it is critical to examine the fiber orientation with respect to the direction of tool tip motion near tool position (2).

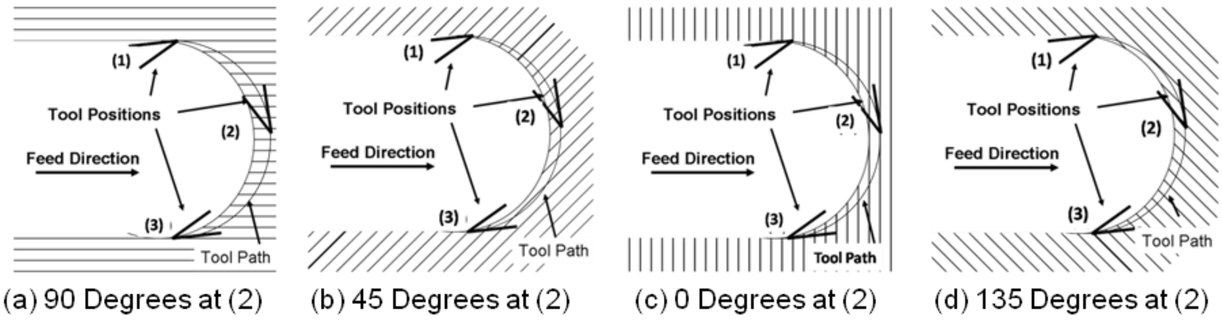

Figure 3.7. Chip Formation Locations

Chip Appearance. Figure 3.8 shows the images of the chips collected for the four different fiber orientations specified in Fig. 3.7. These chips reveal the underlying mechanisms of failure that come into play for these CFRPs. In examining the chips, there were two distinct types of chips observed. The chips collected for the 0 and 135 degree orientations at (2) (Fig. 3.7) show chips with large fiber segments where the individual fiber pieces are discernable in what appears to be irregular fiber bundles, most of which appear to be significantly longer (~100 μm in length) than the FPT value of the cutting process (Fig. 3.8). For the 45 and 90 degree orientations (Fig. 3.8) the length of the fibers observed in the chips were found to vary approximately between 5 and 12 μm, or comparable to the FPT value.

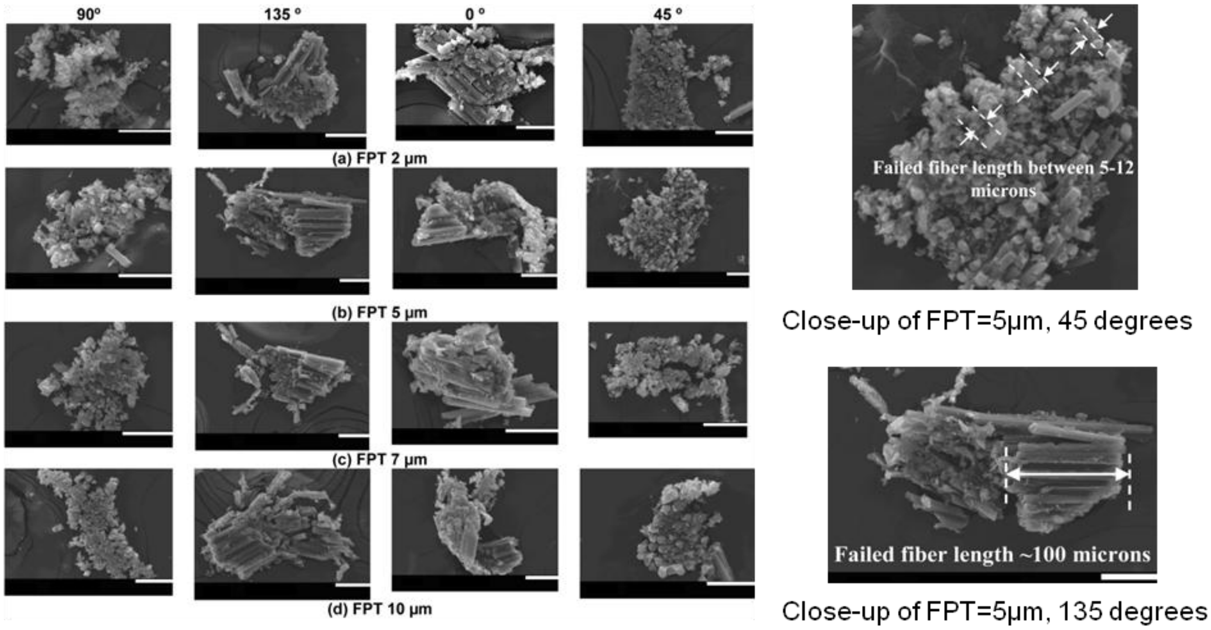

Figure 3.8. Typical Chips Formed at Tool Position (2) as Defined in Fig. 5 (Scale: Bar = 50 µm)

Orientation Effects. For the fiber orientations shown in Figs. 3.7a-b, near tool position (2), the tool will be moving 90 and 45 degrees, respectively, to the fiber axis. The chips collected for the 90 and 45 degree fiber orientations show small fiber fragments within the chips (Fig. 3.8). This seems to indicate a crushing failure at point A (Figs. 3.1a-b) rather than a bending failure as typically observed at the macro-scale, which agrees with the proposed model. The lengths of the fiber fragments appear to increase with the FPT value (Fig. 3.8, close-up of FPT = 5µm, 45 degrees).

For the fiber orientation shown in Fig. 3.7c, at tool position (2) the tool will be moving 0 degrees with respect to the fiber axis. Similarly, for the fiber orientation shown in Fig. 3.7d, at tool position (2), the tool will be moving in the 135 degree orientation. The chips collected for these cases show fibers within the chips that are significantly longer than the FPT value (Fig. 3.8, close-up of FPT=5µm, 135 degrees). The failure length of the fibers (L_f in Fig. 3.1c-d) is found to be approximately 100 µm for the 0 and 135 degree orientations, indicating buckling- and bending-dominated failures, respectively. These failure lengths appear to be independent of the FPT values used in this study, which is consistent with the proposed model.

3.3.2. Delamination

Figure 3.9 shows representative images of slots machined at a cutting velocity of 187.5 m/min and FPT of 6 μm for all four fiber orientations. Because delamination only occurs at the edge of the slots, delamination depends primarily on the fiber orientation close to the edge of the slot (positions (1) and (3) in Fig. 3.7). Figure 3.10 shows the delamination measurements for several cutting conditions and shows that both positive and negative delamination occur independently of each other. The 62.5 m/min cutting speed results in higher positive delamination while the 187.5 m/min cutting speed results in higher negative delamination. Neither positive nor negative delamination appears to exhibit any apparent correlation with feedrate.

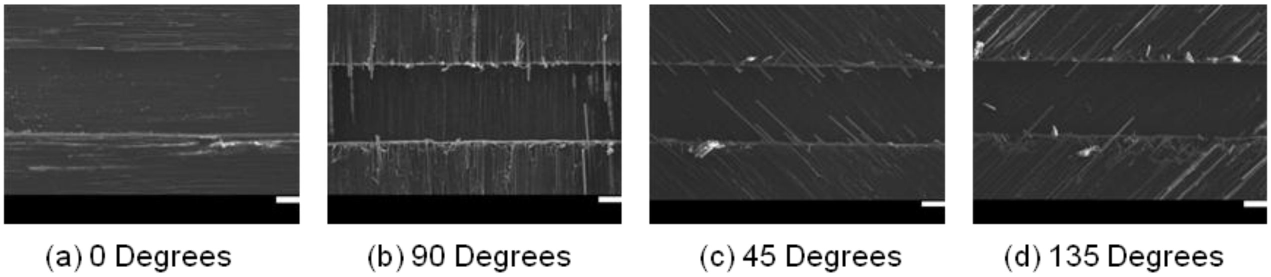
(a) 0 Degrees (b) 90 Degrees (c) 45 Degrees (d) 135 Degrees

Figure 3.9. Slot Edge Delamination (Scale: Bar = 100μm)

<u>0 Degree Orientation.</u> Figure 3.10 shows that there is almost no positive or negative delamination observed for any of the cutting conditions when machining with the fibers in the 0 degree orientation. This is likely due to the fact that the tool buckles a portion of the fiber longitudinally and since fracture tends to grow along the fiber axis, the W_D value as measured according to Eqs. 1 and 2 will never differ by more than the diameter of a single fiber from the nominal width. F_{DN} and F_{DP} are close to 1 (Fig. 3.10), which agrees with the proposed failure model.

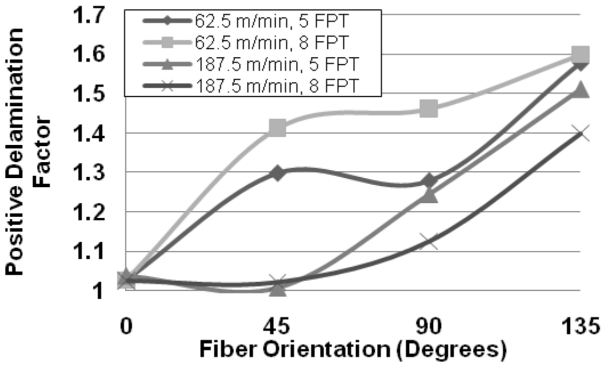

(a) Positive Delamination

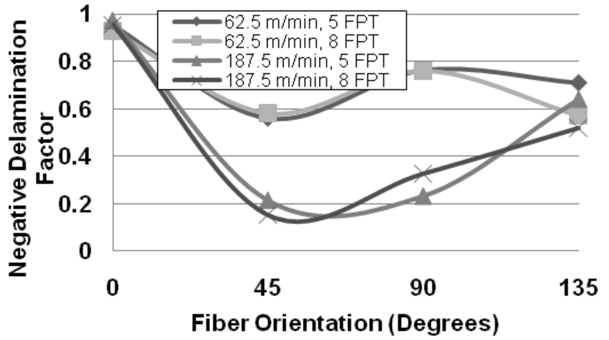

(b) Negative Delamination

Figure 3.10. Nature of Delamination at Various Fiber Orientations

135 Degree Orientation. The 135 degree tool-fiber orientation yields the highest positive delamination among the four orientations (Fig. 3.10a). When the tool tip comes in contact with the fibers at the edge of the slot, the fibers are subjected to bending stress, and generally fracture at a point beyond the edge of the slot wall (Point B, Fig. 3.1d) resulting in subsurface damage or in this case, positive delamination. Thus, the fact that the positive delamination is the highest for the 135 degree case is therefore consistent with the proposed model. Furthermore, negative delamination also appears to be prevalent in that fibers are seen to have bent and sprung back after the passing of the tool (Fig. 3.10b).

45 and 90 Degree Orientations. For the 45 and 90 degree orientations, the relatively low positive delamination (Fig. 3.10a) in comparison to the 135 degree orientation indicates that the fibers are being crushed rather than bent, which would result in subsurface damage (positive delamination). While most of the fibers are crushed, some fibers are bent under the tool and spring back after the tool has passed resulting in negative delamination (Fig. 3.10b). This behavior is consistent with the proposed model.

3.3.3. Cutting Forces

Figure 3.11 shows a series of force signals and spectra in the direction orthogonal to the feed direction collected over 10 revolutions for each fiber orientation. The cyclic nature of the single-fluted cutting process can be clearly seen in Fig. 3.11 as the cutting edge of the tool enters the cut for one half revolution and exits the cut for the other half revolution. A smaller sub-peak is noted between the main peaks, which may be attributed to the tool rubbing against the elastically recovered surface. The spectrum plots clearly show the spindle frequency of 850 Hz to be dominant. The reduced energy level observed in the second harmonic of the spindle frequency for the 135 degree orientation may be indicative of reduced back rubbing in this fiber orientation. The forces orthogonal to the feed direction were chosen to analyze because the majority of the chip is formed when the tool is in the vicinity of position (b) (Fig. 3.7) and moving orthogonal to the feed direction. It is at this point (b) that the force reaches its maximum value.

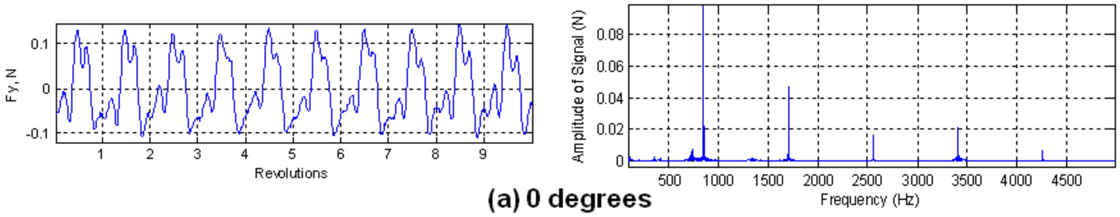

(a) 0 degrees

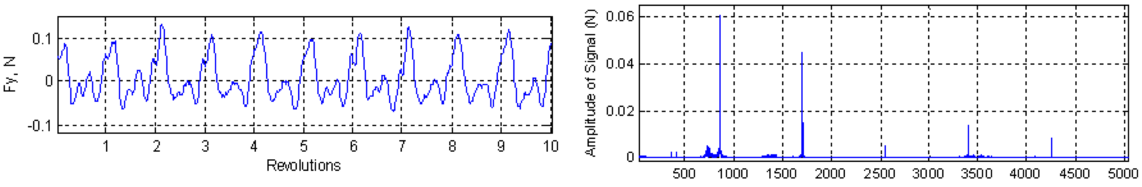

(b) 45 degrees

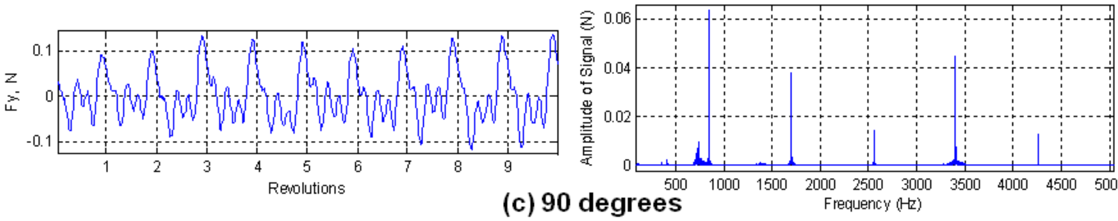

(c) 90 degrees

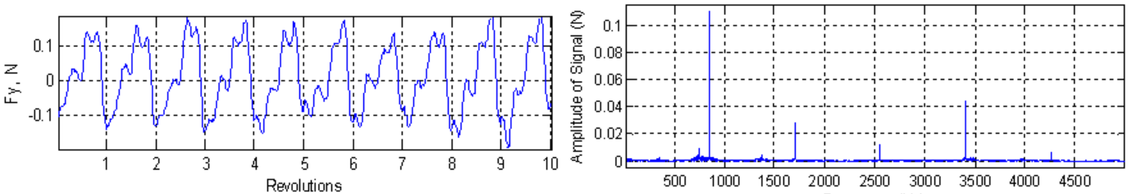

(d) 135 degrees

Figure 3.11. Cutting Force Profiles and Spectra for Collected Force Signals

Figure 3.12 shows the average peak-to-peak forces orthogonal to the feed direction (at tool position (2) in Fig. 3.7) collected over the entire length of the slot. Figure 3.12 shows that the forces for the 45 and 90 degree orientations at (2) are about 40 percent higher than for the 0 and 135 degree orientations at (2). As proposed by the model, the chip at tool position (2) (Fig. 3.7) is formed by a crushing-dominated process for the 45 and 90 degree orientations. Though the compressive strength of carbon fibers (3 GPa) is lower than their tensile strength (3.5 GPa), a crushing-dominated fiber failure has been observed to result in a higher cutting force when compared to buckling or bending-dominated failure [17,39]. Unlike crushing, in a bending-mode the tool induces a moment at the location of failure which aids the failure process.

Therefore, even though the tensile strength of the fibers is higher than the compressive strength, lower cutting forces are observed. The lower force observed for the 0 and 135 degree orientations can be attributed to the buckling and bending-dominated failures occurring at those orientations, respectively. These observations agree with the studies of Hocheng et al. [17] and Zhang et al. [39] and support the proposed model.

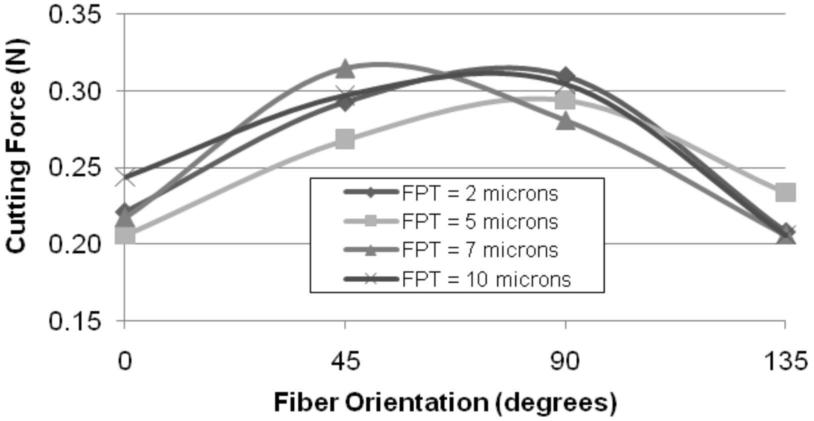

Figure 3.12. Effect of Fiber Orientation on Cutting Forces

3.4. Chapter Summary

A failure model is proposed to capture the fiber failure mechanisms that occur while machining CFRP composites at the micro-scale. Carbon fibers oriented at 90 and 45 degrees to the direction of motion of the tool edge are proposed to fail predominantly in crushing/compression while buckling- and bending-dominated tensile failures are proposed for the 0 and 135 degree orientations, respectively according to Fig. 3.1. The model proposes a location of failure, mode of fiber failure (viz., bending, crushing, buckling), and a relative length of fiber that will be found in the chips generated from the process. The micro-scale fiber failure model proposed in this study specifies micro-scale fiber failure mechanisms that are uniquely different than their macro-scale counterparts.

In order to validate the machining model based on experimental observations, the results from an experimental validation study are examined and compared to the developed model. Parameters such as chip morphology, delamination trends, and cutting forces are used as validation measures. The chip morphology validates the proposed model since the chips for the 45 and 90 degree orientations show small fragmented chips indicating crushing (compressive) failure while the chips collected for the 0 and 135 degree orientations have fibers significantly longer than the feed-per-tooth indicating buckling and bending (tensile) failures, respectively. The delamination patterns observed support the failure modes proposed. The buckling failure at 0 degree orientation results in negligible delamination whereas the bending failure at 135 degree orientation results in the highest positive delamination. Both 45 and 90 degree orientations show low positive delamination because of the crushing mode of failure. The trends in the cutting forces correlate with the proposed modes of failure. The cutting forces were found to be 40 percent higher for the crushing-dominated failure as compared to bending or buckling failures. In a bending mode the tool induces a moment that aids the fiber failure process, thereby reducing the cutting force.

The fiber failure model proposed and subsequently substantiated based on experimental data in this chapter is useful in understanding the fiber failure mechanisms occurring in the micro-scale machining process as a function of fiber orienntation, however, its usefulness is limited for two reasons. First, the model is limited in describing the failure mechanisms only as a function of the process parameter values (viz., feedrate, cutting speed, tool rake angle, and tool edge radius) analyzed in this study. Furthermore, in this study, the failure mechanisms were not directly observed, but instead inferences were drawn from the machining responses observed in the experimental validation study. To gain a more fundamental understanding of the micro and macro-scale fiber failure mechanisms occurring in the machining process, a more comprehensive model is required in which the fiber failure mechanisms can be directly observed throughout the chip formation process for any process parameter under consideration.

4. Development of a Finite Element-based Machining Model

Chapter 3 outlines a fiber failure model for machining of CFRPs at the micro-scale. While the failure mode and location of fiber failure were inferred from examination of the experimental machining responses, the specific nature of the fiber-failure mechanisms is still not fully understood as the chip formation process cannot be directly observed.

In this chapter, what will be referred to as a dynamic machining simulation will be developed where the tool is assigned a velocity-based boundary condition instead of a displacement-based boundary condition as is typical in quasi-static simulations. A dynamic finite element machining model (FEMM) is capable of capturing the failure mechanisms occurring throughout the chip formation process. Thus, along several points throughout the cut, the chip formation and fiber failure mechanisms can be captured and analyzed, illustrating the specific nature of the chip formation process. In order to facilitate this new modeling approach, a unique approach to fiber-matrix interfacial modeling will be presented and implemented into the finite element machining model.

The remainder of this chapter is organized as follows. Section 4.1 explains the FEMM development and material/failure models, followed by Section 4.2, which employs an experimental study to validate the FEMM using fiber failure mode, the characteristic fiber length in the chips, and cutting forces as validation measures. Section 4.3 outlines a parametric study which implements the model to find improved tool geometry conditions for machining microstructures of differing fiber sizes. Section 4.4 presents the specific conclusions that can be taken from this work.

4.1. Finite Element Machining Model Development

Figure 4.1 outlines the modeling strategy to develop the FEMM for carbon fiber-reinforced polymer composites. First, the overall material microstructure was characterized and this was used to simulate separate material microstructures for each fiber orientation under consideration. The simulated microstructures and interfacial model along with the material and failure models of carbon fiber and epoxy from literature were used as model inputs for the finite element solver. With these parameters, the model is then capable of predicting the machining behavior of these materials, specifically, the fiber failure mode, characteristic fiber length in the chips, and machining forces. In chapter 5, the model will be validated by comparing the model simulation results to the results of a set of micro-scale orthogonal machining experiments.

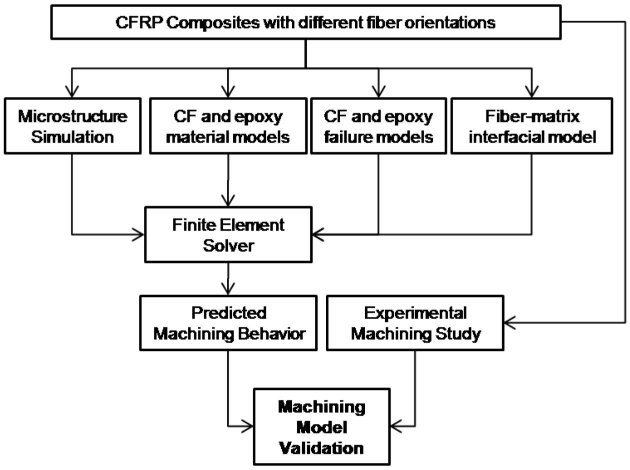

Figure 4.1 . Model Development and Validation Strategy

4.1.1. Microstructure Simulation

The material used in this study was a unidirectional carbon fiber-reinforced polymer obtained from ACP Composites with a fiber volume percentage of 60 percent and diameter of 7.5 µm [61]. SEM images of the machined material surface were taken to characterize the microstructure as shown in Fig. 4.2.

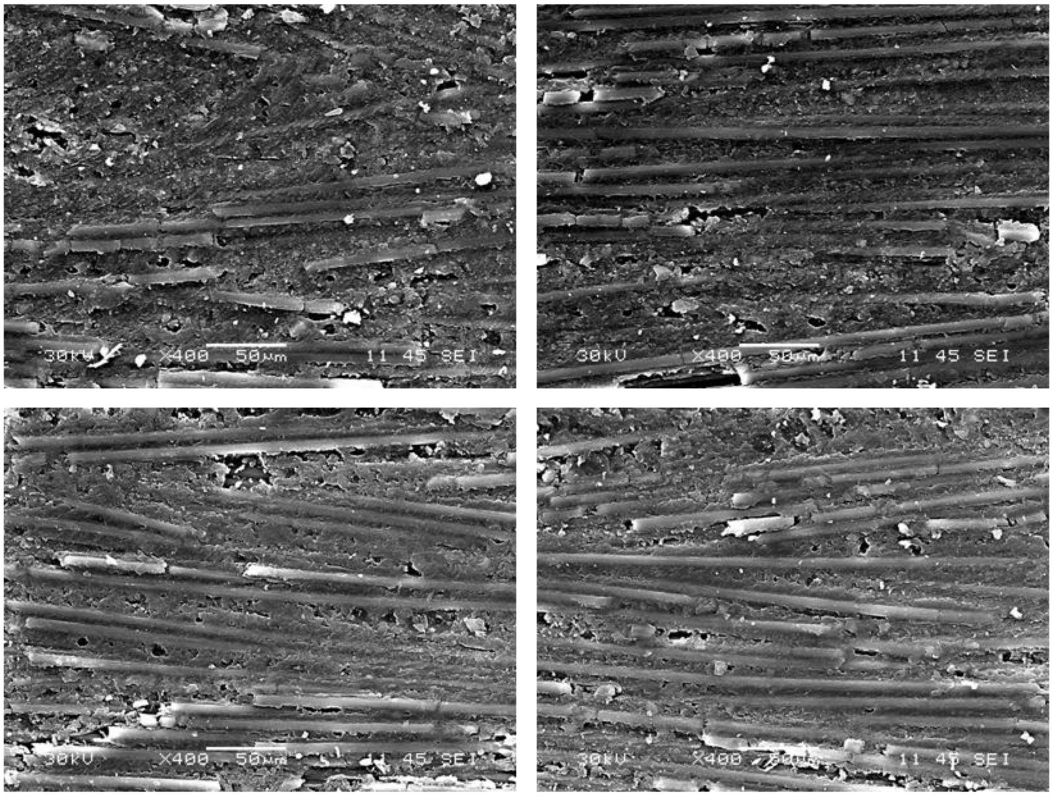

Figure 4.2 Images Used for Microstructure Characterization

The three parameters used to characterize the microstructure are illustrated in Fig. 4.3. The three parameters are fiber angle, fiber grouping number, and matrix spacing. The fiber angle (Φ) is defined as the local fiber angle in reference to the mean fiber angle, θ (θ = 0 for fiber orientation in Fig. 4.3). Variability in fiber angle is inherent to most CFRP microstructures and caused from the high temperature curing of the composite panels. The fiber grouping number (N) is defined as the number of fibers in a group at a specific fiber angle (Φ). The matrix spacing (t) is defined as the thickness of the matrix sections between adjacent fibers.

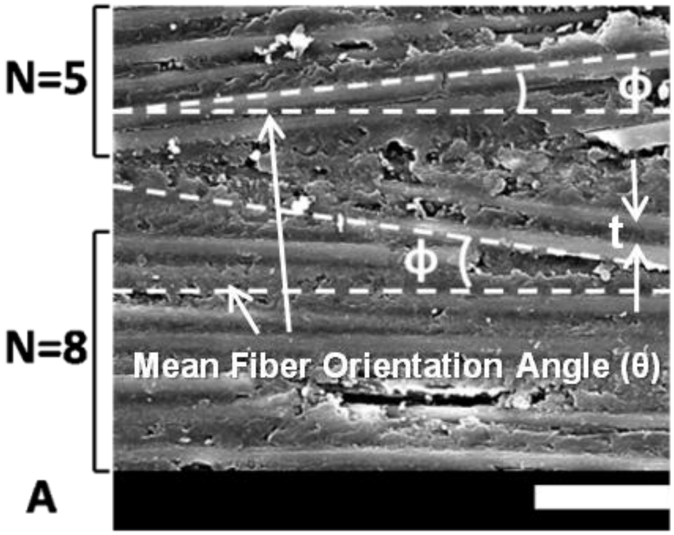

Figure 4.3. Microstructure parameters used for microstructure simulation (Scale: Bar = 50μm)

To estimate each of the three parameters, ten 300 μm square microstructures similar to that shown in Fig. 4.3 were imaged using SEM. To determine the fiber angle statistics, the local angle (Φ) of each individual fiber on the surface of the microstructure was measured in reference to the mean fiber orientation angle (θ) and the average and sample variance pooled over the ten specimens were calculated. In examining the fiber angle histogram in Fig. 4.4, the data was shown to well-approximate a normal distribution. A similar technique was used to determine the average and sample variance of the fiber grouping number (N). Based on the data, the distribution of the matrix spacing was approximated as a uniform distribution between 2 and 5 μm. Table 4.1 outlines the estimated parameters used to characterize the microstructure.

Table 4.1. Estimated parameters used in microstructure characterization

	Average	**Stdev**	**Distribution**
Fiber Angle (degrees)	0	3.28	Normal
Fiber Grouping Number	5.52	2.01	Normal
Matrix Spacing	3.5	0.75	Uniform

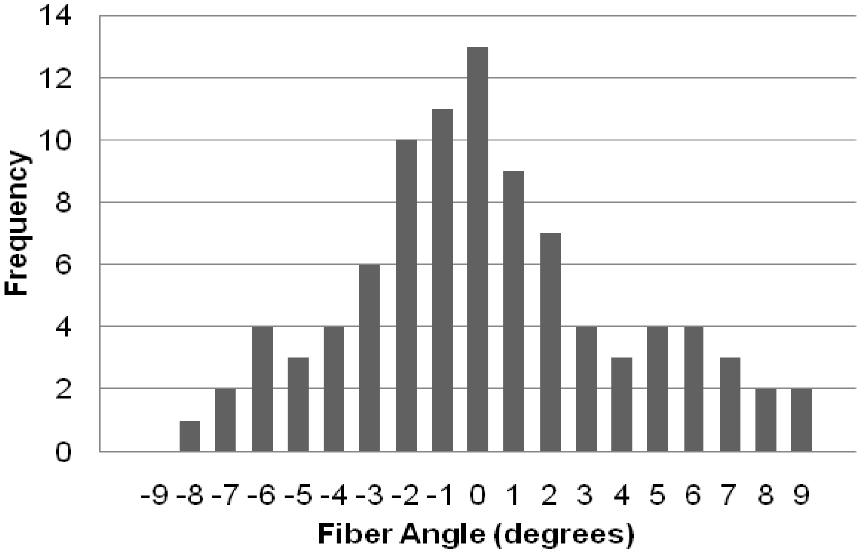

Figure 4.4 Histogram of fiber angle data

The estimated microstructure parameters were used to simulate the material microstructure using the following algorithm. First, a fiber angle (Φ) and matrix spacing (t) were generated according the appropriate distributions outlined in Table 4.1. Second, a fiber grouping number (N) was generated according the appropriate distribution and rounded to the nearest integer. Next, N fibers were generated and placed in a group into the microstructure with angle 'Φ' with a separate spacing (t) generated for the spacing between adjacent fibers. This process was repeated as groups of fibers of differing angles and fiber numbers were stacked to create the microstructure. Figure 4.5 shows examples of two 300μm square microstructures simulated from data in Table 4.1 where the black lines denote fibers and the white areas denote the matrix phase. Once the two-phase microstructure was simulated, an EHM backing was added to the overall microstructure to add extra stiffness in the cutting direction [43].

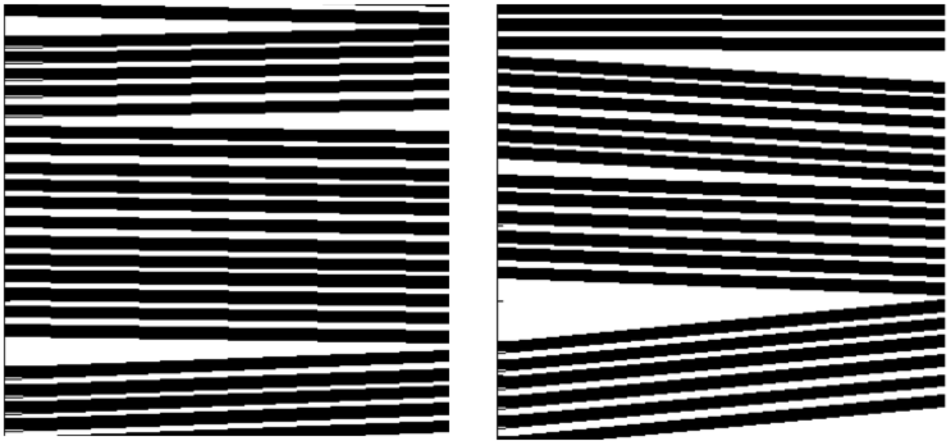

Figure 4.5. Examples of two simulated microstructures (Scale: Bar = 50μm)

4.1.2. Material and Failure Modeling

Since a microstructure-based approach was used in the development of the model, unique material and failure models are required for each of the three phases.

Carbon Fiber/Epoxy/EHM Model. The carbon fiber and epoxy material and failure models used in this analysis are standard for many finite element machining simulations [43,63]. The carbon fiber is assumed to be an elastic and anisotropic material. The carbon fiber material model could be fully characterized by the anisotropic elasticity matrix of the material (E). The carbon fibers are assumed to fail at the onset of stress-induced damage initiation (σ_f). The epoxy matrix was modeled as an isotropic, elasto-plastic material. The elastic region is characterized by the Elastic Modulus (E) and the poisson ratio (ν). A progressive damage model was used to model the epoxy material as is available in the ABAQUS/Explicit finite element code. The EHM backing was modeled as elastic and anisotropic. The elastic constants of this material were calculated according to a micromechanics approach with the combined properties of the two constituent materials. Because failure did not take place in the EHM regions, plasticity or failure models were not required.

Fiber-Matrix Interfacial Model. For the continuum interfacial elements used in the new interfacial model, the elastic region was modeled as isotropic with an arbitrary penalty stiffness (P). The progressive damage is then said to initiate at the maximum normal or tangential stress (σ_{max} or τ_{max}). Because the damage initiation stress primarily dictates the behavior of the elements, the elastic stiffness of the elements is of secondary importance [52,43].

In order to accurately model the normal and tangential failure of the interfacial continuum elements, two separate damage models were implemented simultaneously. The normal damage behavior of the interfacial elements is modeled with a tensile progressive damage model, which dictates the normal separation of the interface. After damage initiation occurs, as the normal strain increases, the elastic modulus of the interfacial elements decreases according to:

$$E = (1-d)E_e \tag{4.1}$$

where E is the degraded elastic modulus, E_e is the elastic modulus before damage initiation, and d is the damage variable. The material is said to fail when the damage variable is equal to unity, at which point the material stiffness is equal to zero. The damage variable ‘d’ evolves exponentially according to:

$$d = 1 - \exp\left(-\int_0^{u^{pl}} \frac{\sigma_y L_e \dot{\varepsilon}^{pl}}{G_f} \right) \tag{4.2}$$

where $\dot{\varepsilon}^{pl}$ is the rate of plastic strain, σ_y is the yield stress, L_e is the characteristic element length, G_f is the material fracture energy, and u^{pl} is defined according to:

$$u_f^{pl} = \frac{2G_f}{\sigma_y} \quad . \tag{4.3}$$

The fracture energy (G_f) is defined for the normal and tangential fracture energies, respectively, viz.,

$$G_n = \int_0^{\varepsilon_f} \sigma d\varepsilon \tag{4.4}$$

$$G_t = \int_{-\gamma_f}^{\gamma_f} \tau d\gamma \quad , \tag{4.5}$$

where ε_f and γ_f are the normal and shear failure strains, respectively. Similarly, the shear damage of the interfacial elements is modeled with the progressive damage approach accounting for failure under positive or negative shear strains. After damage initiates, the progression of shear damage evolves exponentially according to Eq. 4.2 until the elements are assumed to fail at a strain of $\pm\gamma_f$ and when the damage variable is equal to unity.

Because multiple damage modes are implemented for the interfacial elements, a multiplicative damage variable is defined which combines the current state of damage of each of the two damage variables according to:

$$d_{mult} = 1 - \prod_{k \in N_{mult}} (1 - d_k) \quad , \tag{4.6}$$

where d_{mult} is an intermediate damage variable and N_{mult} is the number of damage variables used in the model. The overall damage variable (D) can then be calculated according to:

$$D = \max \ d_{mult}, \max_{j \in N_{\max}} (d_j) \quad . \tag{4.7}$$

Researchers have noted that the overall shape of the normal and tangential traction-separation curves for interfacial elements has little effect on their behavior [52]. Instead, the damage initiation stress and fracture energy are the two key factors which dictate the behavior of the material interface. The behavior of the interface phase can then be fully described with normal and tangential strengths, fracture energy, and penalty stiffness in the elastic region. The overall stress-strain relationships for the normal and tangential behavior of the interfacial elements can thus be defined for the normal and tangential behaviors, respectively, viz.,

$$\sigma(\varepsilon) = \begin{cases} P\varepsilon & : \varepsilon \le \varepsilon_d \\ (1-D)P\varepsilon & : \varepsilon_d < \varepsilon < \varepsilon_f \\ 0 & : \varepsilon \ge \varepsilon_f \end{cases} \tag{4.8}$$

$$\tau(\gamma) = \begin{cases} P\gamma & : -\gamma_d \ge \gamma \ge \gamma_d \\ (1-D)P\gamma & : -\gamma_d > \gamma > -\gamma_f ; \gamma_d < \gamma < \gamma_f \\ 0 & : \gamma \le -\gamma_f ; \gamma \ge \gamma_f \end{cases} \quad . \tag{4.9}$$

where ε_d and γ_d are the normal and tangential damage initiation strains, respectively.

Figure 4.6 summarizes the stress-strain behavior of each of the three materials under consideration. Figure 4.6a-b outlines the carbon fiber and epoxy material and failure models used from literature. Figures. 4.6c-d are developed using Eqs. 4.8-4.9 where the three regions from Eqs. 8-9 are dependent on the state of strain.

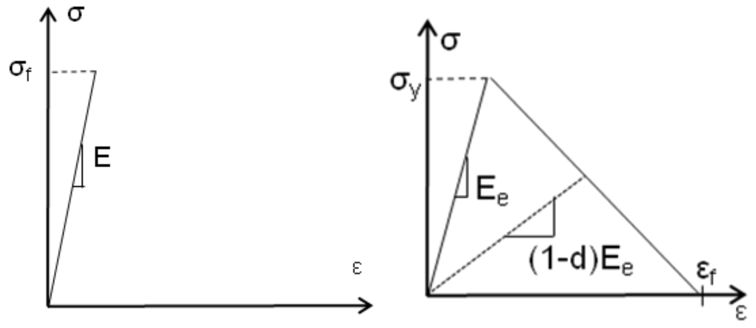

(a) Carbon Fiber Behavior (b) Epoxy Behavior

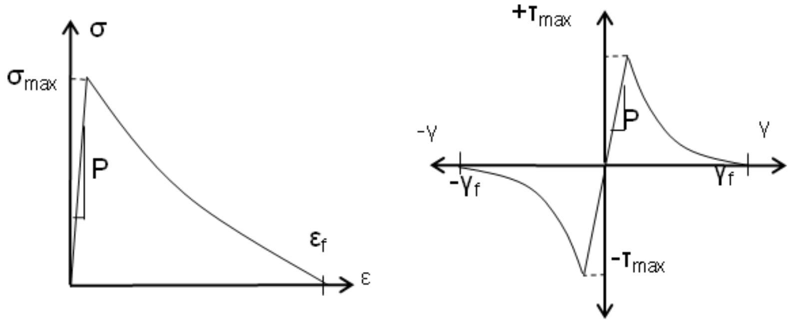

(c) Interfacial Normal Behavior (d) Interfacial Tangential Behavior

Figure 4.6. Material and Failure Models

4.2.Machining Model Implementation

A microstructure-based FEMM can be generated by combining the simulated microstructure with the appropriate material/failure models assigned for each of the three individual phases. The simulation is carried out using commercially available finite element software ABAQUS/EXPLICIT. The model will be capable of predicting the mode of fiber failure, fiber length in the chips, and cutting forces. Table 4.2 outlines the material properties used in the machining simulations obtained from literature [52,56,64,65,54,55,66,67,68].

Table 4.2. Material Properties Used in Machining Simulations

Material	**Property**	
Carbon Fiber	Elastic Constants	E_{11}=235GPa, E_{22}=14GPa, ν=0.2
	Longitudinal Strength	X=3GPa
	Transverse Strength	Y=0.5GPa
Epoxy	Elastic Constants	E=4GPa, ν=0.4
	Yield Strength	σ_y=85MPa (Static)
Interface	Normal Strength	σ_{max}=167.5MPa
	Shear Strength	τ_{max}=25MPa
	Fracture Energy	0.05 N/mm^2
EHM	Elastic Constants	E_{11}=147GPa, E_{22}=10GPa, ν=.27

In this machining simulation, four fiber orientations are considered: 0, 45, 90, and 135 degrees, defined according to Fig. Figure 4.7. A separate microstructure is simulated for each fiber orientation according to the parameterization scheme outlined in Section 4.1.1. The workpiece size was determined to be 300 by 300 µm in order to accommodate the chip size and failure modes typical in the micro-machining process. To construct the overall microstructure, each separate phase was modeled as a separate part and each individual part was added into the overall microstructure. To ensure the nodes between sections remained intact, tie constraints were used along all adjacent boundaries. During the simulation, the workpiece was constrained along the bottom and far left edges according to Fig. Figure 4.7.

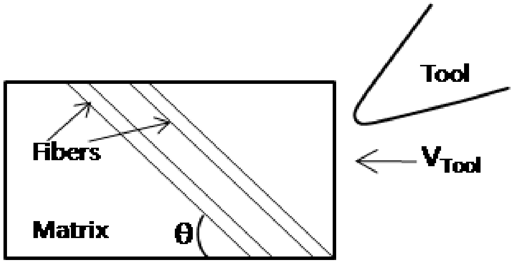

Figure 4.7. Fiber Angle Definition

The elastic modulus of the tungsten carbide tool material is significantly higher than the elastic modulus of either carbon fiber or the epoxy matrix and thus, the tool was modeled as an analytical rigid body. The tool was assigned an edge radius of 5μm and rake and clearance angles of 25 and 10 degrees, respectively. This tool geometry was chosen because it was determined to yield generally lower forces as compared to lower rake and clearance angle geometries [24,69]. To simulate the machining process, a constant velocity boundary condition (V_{Tool}) was assigned to the tool in the direction shown in Fig. Figure 4.7. A 40 μm length of cut was used for the simulations. The friction between the tool and the workpiece is accounted for and assumed to be a function of fiber orientation and was set to 0.3, 0.6, 0.9, and 0.6 for the 0, 45, 90, and 135 degree orientations, respectively according to Nayak et al. as shown in Fig. 4.8. For the 135 degree orientation it was assumed that the coefficient of friction was the same as for the 45 degree orientation.

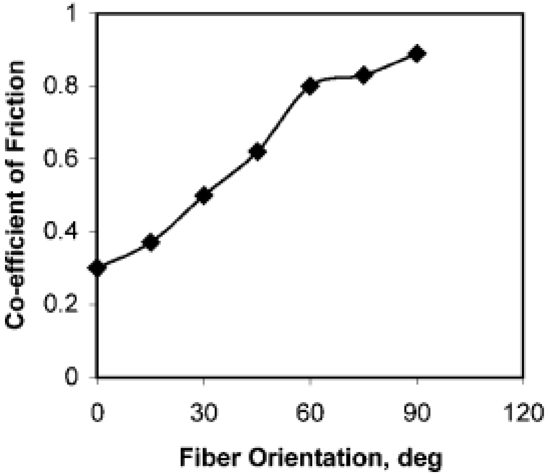

Figure 4.8. Coefficient of Friction with Respect to Fiber Orientation [59]

The microstructures are meshed in the cutting region using a combination of quadrilateral and triangular 2D, 0.5 μm elements. In order to improve computation time, a more course mesh was used in the EHM sections as no element failure takes place in these regions. The fine 0.5 µm mesh in the cutting region was swept to the course mesh at the outer surface of the EHM.

Because the interfacial elements are not able to hold any stress after failure, it became necessary to specify contact between each of the material phases to avoid the penetration of intact surfaces around the interfacial elements. Two forms of penalty contact were defined within each microstructure. The first was contact between each fiber external surface with each adjacent epoxy nodal surface. The second type of contact implemented was between each fiber external surface and the external surface of each adjacent fiber. Using the combination of these two contact conditions, the un-failed elements remained relevant in the simulation until the point of failure. The penalty contact algorithm is available in ABAQUS/Explicit finite element code [57].

Orthogonal machining simulations were run with a cutting speed of 500 mm/min and depths of cut of 15 and 30µm. The three machining responses of primary interest in this machining simulation were fiber failure mode, characteristic fiber length in the chips, and machining forces. Table 4.3 outlines the process parameters used in the finite element machining simulation.

Table 4.3. Process Parameters Used in Simulation

Tool	• 5 µm edge radius • 10 degree clearance angle • 25 degree rake angle
Depths of cut	15 and 30 µm
Cutting Speed	500 mm/min
Fiber Orientations	0, 45, 90, and 135 degrees
Machining Responses	• Fiber failure mode • Characteristic fiber length in chips • Cutting forces

4.3. Simulation Results

In this section, the three model machining responses of primary importance are outlined including fiber failure mode, characteristic fiber length in the chips and machining forces.

4.3.1. Fiber Failure Mode

Figure 4.9 shows the results from the 0 degree cutting simulation. Figure 4.9a shows the material failure modes leading to the formation of the chip. As the tool enters the workpiece, the phases are seen to separate due to interfacial failure. Once the interface has failed sufficiently, bending stresses build up in the fibers ahead of the cutting tool. The fiber-matrix interface continues to fail until the bending stresses in the fiber exceed the failure stress of the fiber resulting in bending-dominated fiber failure ahead of the cutting tool. Figures 4.9b and c show the fiber just after failure occurs. The fiber failure mode is seen to be independent of the DOC of the process, which dictates the number of fibers in a chip rather than the fiber failure mechanisms.

The bending-dominated failure observed in Fig. 4.9 is notably different from the buckling-dominated failure proposed in the model based on experimental observations developed in Chapter 3. This may occur for several reasons. First, in this simulation study, the depths of cut analyzed are 15 and 30 μm, which are notably higher than used in the study in Chapter 3. Thus, with a higher DOC, it is more likely that the tool will bend a larger bundle of fibers rather than buckle an individual fiber as proposed in the experimentally-based model developed in Chapter 3. Furthermore, the model developed in Chapter 3 was proposed with a tool edge radius of 1 μm whereas the tool in the simulation study had an edge radius of 5 μm and thus, the longitudinal stresses in the fiber observed in the simulation are spread between several fiber making it less likely for a single fiber to failure under buckling-dominated failure.

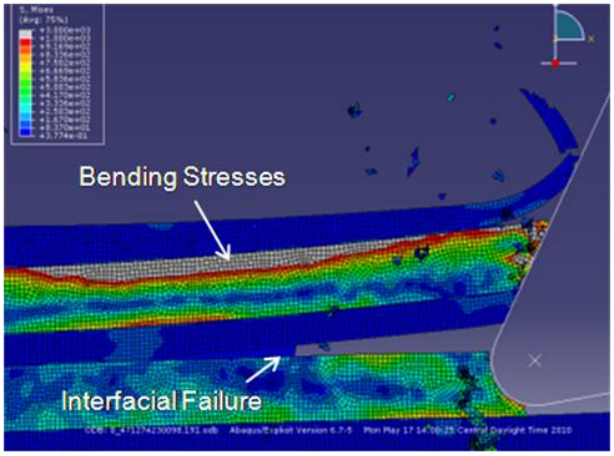

(a) 0 degree failure modes

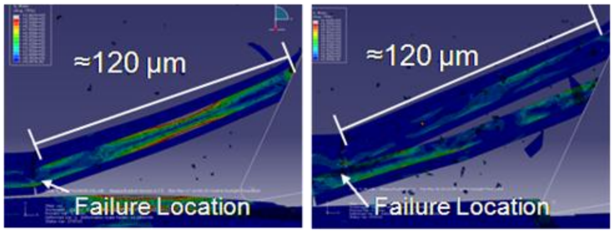

(b) 15 µm DOC (c) 30 µm DOC

Figure 4.9. 0 degree simulation results

Figure 4.10 shows the results from the 45 and 90 degree simulations. As the tool progresses into the workpiece, each fiber is crushed and fails at the point of contact of the tool (Fig. 4.10a). There is also observed to be some bending stresses in the fibers below the cutting plane, however, these do not lead to sub-surface fiber failure as typically observed in macro-machining studies. The bending stresses below the cutting plane do, however, result in sub-surface damage in the form of fiber-matrix interfacial failure. Figures 4.10b-e show the chip formed after several fibers have been crushed for the 45 and 90 degree orientations at the two DOCs under consideration.

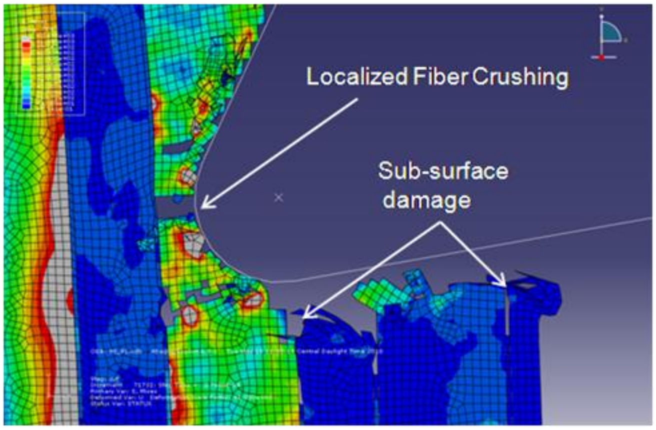

(a) 45 and 90 degree failure modes

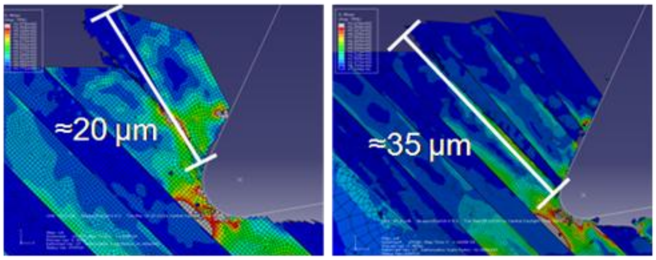

(b) 45 degrees, 15 μm DOC (c) 45 degrees, 30 μm DOC

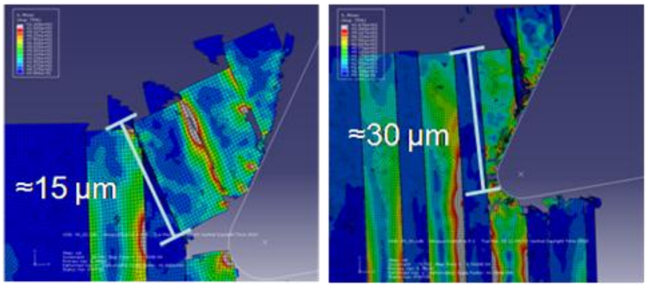

(d) 90 degrees, 15 μm DOC (e) 90 degrees, 30 μm DOC

Figure 4.10. 45 and 90 Degree Simulation Results

Figure 4.11 shows the simulation results for the 135 degree orientation. Figure 4.11a shows the failure modes occurring in the 135 degree machining simulation. As the tool enters the workpiece, it catches on a fiber which is peeled from the rest of the workpiece due to fiber-matrix interfacial failure below the cutting plane. After sufficient fiber peeling and separation, bending stresses develop below the surface of the cut, eventually leading to bending-dominated fiber failure below the cutting plane (Figs 4.11b and c). The fibers are seen to fail in a similar failure mode for each of the two DOCs under consideration.

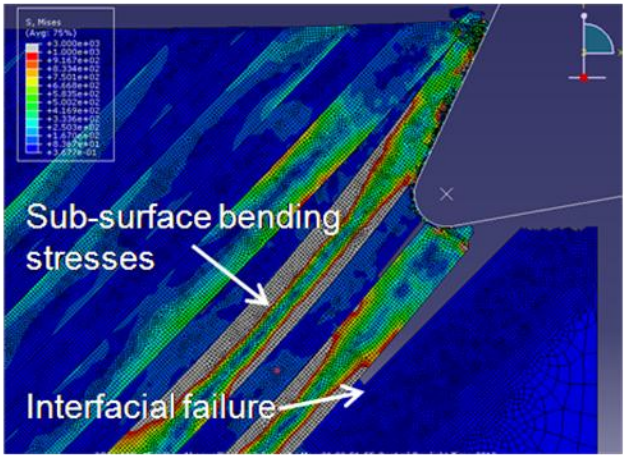

(a) 135 degree failure modes

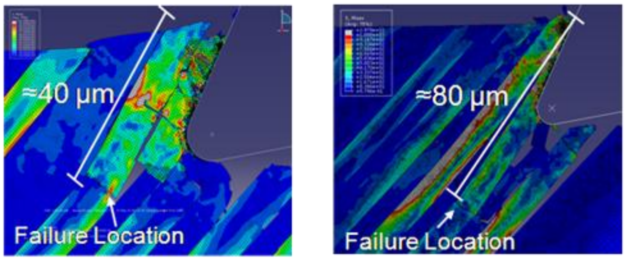

(b) 15µm DOC (c) 30µm DOC

Figure 4.11. 135 Degree Simulation Results

4.3.2. Characteristic Fiber Length in the Chips

Figures 4.9-4.11 also illustrate the characteristic length of the fiber found in the simulation chips. For the 0 degree orientation, the fibers in the chip are seen to be approximately 120 µm in length. This is expected as the fibers in the 0 degree orientation fail in bending-dominated failure away from the point of contact of the tool. For the 45 and 90 degree orientations, the fibers are seen to fail at the point of contact of the tool in a crushing-dominated failure and thus, the chips contain short fibers of approximately 15-35 µm in length. Because of the location of failure, the fiber lengths in the chip are seen to be dependent on the DOC of the process. For the 135 degree orientation, the sub-surface bending-dominated failure is seen to result in fibers in the chips that are approximately 40-80 µm in length and significantly longer than the DOC of the process.

4.3.3. Machining Forces

Figure 4.12 shows the simulated cutting force profiles for the 40 µm length of cut and for each fiber orientation under consideration for the 30 µm DOC. All of the cutting force profiles show a considerable amount of variability cause by the two-phase nature of the simulated microstructure. This force variability is the most prevalent in the 90 and 135 degree orientations as machining in these orientations result in the most significant out-of-plane forces [28]. These force profiles agree well with those observed by Rahman et al. in Fig. 2.8 [28].

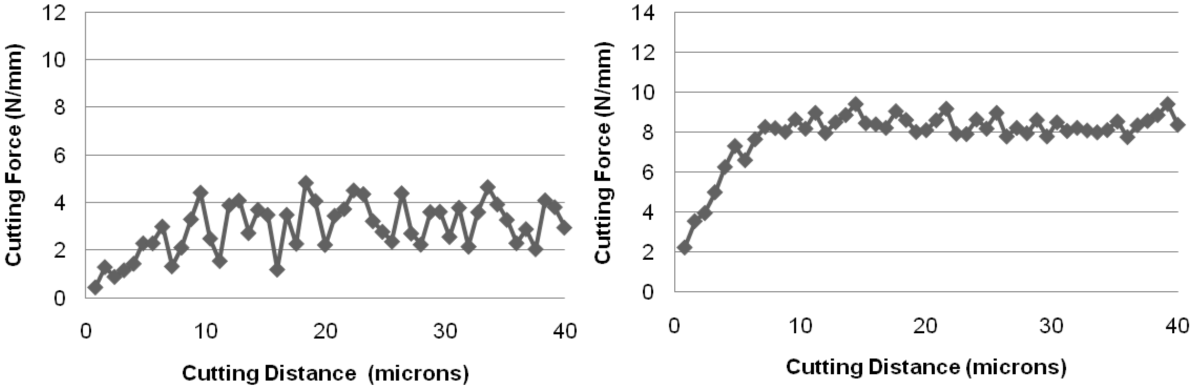

(a) 0 degrees

(b) 45 degrees

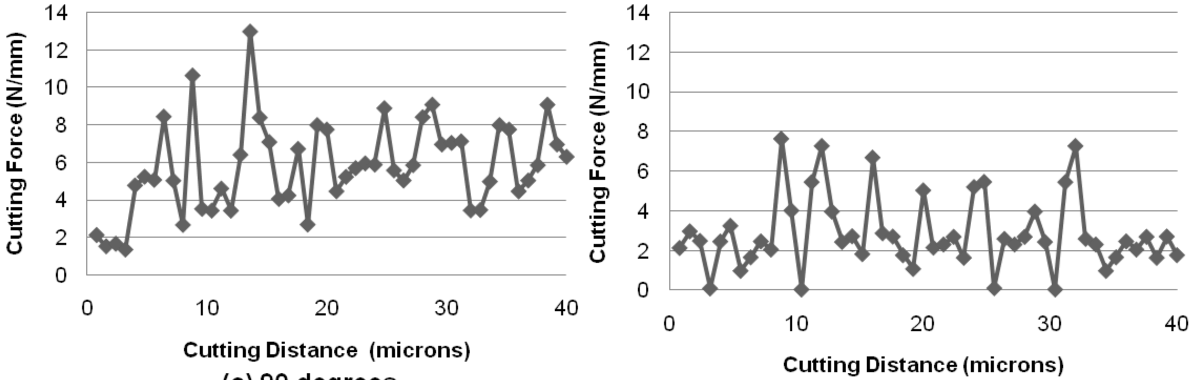

(c) 90 degrees

(d) 135 degrees

Figure 4.12. Simulated Cutting Force Profiles

Figure 4.13 shows the simulated thrust force profiles for each fiber orientation. It can be noted that the overall magnitude of the simulated thrust forces is significantly lower than for the cutting forces. In finite element machining models, it is typical for the thrust forces to be significantly underpredicted. This occurs because in a finite element simulation, as elements in the microstructure fail, they are deleted from the simulation and can no longer hold stresses. In the vertical (thrust) direction, this phenomenon has the most significant effect as after the elements along the surface of the cut fail, they are deleted and fewer elements on the surface of the cut are contributing to the thrust forces. The cutting forces; however, are effected less significantly by the element deletion algorithm as the tool continues to come in contact with elements after the previous ones have been deleted. The variability within the thrust force signal remains high and comparable for all four fiber orientations.

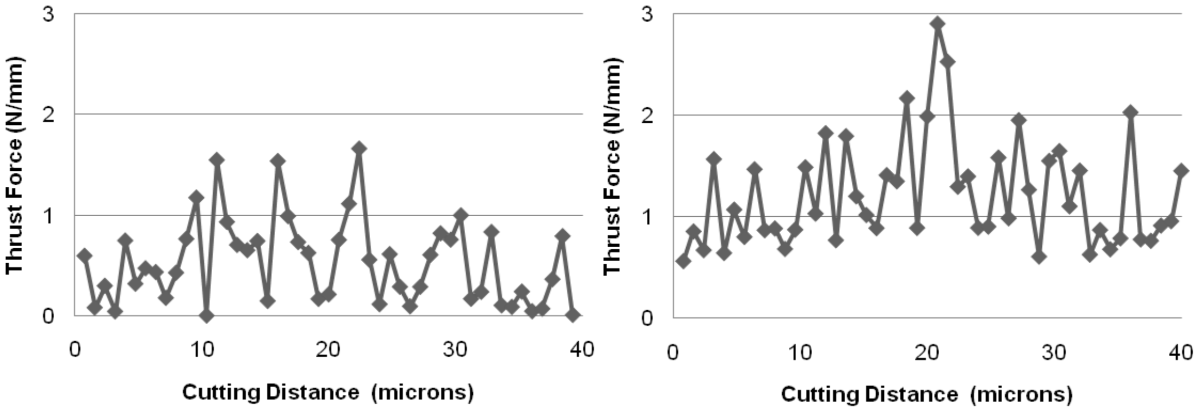

(a) 0 Degrees

(b) 45 Degrees

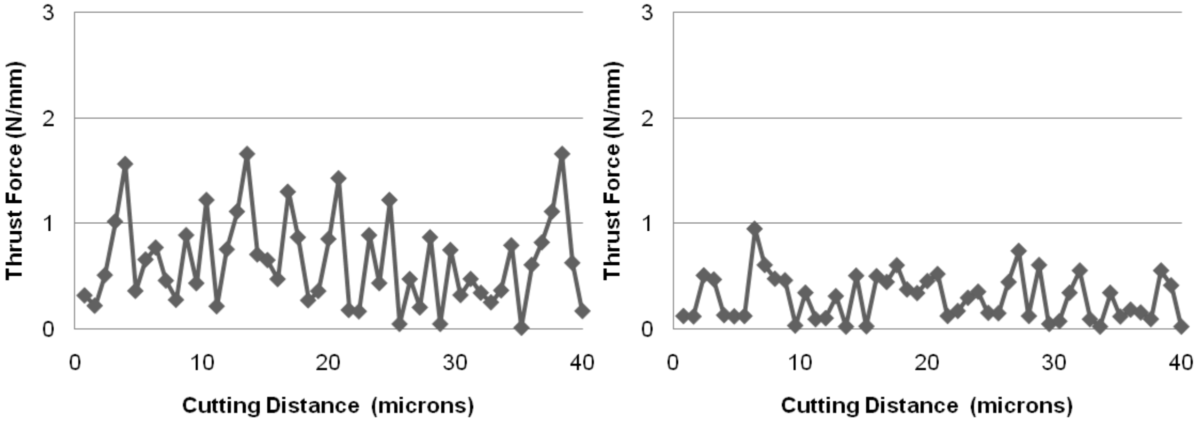

(c) 90 Degrees

(d) 135 Degrees

Figure 4.13. Simulated Thrust Force Profiles

4.4. Chapter Summary

In this chapter, a new finite element machining model approach is presented capable of improving on some of the shortcomings of both the experimentally-based models and the finite element models developed in literature. This model is capable of capturing the failure mechanisms occurring at several points throughout the chip formation process. The model was capable of predicting fiber failure mode, characteristic fiber length in the chip, and machining forces for microstructures with fibers oriented at 0, 45, 90, and 135 degrees. The fibers were observed to undergo crushing-dominated failure for the 45 and 90 degree orientations and bending-dominated failure for the 0 and 135 degree orientations for the process parameters under consideration.

The new interfacial model developed for this study was composed of traditional continuum elements, which are allowed to fail in tension or compression, thus preventing the interfacial sections from distorting excessively. Furthermore, the sections have a thickness comparable to the smallest element size in the fiber and matrix sections, which prevents a dramatic increase in the smallest stable time increment. To accommodate the normal and tangential deformation modes from traditional interfacial models, two separate damage modes were implemented simultaneously to the continuum interfacial elements. This interfacial model was able to describe chip formation mechanisms along with sub-surface damage in the form of fiber-matrix interfacial failure.

5. Validation and Interpretation of Finite Element Machining Model

In chapter 4 what was referred to as a dynamic finite element machining model was developed using a unique modeling approach. Material and failure models for the separate materials phases (viz., carbon fibers, epoxy, and interface) were developed and assigned to each microstructural component. The model is capable of predicting the fiber failure mode, characteristic fiber length in the chips, along with machining forces. In this chapter, the model will be validated by first comparing the simulated machining responses from the model to the machining responses from a set of orthogonal machining experiments, and then the model is used to find a more robust tool geometry.

The remainder of this chapter is organized as follows. In section 5.1, the experimental machining testbed is described and the details of the orthogonal machining experiments are outlined. Section 5.2 compares the results from the machining simulations and the experimental analysis with the aim of validating the finite element machining model. Section 5.3 outlines the application of the developed and validated finite element machining model with an aim to determine the effects of fiber diameter and tool geometry on the machining process.

5.1. Validation Machining Experiments

The orthogonal micro-machining experiments were performed on a 3-axis CNC micro-scale machining testbed developed at the University of Illinois. This testbed is equipped with linear voice-coil motors and encoders having a resolution of 100 nm. The testbed was suitably modified to facilitate orthogonal machining experiments. A stationary tool mount was designed for orthogonal machining with an embedded Kistler 9018 triaxial load cell. A Phantom v. 7.0 high-speed camera is implemented into the experimental setup to monitor the cutting process. Figure 5.1 shows a schematic of the experimental testbed used for model validation while Fig. 5.2 illustrates the actual orthogonal machining testbed.

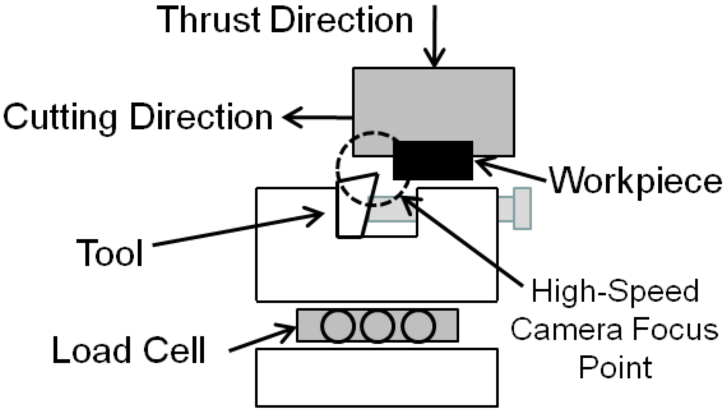

Figure 5.1. Schematic of Orthogonal Machining Testbed

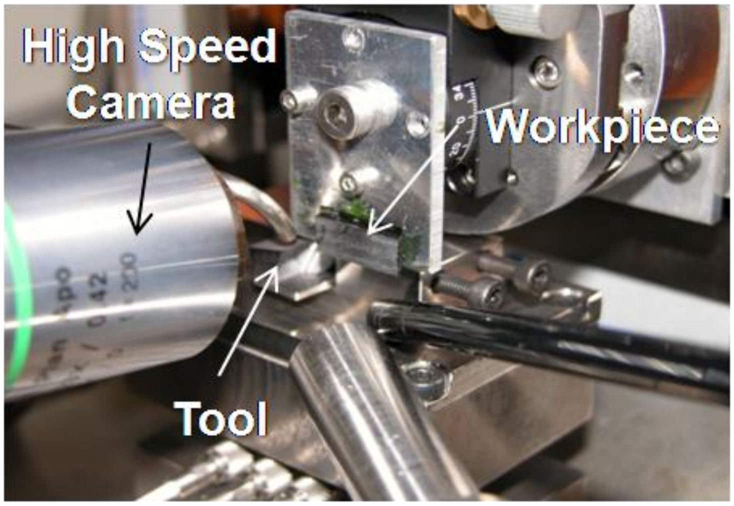

Figure 5.2. Orthogonal Machining Experimental Setup

A micro-scale orthogonal machining tool with an edge radius of 5μm and rake and clearance angles of 25 and 10 degrees, respectively, was used for the cutting operation. This tool geometry was chosen because it was identical to the tool geometry used in the machining simulations. The tool remained stationary on the mount while the cutting operation was performed with the moving of the workpiece over the tool.

The micro-scale orthogonal machining experiments were performed with depths of cut of 15 µm and 30 µm. The machining experiments were carried out at a cutting speed of 500 mm/min. Four different fiber orientations were tested: 0, 45, 90, and 135 degrees according to Fig. Figure 4.7. For each experimental condition, two replicate experiments were performed. A new tool was used for every two test conditions to avoid confounding machining responses with tool wear effects.

The machining responses were collected with two separate cutting operations. During the first cut, the high-speed camera images were collected at 400 pps. In order to prevent the forming chips from interfering with the images, an air stream was directed at the tool to clear chips from the cutting surface. The high-speed camera images were used to validate the fiber failure mode observed in the machining simulations.

During the second cut, the chips and cutting forces were collected. The chips from the cutting process were collected and examined using scanning electron microscopy (SEM) with specific attention being given to the fiber lengths in the chips collected. The chip morphology analysis was used to validate the characteristic fiber lengths in the chips from the machining simulations.

The cutting and thrust forces were collected using the Kistler load cell. Figures 5.3 and 5.4 show the raw data collected over the full 10 mm length of cut. The force values were then averaged during the steady-state region of each of the force signals. While the workpieces were approximately 1 mm thick, there was found to be some slight variance, and thus, the overall average machining force was divided by the thickness of each individual workpiece to obtain the machining forces per unit thickness (N/mm). Finally, these values were averaged across the two replicate experiments.

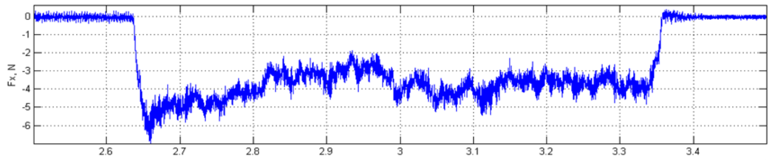

(a) 0 Degrees

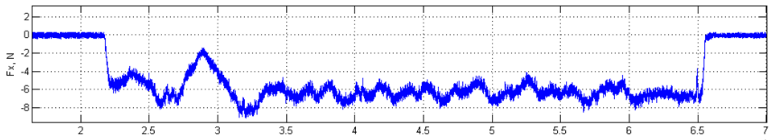

(b) 45 Degrees

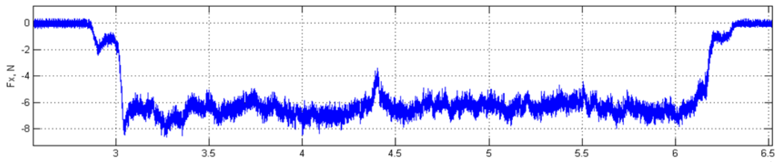

(c) 90 Degrees

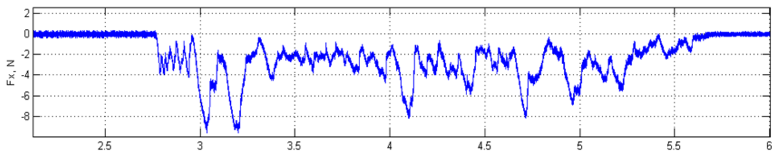

(d) 135 Degrees

Figure 5.3. Raw Cutting Force Signal

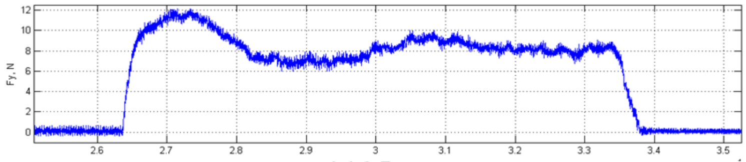

(a) 0 Degrees

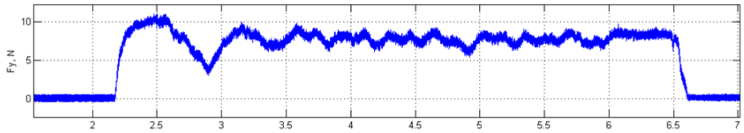

(b) 45 Degrees

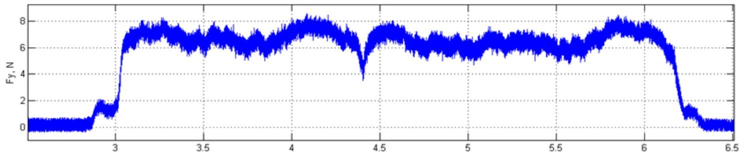

(c) 90 Degrees

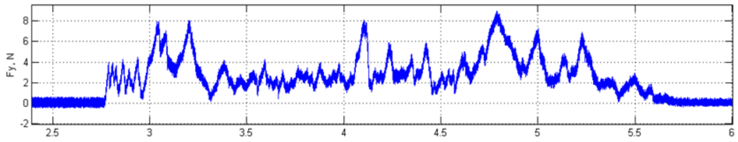

(d) 135 Degrees

Figure 5.4. Raw Thrust Force Signal

5.2. Finite Element Machining Model Validation

In validating the finite element machining model developed in Chapter 4, the machining responses from the simulation are compared to their experimental counterparts. The machining responses used for validation purposes are fiber failure mode, characteristic fiber length in the chips, and machining forces.

5.2.1. Fiber Failure Mode

To validate the fiber failure mode, the fiber failure modes (viz., bending, crushing, etc.) observed in the machining simulation are compared to the high-speed camera images captured in the experiment. Figures 4.9-4.11 are repeated here as Figs. 5.5-5.7 showing representative images from the machining simulations for each fiber orientation and DOC under consideration.

For the purpose of comparison, Fig. 5.8 shows several high-speed camera images collected for each fiber orientation and DOC.

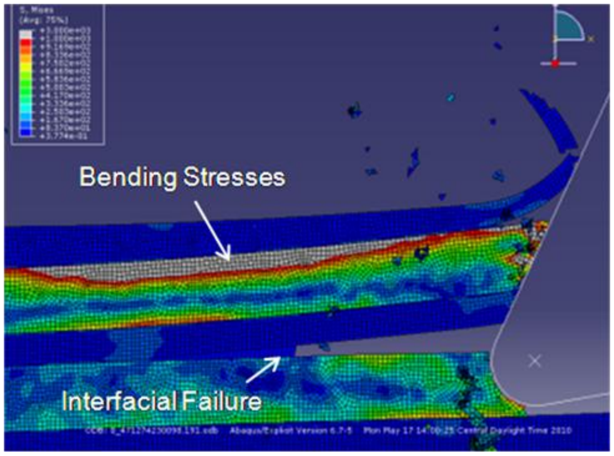

(a) 0 degree failure modes

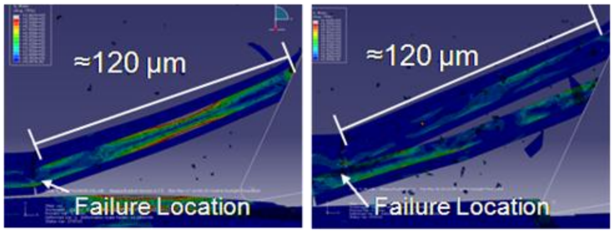

(b) 15 µm DOC (c) 30 µm DOC

Figure 5.5 . 0 Degree Simulation Reults

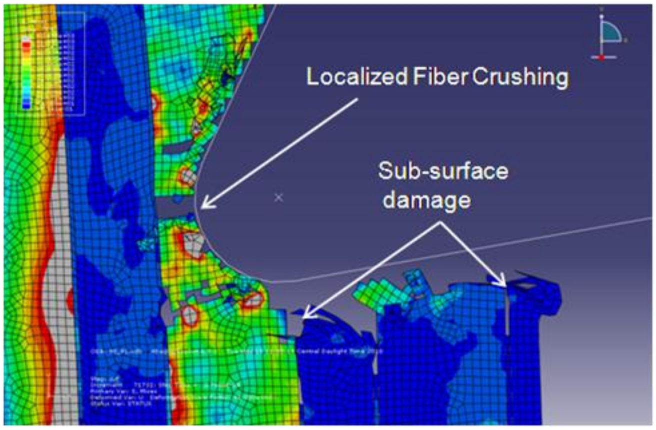

(a) 45 and 90 degree failure modes

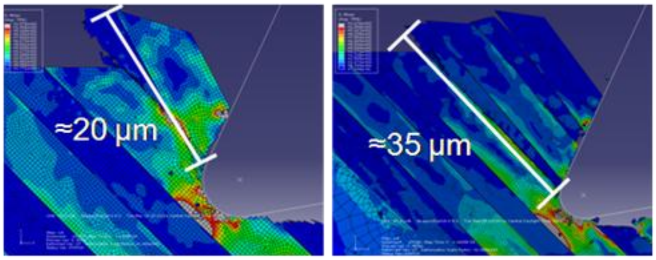

(b) 45 degrees, 15 µm DOC (c) 45 degrees, 30 µm DOC

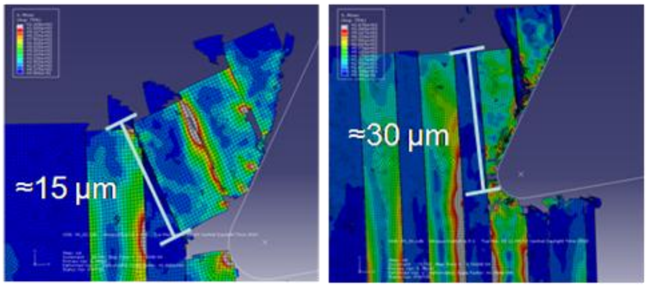

(d) 90 degrees, 15 µm DOC (e) 90 degrees, 30 µm DOC

Figure 5.6. 45 and 90 Degree Simulation Results

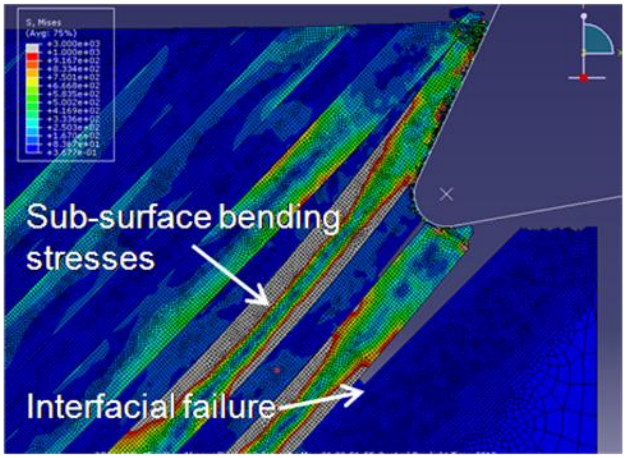

(a) 135 degree failure modes

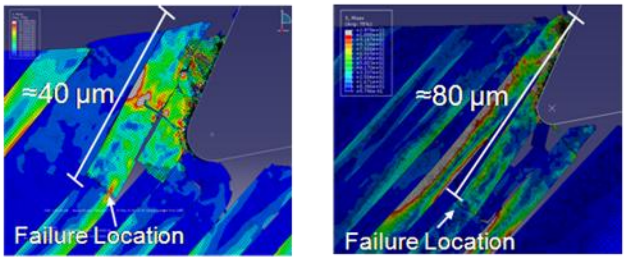

(b) 15µm DOC (c) 30µm DOC

Figure 5.7. 135 Degree Simulation Results

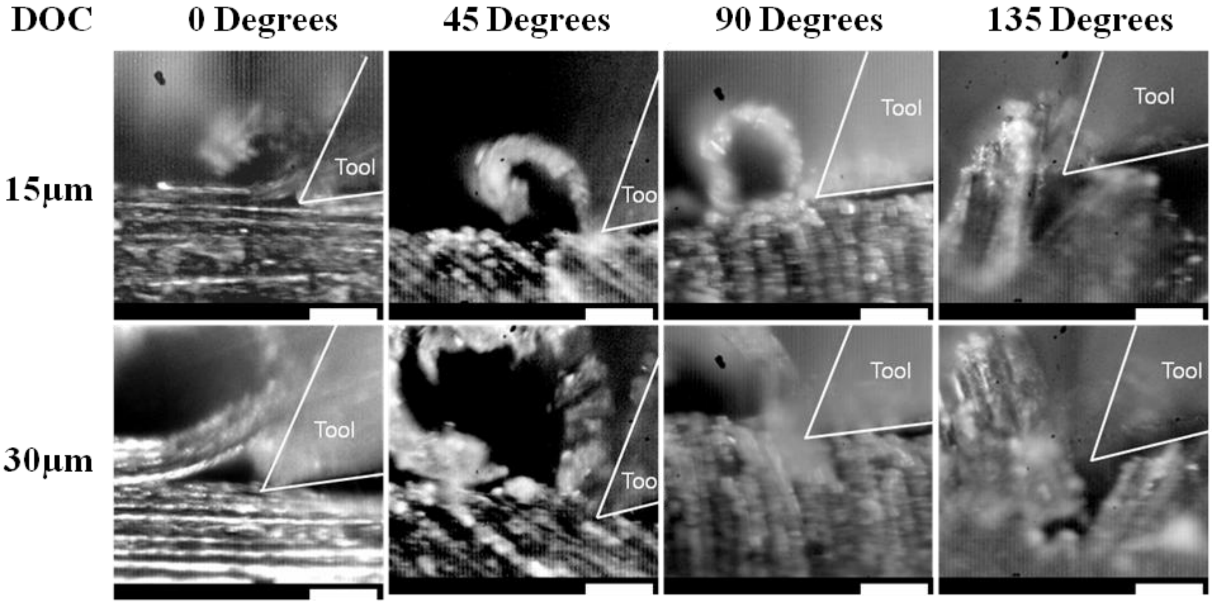

Figure 5.8. Experimental High-Speed Camera Images for Each Fiber Orientation and DOC under Consideration

The high-speed camera images for the 0 degree orientation in Fig. 5.8 agree well with the simulated failure mechanisms as the fiber bundles are seen to bend from the progressing tool and fail ahead of the cutting tool. This failure mode is also illustrated in Fig. 5.9a. While the tool contacts the fiber at Point A, the bending stresses eventually cause it to fail at Point B ahead of the tool but still along the cutting plane. The fiber failure mode observed in the 45 and 90 degree simulations agrees well with the experimental high-speed camera images seen in Fig. 5.8. The 45 and 90 degree high-speed camera images show the fibers undergo a crushing-dominated failure at the point of contact of the tool for both depths of cut under consideration. This phenomenon is further illustrated in Fig. 5.9b and c, where the fiber is seen to fail at the point of contact of the tool (Point A). The bending-dominated fiber failure mode observed for the 135 degree simulations also agrees well with the experimental high-speed camera images. The tool is seen to peel back a small bundle of fibers which fail below the cutting plane (Fig. 5.8). Figure 5.9d illustrates the failure mechanisms observed in the 135 degree simulations and experiments. The tool rake face first contacts the fiber at Point A; however, failure due to bending takes place at Point B, below the surface of the cut.

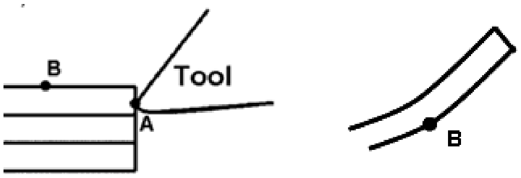

(a) 0 Degrees

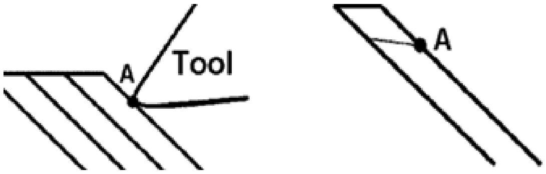

(b) 45 Degrees

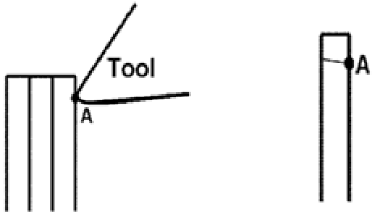

(c) 90 Degrees

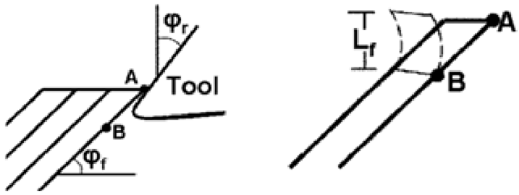

(d) 135 Degrees

Figure 5.9. Illustration of Failure Mechanisms for Fiber Orientations under Consideration

5.2.2. Characteristic Fiber Length in Chips

The characteristic fiber length in the chips is validated by comparing the characteristic fiber length in the simulated chip (Figs. 4.9-4.11) to the fiber lengths observed from the experimental chip morphology analysis. Figure 5.10 shows representative chips collected for each of the four fiber orientations and depths of cut under consideration. While there is some variability in the fiber lengths found in the chips, the general lengths are labeled and shown in Fig. 5.10.

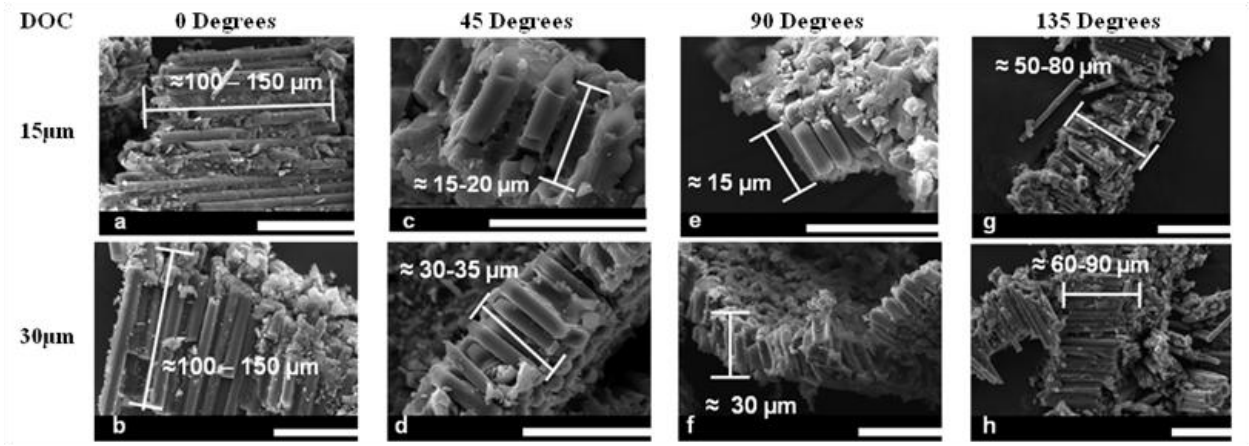

Figure 5.10. Chips Collected from Machining Experiment for Each Fiber Orientation and DOC under Consideration (Scale: Bar = 50μm)

For the 0 degree machining simulations, the fractured fibers in the chip are approximately 120μm in length. The fiber length in the chips appears to be consistent for both of the DOCs, with the only difference being the number of fibers in the chip. This agrees well with the experimental chip morphology analysis as the chips appear in the form of irregular fiber bundles with fibers approximately 100-150μm in length (Fig. 5.10a-b). Furthermore, the length of the fibers in the chips appears to be independent of the DOC of the process, which agrees well with the simulation results.

The fibers in the simulated chips for the 45 and 90 degree orientations are found to be approximately 15-35μm in length. The fiber lengths are found to correspond to the DOC of the process as failure takes place at the point of contact of the tool. The chips observed in the experimental chip morphology analysis are continuous with fibers extending through the thickness of the chip. The fiber pieces in the chip are also seen to correspond to the DOC of the process for both the 45 and 90 degree orientations as is evident in Fig. 5.10c-f.

The 135 degree simulations show chips that are approximately 40-80μm in length. The fiber length in the simulated chip is seen to be effected by the DOC of the process as the fiber length for the 30μm DOC is double that for the 15 μm DOC. For both cases, the fiber length is seen to be significantly higher than the DOC of the process as the fiber length is dictated by the location of sub-surface fiber failure. The experimental chip morphology analysis shows chips in the form of irregular fiber bundles similar to those collected from the 0 degree orientation. There is a high variability in fiber length but the majority of the fibers in the chips are found to be approximately 40-90μm in length corresponding well to the simulated chips (Fig. 5.10g-h).

Table 5.1 provides a summary of the fiber lengths in the simulated chips for each fiber orientation under consideration and a comparison with the experimental fiber lengths in the chips.

Table 5.1. Comparison of Approximate Fiber Lengths in Simulation and Expeirment

Experimental Condition		**Fiber Length (μm)**	
Orientation (degrees)	**DOC (μm)**	**Simulation**	**Experiment**
0	15	120	100-150
45	15	20	15
90	15	15	15
135	15	40	50-80
0	30	120	100-150
45	30	30	35
90	30	30	30
135	30	80	60-90

5.2.3. Cutting Forces

The simulated machining forces are validated by comparing the simulated machining force trends across the four fiber orientations to their experimental counterparts. In the cutting force comparison, attention here is given to relative force trends across the four fiber orientations.

Figure 5.11 shows a comparison of the simulated and experimental machining forces. The highest simulated cutting forces exist for the 45 and 90 degree orientations, where crushing-dominated failure is observed. Significantly lower cutting forces are seen for the 0 and 135 degree orientations where bending failure is observed. This agrees well with the experimental cutting force magnitudes and cutting force trends, as the failure mode is seen to primarily dictate the cutting forces.

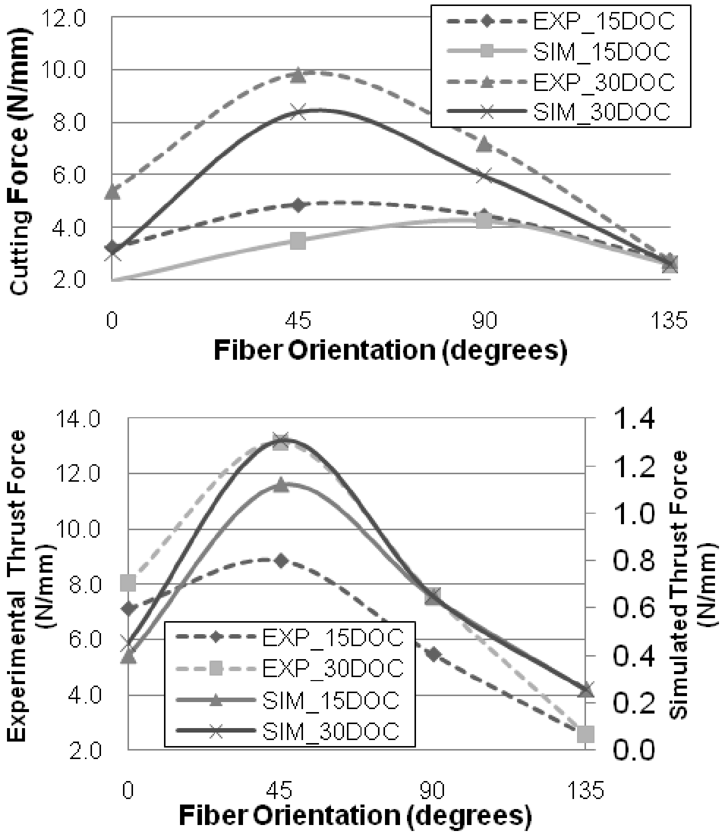

Figure 5.11. Machining Force Comparison

For thrust forces, it can be noted that while the magnitude of the thrust forces from the simulation is significantly underpredicted (see right-hand axis), the simulated thrust force trends as a function of fiber orientation agree well with the experimental results. It is noted that for both the simulated and experimental thrust forces, the highest force exists in the 45 degree orientation with a progressively lower thrust force with increasing or decreasing fiber orientation.

In examining the model machining responses (viz. fiber failure mode, characteristic fiber length in chips, and machining forces), it can be concluded that these correspond well to the experimentally obtained machining responses. Thus, the developed finite element machining model can be considered to be sufficiently validated and as such, can be applied in further machining process analysis.

5.3. Application of Machining Model

5.3.1. Motivation for Parametric Study

In the machining of more complex geometries such as rounded edges and curvilinear features in CFRPs, the tool will encounter a full range of fiber orientations, and thus, the process conditions must be selected with this in mind. While the micro-scale machining of CFRPs has been shown to be a feasible manufacturing option, there are several manufacturing complications which arise in specific fiber orientations. First, the sub-surface fiber and interfacial failure occurring in the 135 degree orientation has been observed to yield a poor quality surface finish, which leads to tolerance limitations and poor structural integrity of the machined surface [9]. Secondly, the high cutting and thrust forces observed in machining in the 45 and 90 degree orientations lead to high rates of tool wear, which is a major limitation of composite machining [70].

While fiber orientation has been observed to play a dominant role in determining the fiber failure mechanisms, other factors have been found to play secondary roles. As new carbon fiber manufacturing processes are developed, it is likely that the fiber diameter may vary for material design purposes. It is possible for the fiber failure mechanisms to be affected by the fiber size and as such, it is important to understand the effect of fiber diameter on the machining response of the material.

5.3.2. Experimental Design

In this simulation study, two process parameters will be investigated in determining their effects on the fiber failure mechanisms occurring in the machining process. Specific attention will be given to the reduction of sub-surface damage in the 135 degree orientation and reduction of machining forces in the 45 degree orientation. Model simulations with a new tool geometry and smaller fiber diameter will be investigated with the aim of improving the machining response of the material.

The new tool geometry used for the study had a rake angle (α) of 50 degrees and a tool edge radius (r_e) of 1 µm as compared to the original tool having a rake angle of 25 degrees and edge radius of 5 µm. To examine the effect of fiber size on machining forces, secondary microstructures were simulated with 3.5 µm diameter fibers as compared to the original 7.5 µm diameter fibers with the remainder of the microstructure simulation parameters being identical to those outlined in Table 4.1. For each fiber orientation under consideration, a separate 2^2 factorial design experiment was run with levels outlined in Table 5.2. The simulations were run with a 30 µm DOC in all four fiber orientations with the other simulation conditions remaining identical to the previous validation analysis.

Table 5.2. Levels for Facotial Design Experiment

	Level	
Parameter	**Low**	**High**
Tool Geometry	α=25µm , r_e=5µm	α=50µm , r_e=1µm
Fiber Diameter (µm)	3.5	7.5

5.3.3. Simulation Results

Figure 13 shows a comparison of the cutting and thrust forces for both tool geometries and fiber diameters under consideration. For the 45 and 90 degree fiber orientations, the cutting force is seen to reduce significantly with the new tool geometry for both fiber diameters. The higher rake angle allows the chips to flow up the rake face of the tool with less resistance resulting in a lower cutting force. This phenomenon is also exhibited in the 0 degree orientation, but to a lesser degree. The thrust forces are seen to be similarly affected by tool geometry as the thrust forces in the 45 degree orientation are notably lower with the new tool geometry. While a decrease in machining forces is observed for the 0, 45, and 90 degree orientations, the failure modes remain identical to those found with the original tool geometry.

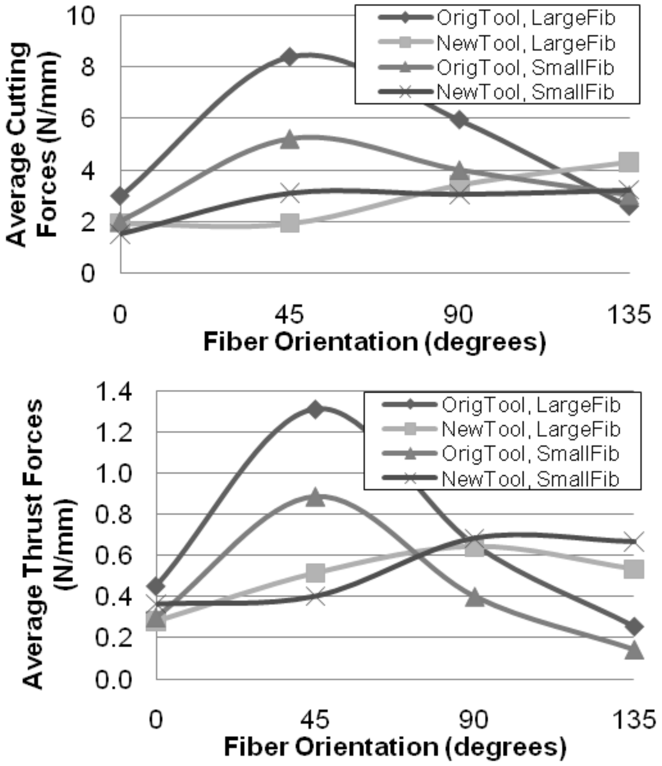

Figure 5.12. Cutting and Thrust Forces from Parametric Study

The cutting and thrust force in the 135 degree orientation are observed to increase with the new tool geometry. With the original tool geometry, the tool first contacts the fiber with the tool rake face because of the fiber angle-rake angle relationship. The tool contacts a large area of the fiber along the rake face instead of providing a concentrated stress on the fiber from the tool tip. This leads to bending-dominated failure below the surface of the cut as seen in Fig. 14a. With the new tool geometry, the lower tool tip edge radius provides a much more concentrated stress on the fiber while the higher rake angle allows the tool to contact the fiber with the tip before the rake face as seen in Fig. 14b. This results in a crushing failure similar to that observed for the 45 and 90 degree orientations instead of a bending failure with the original tool geometry, which causes an increase in cutting and thrust forces.

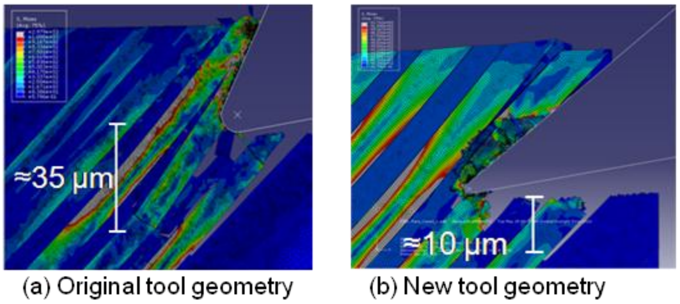

(a) Original tool geometry (b) New tool geometry

Figure 5.13. Effect of Tool Geometry on Sub-Surface Damage in the 135 Degree Orientation

With the new tool geometry, the cutting forces are much more consistent with lower force variability across fiber orientations. Also, the overall cutting and thrust force magnitudes decrease significantly, which would result in a significant decrease in tool wear. At the same time, the tool is capable of locally crushing the fibers in the 135 degree orientation which results in a decrease in sub-surface damage.

When machining with the original tool geometry, the force magnitudes are seen to decrease significantly with the 3.5 µm diameter fibers. This effect is observed to be the most significant in the 45 and 90 degree orientations, implying that the fiber size primarily affects the machining forces in a fiber orientation where crushing failure is dominant. With the new tool geometry, the fiber diameter has little affect on the machining force trends or magnitudes.

In summary, the new tool geometry is found to reduce the cutting and thrust forces in the 45 degree orientation and reduce the depth of sub-surface damage in the 135 degree orientation. Furthermore, the new tool geometry is more robust as factors such as variation in fiber orientation and fiber diameter have a comparatively insignificant affect on the machining forces.

5.4. Chapter Summary

The model was validated by comparing the model simulation results to the results from a set of CFRP machining experiments with identical process parameters. The developed finite element machining model was found to be capable of accurately predicting fiber failure mode, characteristic fiber length in the chip, and machining forces. In particular, the model was found to accurately describe fiber failure mode, characteristic fiber length in the chips, and machining forces.

Using the model, the affects of tool geometry and fiber size were investigated. A new more robust tool design was found where the affect of fiber size and orientation on machining forces was reduced significantly. Furthermore, the tool geometry caused the fibers in the 135 degree orientation to fail in crushing instead of bending, thus reducing the depth of sub-surface damage.

6. Conclusions and Recommendations.

The objective of this research was to gain a better understanding of the fiber failure mechanisms occurring in the micro-scale CFRP machining process. To this end, a model was proposed and experiments were conducted to shed light on the validity of the proposed failure mechanisms. Subsequently, a finite element-based model was developed to obtain a more fundamental understanding of the failure mechanisms involved in micro-scale CFRP machining as a function of fiber orientation.

This research was focused on determining the effect of fiber orientation on the fiber failure mechanisms occurring in the micro-machining process. Specific attention was given to carbon fiber reinforced composites with fiber orientations of 0, 45, 90, and 135 degrees with respect to the direction of tool motion in an effort to cover the full range of fiber orientations encountered in the machining of CFRP composites.

6.1. Conclusions

The following is a set of conclusions that can be taken from this work:

Micro-Scale Fiber Failure Mechanisms

1. The fiber failure mechanisms occurring in the micro-scale machining process were found to be notably different than their macro-scale counterparts. These differences exhibited themselves most significantly in the 45 and 90 degree orientations where the fibers were found to fail in crushing rather than bending as is typical at the macro-scale. For the 0 degree fiber orientation, the fibers were found to either fail in bending or buckling dominated failure, depending on the tool edge radius and DOC under consideration. For

the 135 degree orientation, the fibers were observed to fail in bending at the micro-scale, similar to the macro-scale failure mechanisms.

2. The chip morphology analyses agrees with the proposed micro-scale failure mechanisms since the chips in the 45 and 90 degree orientations show small fragmented chips indicating crushing-dominated failure, while the chips collected for the 0 and 135 degree orientations had fiber significantly longer than the FPT or DOC of the process indicating bending or buckling dominated failure.
3. The delamination patterns observed support the failure modes proposed as the bending or buckling-dominated failure in the 0 degree orientation results in negligible delamination while the sub-surface bending failure in the 135 degree orientations results in the highest positive delamination. Both the 45 and 90 degree orientations showed low positive delamination because the fiber failed in crushing at the point of contact of the tool.
4. The cutting force trends correlate with the proposed fiber failure modes. The machining forces in the 45 and 90 degree orientations are significantly higher than the force in the 0 and 135 degree orientations, indicating that a crushing failure results in a higher force than a bending or buckling-dominated failure.

Finite Element Machining Model Development and Interpretation:

5. The microstructure of a carbon fiber-reinforced polymer composite was characterized using three parameters: fiber angle, fiber grouping number, and matrix spacing. Statistical distributions for each parameter were determined and used to simulate the microstructure.
6. A new finite element machining modeling approach is outlined in this work capable of capturing the fiber failure mechanisms occurring at several points throughout the chip

formation process. This unique approach was referred to as a dynamic analysis as it is capable of illustrating the full chip formation process and sub-surface damage. The model was capable of predicting fiber failure mode, characteristic fiber length in the chip, and machining forces for fiber orientations of 0, 45, 90, and 135 degree orientations.

7. The interfacial model developed in this study is based on the use of continuum elements to model the fiber-matrix interface. The continuum interfacial elements used to model the fiber-matrix interface are assigned two separate damaged models and allowed to fail in both tension and compression. The fiber-matrix interface was found to play a critical role in the fiber failure mechanisms occurring in the chip formation process.
8. The fibers were determined to fail in bending for the 0 degree orientation along the trim plane while for 135 degree orientation, the fibers failed in bending below the trim plane. For the 45 and 90 degree orientations, crushing at the point of contact of the tool was found to be the dominant failure mode.
9. For the 0 and 135 degree orientations where bending-dominated failure is prevalent, the characteristic fiber lengths in the chips were found to be significantly longer than the DOC of the process as the failure takes place away from the cutting tool. In the 45 and 90 degree orientations, the crushing-dominated failure resulted in short fiber fragments in the chips of length comparable to the DOC of the process.
10. The simulated cutting forces with respect to fiber orientation were found to agree well with the experimentally obtained machining forces. The simulated thrust force trends with respect to fiber orientation were found to accurately represent those obtained experimentally; however, the overall thrust force magnitude was found to be significantly underpredicted.

11. To determine model validity, the simulation results based on fiber failure mode, characteristic fiber length in the chips, and machining forces were compared to the results from a set of CFRP orthogonal machining experiments with identical process parameters. The developed finite element machining model was determined to be valid and capable of accurately predicting machining responses.
12. To examine the affects of tool geometry and fiber diameter on the machining responses, the model was used to simulate the cutting process for a tool with a higher rake angle (50 degrees) and lower edge radius (1 µm) as compared to the original tool geometry (rake angle: 25 degrees, edge radius: 5 µm) along with microstructures with a smaller fiber diameter. This parametric study was used to show the capabilities of the developed finite element machining model in predicting machining responses.
13. It was determined that the new tool geometry allowed for the fibers in the 135 degree orientation to fail in crushing instead of bending, thus reducing the depth of subsurface damage and indicating that tool geometry plays an important role in the fiber failure mechanisms. Furthermore, the new tool geometry studied was more robust as the affect of fiber size and fiber orientation on machining forces was reduced significantly.

6.2. Recommendations for Future Work

1. While the finite element machining model and experimentally-based micro-scale model in this work focused on CFRP composites, there are many other fiber reinforced materials which are commonly used in both micro and macro-scale applications. These include glass, boron, and aramid fiber composites. While some of the orientation-based failure mechanisms may be similar for these materials, it would be helpful to develop similar

finite element machining models to explore any significant differences. In order to simulate the machining process for these new fiber reinforcement materials, new material and failure models would need to be developed. Furthermore, validation experiments similar to those used in this study for CFRP composites could be executed in an aim to validate the new material and failure models.

2. While the models developed in this work were validated for the process parameters under consideration, it would be beneficial to observe if the machining responses remain similar for other process parameters (viz., increase DOC, negative rake angles, large edge radii). Thus, a secondary parametric study could be executed using different process parameters to observe if the model is valid for process parameters outside the range considered in the original simulations.
3. While this work was focused on long aligned unidirectional fiber composites, other fiber configurations are commonly used. Randomly orientated short fibers, aligned short fibers, or plies of differing fiber orientations are all common FRP microstructures whose machining behavior could be more fully investigated. In order to simulate the machining process on other fiber configurations, new parametrization schemes could be developed in order to characterize these new material microstructures. To examine the effect of other fiber configurations on the machining process, simulations could be carried out using the new developed microstructures.
4. Now that a fundamental understanding of CFRP failure mechanisms occurring in the machining process has been achieved, this information can be applied to designing machining processes for actual CFRP components. Specifically, the manufacturing processes for more complex features such as curvilinear and three-dimensional features

can be developed. Using the results obtained in this study, complex geometries could be machined experimentally with improved processing results.

References

[1] Sheikh-Ahmad, J.Y. *Machining of Polymer Composites.* Springer Science, 2009.

[2] DiPaolo, G. *Drilling Fiber-Reinforced Composite Matierials: A Hole Quality Modeling Investigation with Emphasis on Crack Growth.* M.S. Thesis, Urbana-Champaign: University of Illinois, 1995.

[3] Hull, D. *An Introduction to Composite Materials.* Cambridge: Cambridge University Press, 1981.

[4] Isaac M. Daniel, Ori Ishai. *Engineering Mechanics of Composite Materials.* New York: Oxford University Press, 2006.

[5] Puw, H.Y., Hocheng, H., Kuo, H.C. "Anisotropic Chip Formation Models of Cutting of FRP." *MED Vol. 2(1)*, 1995: 259-282.

[6] Sakuma, K., Seto, M. "Tool Wear in Cutting Glass-Fiber-Reinforced Plastics." *Bulletin of the JSME, Vol. 26(218)*, 1983: 1420-1427.

[7] Konig, W., Wulf, C., Gra, P., Willersceid, H. "Machining of Fiber Reinforced Plastics." *Ann. CIRP, Vol. 34*, 1985: 537-547.

[8] Koplev, A. "Cutting of CFRP with Single Edge Tool." *ICCM3.* Paris, 1980. 1597-1605.

[9] Ramulu, M. "Machining and Surface Integrity of Fiber-Reinforced Plastic Composites." *Sadhana, Vol. 22(3)*, 1997: 449-472.

[10] Santhanakrishnan, G., Krishnamurthy, R., Malhotra, S.K. "High Speed Steel Tool Wear Studies in Machining of Glass-Fiber-Reinforced Plastics." *Wear, Vol. 132*, 1989: 327-336.

[11] Sakuma, K., Seto, M., Taniguchi, M. "Tool Wear in Cutting Carbon-Fiber-Reinforced

Plastics." *Bulletin of JSME, Vol. 28(245)*, 1985: 2781-2788.

[12] An, S., Lee, E., Noh, S. "A Study on the Cutting Characteristics of Glass Fiber Reinforced Plastics with Respect to Tool Materials and Geometries." *J. Mat. Process. Tech.*, 1997: 60-67.

[13] Kaneeda, T. "CFRP Cutting Mechanism." *North American Manufacturing Research Inisttute of SME.* 1991. 216-221.

[14] Komanduri. "Machining of Fiber-Reinforced Composites." *Machining Sci. and Tech, Vol. 1(1)*, 1997: 113-152.

[15] Wang, D.H., Ramulu, M., Arola, D. "Orthogonal Cutting Mechanisms of Graphite/Epoxy Composite. Part 1: Unidirectional Laminate." *Int. J. Mach. Tools Manufact., Vol 35(12)*, 1995: 1623-1638.

[16] Koplev, A., Lystrup, A., Vorm, T. "The Cutting Process, Chips, and Cutting Forces in Machining CFRP." *Composites Vol. 14(4)*, 1983: 371-376.

[17] Hocheng, H., Puw, H.Y., Huang, Y. "Preliminary Study on Milling of Unidirectional Carbon Fiber-Reinforced Plastics." *Composites Manufacturing, Vol. 4(2)*, 1993: 103-108.

[18] Arola, D., Ramulu, M., Wang, D.H. "Chip Formation in Orthogonal Trimming of Graphite/Epoxy Composite." *Composites Part A., Vol 27*, 1996: 121-133.

[19] Wang, D.H., Ramulu, M., Arola, D. "Orthogonal Cutting Mechanisms of Graphite/Epoxy Composite. Part II: Multi-Directional Laminate." *Int. J. Mach. Tools Manufact., Vol 35(12),* 1995: 1639-1648.

[20] Pickering, K.L., Bader, M.G., Kimber, A.C. "Damage Accumulation During the Failure of Uniaxial Carbon Fiber Composites." *Composites*, 1998: 435-441.

[21] Bhatnagar, N., Ramakrishnan, N., Naik, N.K., Komanduri, R. "On the Machining of Fiber Reinforced Plastic (FRP) Composite Laminates." *Int. J. Mach. Tools Manufact., Vol. 35(5),* 1995: 701-716.

[22] Pwu, H.Y., Hocheng, H. "Chip Formation Model of Cutting Fiber-Reinforced Plastics Perpendicular to Fiber Axis." *J. Manufacturing Science and Engineering, Vol. 120(1),* 1998: 192-196.

[23] Wern, C.W., Ramulu, M., Shukla, A. "Investigation of Stresses in the Orthogonal Cutting of Fiber-Reinforced Plastics." *Experimental Mechanics*, 1995: 33-41.

[24] Wang, X.M., Zhang, L.C. "An Experimental Investigation into the Orthogonal Cutting of Unidirectional Fiber Reinforced Plastics." *Int. J. Mach. Tools & Manufacture, Vol. 43,* 2003: 1015-1022.

[25] Takeyama, H., Iijima, N. "Machinability of Glassfiber Reinforced Plastics and Application of Ultrasonic Machining." *Annals of the CIRP, Vol. 37(1),* 1988: 93-96.

[26] Pwu, H.Y., Hocheng, H. "Machinability Test of Carbon Fiber-Reinforced Plastics in Milling." *Mat. & Manufact. Proc., Vol. 8(6),* 1993: 717-729.

[27] Gordon, S., Hillery, M.T. "A Review of the Cutting of Composite Materials." *Proc. Instn. Mech. Engrs. Vol. 217L,* 2003: 35-45.

[28] Rahman, M., Ramakrishna, S., Prakash, J.R.S, Tan, D.C.G. "Machinability study of Carbon Fiber Reinforced Composite." *J. Mat. Process. Tech.*, 1999: 292-297.

[29] Nayak, D., Bhatnagar, N., Mahajan, P. "Machining Studies of Uni-Directional Glass Fiber Reinforced Plastic (UD-GFRP) Composites Part 1: Effect of Geometrical and Process Parameters." *Mach. Sci. and Technology, Vol. 9,* 2005: 481-501.

[30] Friend, C.A., Clyne, R.W., Valentine, G.G. "Machining Graphite Composite Materials." 1973: 217-225.

[31] Zhou, L., Wang, C.Y., Qin, Z. "Investigation of Chip Formation Characteristics in Orthogonal Cutting of Graphite." *Mat. and Manufact. Processes, Vol. 24,* 2009: 1365-1372.

[32] Inoue, Hisahiro. "Study on the Cutting Mechanism of GFRP." *Composite Materials and Structures.* Beijing, China, 1986.

[33] Abrate, S., Walton, D.A. "Machining of Composite Materials. Part I: Traditional Methods." *Composites Manufacturing, Vol. 3(2),* 1992: 75-82.

[34] Dandekar, C., Shin, Y. "Multiphase Finite Element Modeling of Machining Unidirectional Composites: Prediction of Fiber Debonding and Damage." *J. Manufacturing Science and Technology*, 2008.

[35] Kalla, D., Lodhia, P., Bajracharya, B., Twomey, J., Sheikh-Ahmad, J. "CN Force Prediction Model in Milling of Carbon Fiber Reinforced Polymers." *SPIE Vol. 5999.* 2005.

[36] Merchant, M.E. "Mechanics of the Metal Cutting Process, Parts 1 and 2." *J. Applied Physics, Vol. 16*, 1945: 318-324.

[37] Everstien, C.G., Rogers, T.G. "A Theory of Machining of Fiber-Reinforced Materials." *Composite Materials*, 1971: 94-106.

[38] Iosipescu, N. "New Acurate Procedure for Single Shear Testing of Metals." *J. Materials Vol. 2(3)*, 1967: 537.

[39] Zhang, L.C., Zhang, H.J., Wang, X.M. "A Force Prediction Model for Cutting Unidirectional Fiber-Reinforced Plastics." *Machining Science and Technology, Vol. 5(3),* 2001: 293-305.

[40] Venu Gopala Rao, G., Mahajan, P., Bhatnagar, N. "Three-Dimensional Macro-Mechanical Finite Element Model for Machining of Unidirectional-Fiber Reinforced Polymer Composites." *Materials Science and Engineering, Vol. 498A*, 2008: 142-149.

[41] Venu Gopala Rao, G., Mahajan, P., Bhatnagar, N. "Micro-Mechanical Modeling of Machining of FRP Composites - Cutting Force Analysis." *Composites Science and Technology*, 2007: pp. 579-593.

[42] Nayak, D., Singh, I., Bhatnagar, N., Mahajan, P. "An Analysis of Machining Induced Damages in FRP Composites - A Micromechanics Finite Element Approach." *Materials Processing and Design*, 2004: 327-331.

[43] Venu Gopala Rao, G., Mahajan, P., Bhatnagar, N. "Machining of UD-GFRP Composites Chip Formation Mechanism." *Composites Science and Technology, Vol. 67*, 2007: 2271-2281.

[44] Mahdi, M., Zhang, L. "A Finite Element Model for the Orthogonal Cutting of Fiber-Reinforced Composite Materials." *J. Mat. Processing Technology, Vol. 113*, 2001: 373-377.

[45] Ramesh, M.V., Seetharamu, K.N., Ganesan, N., Sivakumar, M.S. "Analysis of Machining of FRPs Using FEM." *In. J. Machining Tools & Manufacture, Vol. 38*, 1998: 1531-1549.

[46] Venu Gopala Rao, G., Mahajan, P., Bhatnagar, N. "Three-Dimensional Macro-Mechanical Finite Element Model for Machining of Unidirectional-Fiber Reinforced Polymer Composites." *Materials Science and Engineering, Vol. 498*, 2008: 142-149.

[47] Arola, D., Ramulu, M. "Orthogonal Cutting of Fiber-Reinforced Composites: A Finite Element Analysis." *In. J. Mechanical Science*, 1997: 597-613.

[48] Isaac M. Daniel, Ori Ishai. *Engineering Mechanics of Composite Materials.* New York:

Oxford University Press, 2006.

[49] Hill, R. "A Theory of the Yielding and Plastic Flow of Anisotropic Metals." *Mathematical and Physical Sciences, Vol. 193*, 1947: 281-297.

[50] Jones, R.M. *Mechanics of Composite Materials.* Taylor and Francis, 1999.

[51] Rahulkumar, P., Jagota, A., Bennison, S.J., Saigal, S. *Journal of Solids and Structures, Vol. 37*, 2000: 1873-1897.

[52] Camanho, P.P., Davila, C.G. *Mixed-Mode Decohesion Finite Elements for the Simulation of Delamination in Composite Materials.* Hampton, VA: NASA, 2002.

[53] Pwu, H.Y. "Milling Force Prediction for Fiber Reinforced Plastics." *Machining of Composite Materials II.* Pittsburgh, PA, 1993. 97-108.

[54] Honjo, K. "Fracture Toughness of PAN-Based Carbon Fibers Estimated from Strength-Mirror Size Relation." *Carbon. Vol. 41*, 2003: 979-984.

[55] Lomakin, E.V., Zobnin, A.I., Berezin, A.V. "Finding the Fracture Toughness Characteristics of Graphite Materials in Plane Strain." *Problemy Prochnosti, Vol. 4.*, 1975: 89-92.

[56] Hobbiebrunken, T., Fiedler, B., Hojo, M., Ochiai, S., Schulte, K. "Microscopic Yielding of CF/Epoxy Composites and the Effect on the Formation of Thermal Residual Stresses." *Composites Science and Technology*, 2005: 1625-1635.

[57] Hibbit, K.A.S. *ABAQUS Theory and User Manuals Version 6.9.* ABAQUS, Inc., 2009.

[58] Mkaddem, A., Demirci, I., El Mansori, M. "A Micro-Macro Combined Approach Using FEM for Modeling of Machining of FRP Composites: Cutting Force Analysis." *Composites Science and Technology*, 2008: 3123-3127.

[59] Nayak, D., Bhatnagar, N. "Machining Studies of UD-FRP Composites Part 2: Finite

Element Analysis." *Machining Science and Technology,* 2005: 503-528.

[60] Oshawa, T., Miwa, M., Kawade, M. "Axial Compressive Strength of Carbon Fiber." *Journal of Applied Poymer Science, Vol. 39,* 1990: 1733-1744.

[61] www.ACP-Composites.com.

[62] Bourne, K., Jun. M.B., Kapoor, S.G., DeVor, R.E. "An Acoustic Emission-Based Method for Determining Contact Between a Tool and Workpiece at the Micro-Scale." *Journal of Manufacturing Science and Engineering, Vol. 130,* 2008.

[63] Venu Gopala Rao, G., Mahajan, P., Bhatnagar, N. "Micro-Mechanical Modeling of Machining of FRP Composites - Cutting Force Analysis." *Composites Science and Technology, Vol 67,* 2007: 579-593.

[64] Xia, Z., Ellyin, F. "Time-Dependent Behavior and Viscoelastic Constitutive Modeling of an Epoxy Polymer." *Polymers and Polymer Composites, Vol. 6(2),* 1998: 75-83.

[65] Jordan, J.L., Roley, J.R., Siviour, C.R. "Mechancal Properties of Epon 826/DEA Epoxy." *Mechanics of Time-Dependent Materials, Vol. 12,* 2008: 249-272.

[66] Zhou, Y., Wang, Y., Xia, Y., Jeelani, S. "Tensile Behavior of Carbon Fiber Bundles at Different Strain Rates." *Materials Letters, Vol. 64,* 2010: 246-248.

[67] Pitkethly, M.J., Doble, J.B. "Characterizing the Fiber/Matrix Interface of Carbon Fiber-Reinforced Composites Using a Single Fiber Pull-Out Test." *Composites, Vol. 21,* 1990: 389-395.

[68] Meurs, P.F.M., Schrauwen, B.A.G., Schreurs, P.J.G., Peijs, T. "Determination of the Interfacial Normal Strength Using Single Fiber Model Composites." *Composites, Vol. 29A,* 1998: 1027-1034.

[69] Caprino, G., Nele, L. "Cutting Forces in Orthogonal Cutting of Unidirectional GFRP Composites." *J. Engr. Mat. & Tech.*, 1996: 419-425.

[70] Sung, N., Suh, N.P. "Effect of Fiber Orientation on Friction and Wear of Fiber Reinforced Polymeric Composites." *Wear, Vol. 53*, 1979: 129-141.

[71] Ferreira, J.R., Coppini, N.L., Miranda, G.W.A. "Machining Optomization in Carbon Fiber Reinforced Composite Materials." *J. Mat. Process. Tech.*, 1999: 135-140.

[72] Paulo Davim, J., Reis, P., Conceicao Antonio, C. "A Study on Milling of Glass Fiber Reinforced Plastics Manufactured by Hand-Lay Up Using Statistical Analysis (ANOVA)." *Composites Structures, Vol. 64*, 2004: 493-500.

[73] Gilat, A., Goldberg, R.K., Roberts, G.D. "Strain Rate Sensitivity of Epoxy Resin in Tensile and Shear Loading." *J. Aerospace Engr.*, 2007: 75-89.

[74] Caprino, G., Santo, L., Nele, L. "Interpretation of Size Effect in Orthogonal Machining of Composite Materials. Part I: Unidirectional Glass-Fiber-Reinforced Plastics." *Composites, Vol. 29A*, 1998: 887-892.

[75] Caprino, G., Santo, L., Nele, L. "On the Origin of Cutting Forces in Machining Unidirectional Composite Materials." *Engr. Systems Design and Analysis Conf.* Montpellier, 1996. 83-89.

[76] S.W., Tsai. "A Survey of Macroscopic Failure Criteria for Composite Materials." *J. of Reinforced Plastics and Composites, Vol. 3*, 1984: 40-62.

[77] Wang, X.M., Zhang, L.C. *Abrasive Technology: Current Development and Applications, Vol. 1*, 1999: 429.

[78] Isaac, M.D., Ori, I. *Engineering Mechanics of Composite Materials.* Oxford University

Press, 2006.

[79] Wood, R.J., Avadhanula, S., Sahai, R., Steltz, E., Fearing, R.S. "Microrobot Design Using Fiber-Reinforced Composites." *J. of Mechanical Design, Vol. 130,* 2008: 1-11.

[80] Ramesh, M.V., Seetharamu, K.N., Ganesan, N., Sivakumar, M.S. "Analysis of Machining of FRPs using FEM." *Int. J. of Machine Tools & Manufacture, Vol. 38,* 1998: 1531-1549.

[81] Mahdi, M., Zhang, L. "A Finite Element Model for the Orthogonal Cutting of Fiber-Reinforced Composite Materials." *J. of Materials Processing Technology, Vol. 113,* 2001: 373-377.

[82] Hibbit, K.A.S. *ABAQUS Theory and User Manuals Version 6.9.* USA: ABAQUS Inc., 2009.

[83] Caprino, G., Nele, L. "Cutting Forces in Orthogonal Cutting of Unidirectional GFRP Composites." *J. Engineering Materials and Technology, Vol. 118*, 1996: 419-425.

[84] Hobbiebrunken, T., Feidler, B., Hojo, M., Ochiai, S., Schulte, K. "Microscopic Yielding of CF/Epoxy Composites and the Effect on the Formation of Thermal Residual Stresses." *Composites Science and Technology, Vol. 65*, 2005: 1625-1635.

[85] Honjo, K. "Fracture Toughness of PAN-Based Carbon Fibers Estimated from Strength-Mirror Size Relation." *Carbon, Vol. 41*, 2003: 979-984.

[86] Zhou, Y., Wang, Y., Xia, Y., Jeelani, S. "Tensile Behavior of Carbon Fiber Bundles at Different Strain Rates." *Materials Letters, Vol. 64*, 2010: 246-248.

[87] Hocheng, H., Puw, H.Y., Huang, Y. "Preliminary Study on Milling of Unidirectional Carbon Fiber-Reinforced Composites." *Composites Manufacturing, Vol. 4(2)*, 1993: 103-108.

[88] Ramulu, M. "Machining and Surface Integrity of Fiber-Reinforced Plastic Composites." *Sadhana, Vol. 22(3)*, 1997: 449-472.

[89] Venu Gopala Rao, G., Mahajam, P., Bhatnagar, N. "Machining of UD-GFRP Composites Chip Formation Mechanism." *Composites Science and Technology, Vol. 67*, 2007: 2271-2281.

[90] Nayak, D., Bhatnagar, N. "Machining Studies of UD-FRP Composites Part 2: Finite Element Analysis." *Machining Science and Technology, Vol. 9*, 2005: 503-528.

[91] Arola, D., Ramulu, M. "Orthogonal Cutting of Fiber-Reinforced Composites: A Finite Element Analysis." *In. J. Mechanical Science, Vol. 39(5)*, 1997: 597-613.

[92] Camanho, P.P., Davila, C.G. *Mixed-Mode Decohesion Finite Elements for the Simulation of Delamination in Composite Materials.* Langley, VA.: NASA Research Center, 2002.

[93] Wang, X.M., Zhang, L.C. "An Experimental Investigation into the Orthogonal Cutting of Unidirectional Fiber Reinforced Plastics." *Int. J. Machine Tools & Manufacture, Vol. 43,* 2003: 1015-1022.

[94] Jordan, J.L., Foley, J.R., Siviour, C.R. "Mechanical Properties of Epon 826/DEA Epoxy." *Mechanics of Time-Dependent Materials, Vol. 12,* 2008: 249-272.

[95] Pwu, H.Y., Hocheng, H. "Chip Formation Model of Cutting Fiber-Reinforced Plastics Perpendicular to Fiber Axis." *J. Manufacturing Science and Engineering, Vol. 120(1)*, 1998: 192-196.

[96] Venu Gopala Rao, G., Mahajam, P., Bhatnagar, N. "Machining of UD-GFRP Composites Chip Formation Mechanism." *Composites Science and Technology*, 2007: 2271-2281.